DISSERTATION

ON

EFFECT OF PROCESS PARAMETERS ON WELD JOINT QUALITY DURING SUBMERGED ARC WELDING OF HSLA STEEL

Submitted in Partial Fulfilment of the Requirement for the award of

Degree of

MASTER OF ENGINEERING
IN
CAD/CAM & ROBOTICS

Submitted by

MANISH GARG
ROLL NO: 801081018

Under the Guidance of

Anirban Bhattacharya
Assistant Professor
Mechanical Engineering Department

MECHANICAL ENGINEERING DEPARTMENT
THAPAR UNIVERSITY
PATIALA-147004, INDIA

JULY-2012

DECLARATION

I hereby declare that work done in this Thesis Report entitled, "**EFFECT OF PROCESS PARAMETERS ON WELD JOINT QUALITY DURING SUBMERGED ARC WELDING OF HSLA STEEL**" submitted towards partial fulfilment of requirement for award of **Master of Engineering** degree in **CAD/CAM & Robotics** in **Mechanical Engineering Department** of **Thapar University, Patiala,** is an authentic record of work carried out by me under the supervision and guidance of **ANIRBAN BHATTACHARYA, Assistant Professor** of **Mechanical Engineering Department, Thapar University, Patiala.**

This matter embodied in this report has not been submitted in part or full to any other university or institute for the award of any degree.

MANISH GARG

This is to certify that above declaration made by the student concerned is correct to the best of my knowledge & belief.

16/07/2012

ANIRBAN BHATTACHARYA
ASSISTANT PROFESSOR-MED
THAPAR UNIVERSITY, PATIALA

Countersigned by:

19/7/12

DR. AJAY BATISH
PROFESSOR & HEAD-MED
THAPAR UNIVERSITY, PATIALA

DR. S.K. MOHAPATRA
DEAN, ACADEMIC AFFAIRS
THAPAR UNIVERSITY, PATIALA

ACKNOWLEDGEMENT

I am highly grateful to the authorities of Thapar University, Patiala for providing this opportunity to carry out the thesis work.

I express my deep gratitude and respects to my guide **Anirban Bhattacharya, Assistant Professor of Mechanical Engineering Department, Thapar University, Patiala** for his keen interest and valuable guidance, strong motivation and constant encouragement during the course of the work. I thank him for his great patience, constructive criticism and myriad useful suggestions apart from invaluable guidance to me.

I thank our head of department **Dr. Ajay Batish**, whose excellent leadership and administration made this research project very convenient in term of required stuff and nice working condition. I am extremely thankful to member of distinguished faculty.

I am highly grateful to the authorities of **Defence Research & Development Organisation (DRDO)** and **Defence Material Research Laboratory (DMRL)**, Hyderabad for the support related to this work. I also mention special thank to **Dr. G Madhusudhan Reddy, Scientist-'G', DMRL, Hyderabad** for his technical and all other support extended to us. I am also thankful **to Dr. S. Sankaran, Director, DMRL, Hyderabad** for providing the material used for the present study. I also thank to P.I. / Co-P.I. of DRDO sponsored project for providing me the financial support as 'Project Assistant' under the same project.

The non teaching staff **Mr. Surender Suri, Mr. Surender Singh, Mr. Rath, Mr. Roashan, Mr. Rajender, Mr. A. S. Cheema, Mr. Banerji, Mr. Manoj, Mr. Narender, Mr. Sukhbir** deserve special thanks for their help during this period of this work.

A special thanks to my friend **Mr. Gianender Kajal** for their valorous help and co-operation.

I am also thankful to other faculty members and all the workshop staff of Mechanical Engineering Department of Thapar University, Patiala for their everlasting support.

ABSTRACT

The aim of the present work was to study the effect of various process parameters i.e. current, voltage, travel speed, electrode diameter, flux composition, pre heating of workpiece, electrode stick-out and edge including angle on changes in tensile strength, toughness, microhardness and chemical composition of the weld bead geometry of HSLA Steel and to optimize the process so that minimal changes occur in the material properties after completion of a submerged arc welding (SAW) process following suitable Taguchi experimental design. Tensile strength of the welded specimens were studied and found that Electrode Diameter, welding current and travel speed were the most significant factors leading to changes in tensile strength. The tensile strength tended to increase significantly with the increase in electrode diameter from 3.2-4 mm. whereas higher tensile strength was observed when welding current 450 Ampere and travel speed 15 m/hr was used. Toughness at room temperature of the welded specimen were studied and found that Electrode diameter, electrode stick-out, current, preheat temperature, voltage and were the most significant factors and higher toughness at room temperature was observed when electrode diameter should be 3.2 mm, electrode stick-out should be 28 mm, welding current should be 350 Ampere, preheat temperature should be 150 ^{o}C and welding voltage should be 30 Volts and flux should be of type 3 i.e. GEEFLUX 541 (Basic) was used. Toughness at -40 ^{o}C of the welded specimens were studied and found that type of flux, welding current and electrode stick-out were the most significant factors and higher toughness was observed when welding current 450 Ampere, flux type 3 (GEEFLUX 541-Basic) and electrode stick-out should be 28 mm was used. Edge including angle and welding current were found to be the most significant factors leading to changes in microhardness. The microhardness tended to increase significantly with the increase of welding current from 350 to 450 Ampere and as the edge including angle increases from 60 to 90 degree, microhardness will decrease. Chemical composition of welding specimen was also studied and found that percentage change in phosphorous was increasing in weld region but carbon, sulphur, nickel and chromium contents were decreasing whereas for silicon, manganese and copper shows the mixed trend. So, it concludes that some compounds of flux goes into the weld region.

TABLE OF CONTENT

LIST OF FIGURES

LIST OF TABLES

ABBREVATIONS

ANOVA	Analysis of Variance
BI	Basicity Index
CCT	Centre Cracked Tension
DOE	Design of Experiments
DOF	Degree of Freedom
HAZ	Heat Affected Zone
HSLA	High Strength Low Alloy
MMR	Mis-Match Ratio
PWHT	Post Weld Heat Treatment
SAW	Submerged Arc Welding
SEM	Scanning Electron Microscope
SMAW	Shielded Metal Arc Welding

CHAPTER-1
INTRODUCTION

During the earlier times several attempts were made to mechanize the arc welding process. Developing a continuous coated electrode as an extension of the manual metal-arc welding electrode was ruled out for some reasons. Since the coating is non-conducting, arranging electrical contact with the electrode is not practicable. The coating is likely to peel off when the electrode is coiled, and the coating is also likely to get crushed when fed through the feed rolls. In one of the methods attempted, the work piece was painted with a thin slag flux, while feeding of the bare wire and arc travel were mechanized. Many methods were tried out to provide flux coating in mechanized welding, but all efforts led to failure. The idea of placing a thick layer of dry granular flux on the joint ahead of the carbon electrode was conceived and successfully developed in the U.S.A. and later applied to the welding of penstocks and water conduits in California. Submerged-arc welding was the next logical step and the process became a commercial success both in the U.S.A. and the U.S.S.R. by the middle and late 1930's. [1]

1.1 SUBMERGED ARC WELDING (SAW)

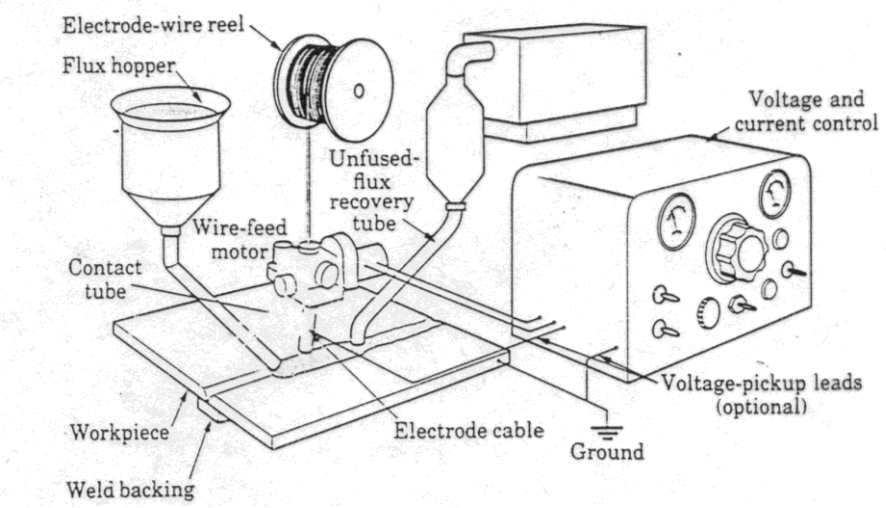

FIGURE 1.1- Submerged arc welding [2]

Submerged Arc Welding (SAW) is an arc welding process in which the arc is concealed by a blanket of granular and fusible flux. Heat for SAW is generated by an arc between a bare, solid-metal (or cored) consumable wire or strip electrode and the workpiece. The arc is

maintained in a cavity of molten flux or slag, which refines the weld metal and protects it from atmospheric contamination. Alloy ingredients in the flux may be present to enhance the mechanical properties and crack resistance of the weld deposit. Figure 1.1 shows the main parts of the machine are control box panel, electrode wire, wire spool and flux hopper. The welding current, welding voltage and welding speed can be regulated, displayed and preset on the panel of the tractor for the convenience of the operator. The function of inch wire feeding and withdrawing makes it convenient for the welder to preset the operating position of the welding wire. Control is provided on the machine for the movement of the tractor on the platform. The movement can be manual or can be automatic. There is also welding head site adjustment function it make the gun move vertically and horizontally. [1]

1.2 PRINCIPLE OF OPERATION

Figure 1.2 shows a typical setup for automatic SAW. A continuous electrode is being fed into the joint by mechanically powered drive rolls. Electrical current, which produces the arc, is supplied to the electrode through the contact tube. The current can be direct current (DC) with electrode positive (reverse polarity), with electrode negative (straight polarity), or alternating current (AC). Figure 1.3 shows the melting and solidification sequence of SAW. After welding is completed and the weld metal has solidified, the un-fused flux and slag are removed. The un-fused flux may be screened and reused. The solidified slag may be collected, crushed, resized, and blended back into new flux. Submerged arc welding is adaptable to both semiautomatic and fully automatic operation, although the latter, because of its inherent advantages, is more popular. In semiautomatic welding, the welder controls the travel speed, direction, and placement of the weld. A semiautomatic welding gun is designed to transport the flux and wire to the operator, who welds by dragging the gun along the weld joint. Semiautomatic electrode diameters are usually less than 2.4 mm to provide sufficient flexibility and feed ability in the gun assembly. Manually guiding the gun over the joint requires skill because the joint is obscured from view by the flux layer. In automatic SAW, travel speed and direction are controlled mechanically. Flux may be automatically deposited in front of the arc, while the un-fused flux may be picked by a vacuum recovery system behind the arc.

To increase deposition rate or welding speed, more than one wire can be fed simultaneously into the same weld pool. For example, in the twin arc process, two electrodes are fed into the same weld pool while sharing a common power source and contact tip. In tandem arc SAW, multiple electrodes are arranged with one in front of the other. Each electrode has an

independent power supply and contact tip. The spacing, configuration, and electrical nature of the electrodes may be arranged to optimize welding speed and bead shape. [1]

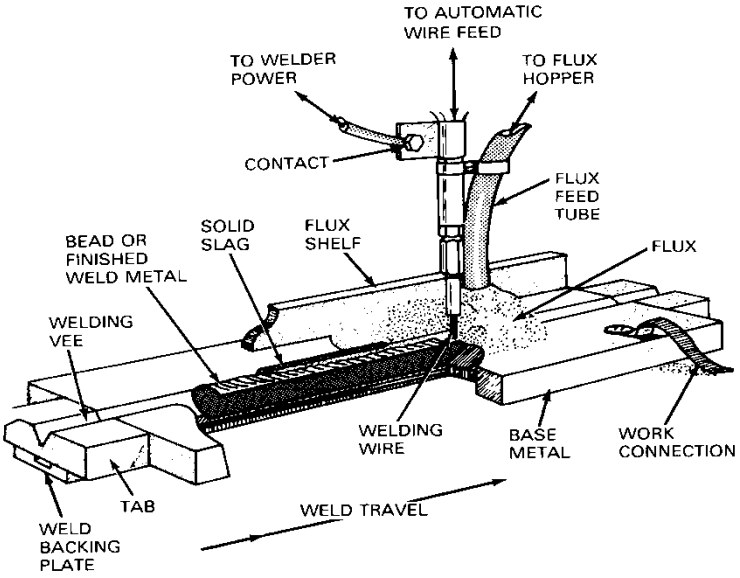

FIGURE 1.2- Mechanism of submerged arc welding [3]

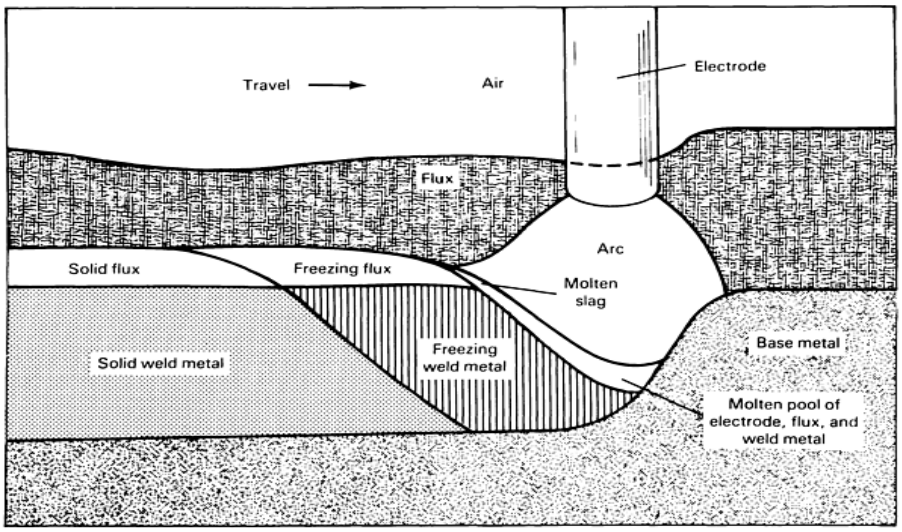

FIGURE 1.3- Melting and solidification sequence of SAW [1]

1.3 SET-UP OF SAW PROCESS

The typical set-up of SAW consists of-

- A wire feeder to drive the electrode to the work through the contact tube of a welding gun or welding head.

- A welding power source to supply electric current to the electrode at the contact tube.
- An arrangement for holding the flux and feeding it ahead of the arc.
- A means to transverse the weld joint. [2]

  This is shown in Figure 1.4.

FIGURE 1.4- Set up of SAW process

(**Courtesy:** Central Workshop, Thapar University, Patiala)

1.4 SAW PARAMETERS

While SAW is the most inexpensive and efficient process for making large, long, and repetitive welds, much time and energy are required to prepare the joint. Care must be taken to line up all joints to have a consistent gap in groove welds and to provide backing plates and flux dams to prevent spillage of flux and molten metal. Once all the pieces are clamped or tacked in place, welding procedures and specifications should be consulted before welding begins. [2]

Procedural Variations and Effect on Weld Bead Characteristics

Procedural variations in SAW include current, voltage, electrode stick out, travel speed, pre-heating of workpiece and post-heating of weldment, size of electrode and flux depth and width. Variation in any of these parameters will affect the shape and penetration of the weld, as well as the integrity of the weld deposit.

1.4.1 Weld Current

Welding current controls the parameters such as deposition rate, penetration, and dilution, it is the most important welding variable. An increase in welding current at a constant voltage will decrease the flux-to-wire ratio, while a decrease in current will increase the flux-to-wire ratio. The effect of current variation on weld bead profile is shown in Figure 1.5. Welds made at excessively low current will tend to have little penetration and higher width-to-depth ratios. Welds made at an excessively high current will have deep penetration, high dilution, more shrinkage, and excess build-up. Low current will also produce a less stable arc than higher currents. [2]

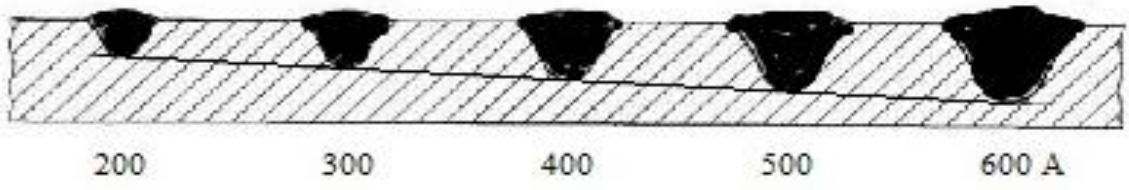

FIGURE 1.5- Effect of variation in welding current on weld bead profile [4]

1.4.2 Travel Speed

Variations in travel speed at a set current and voltage that affect bead shape is shown in Figure 1.6. As welding speed is decreased, heat input per length of joint increases, and the penetration and bead width increase. The penetration will increase until molten metal begins to flow under the arc and interfere with heat flow at excessively slow speeds.

Excessively high travel speeds will promote a crowned bead as well as the tendency for undercut and porosity. [2]

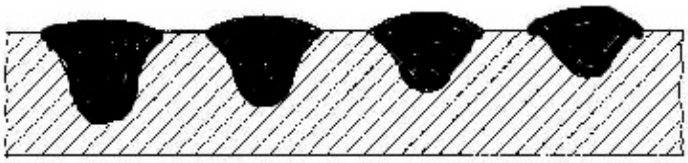

FIGURE 1.6- Effect of variation in welding speed on weld bead profile [4]

1.4.3 Weld Voltage

Like current, welding voltage will affect the bead shape and the weld deposit composition. Increasing the arc voltage at a constant current will increase the flux-to-wire electrode ratio, while decreasing the voltage will reduce the flux-to-electrode ratio. The effect of the magnitude of arc voltage on bead shape is shown in Figure 1.7. Increasing the arc voltage will produce a longer arc length and a correspondingly wider, flatter bead with less

penetration. Higher voltage will increase flux consumption and also produce a hat-shaped concave weld, which has low resistance to cracking and a tendency to undercut. Lower voltages will shorten the arc length and increase penetration. Excessively low voltage will produce an unstable arc and a crowned bead, which has an uneven contour where it meets the plate. [2]

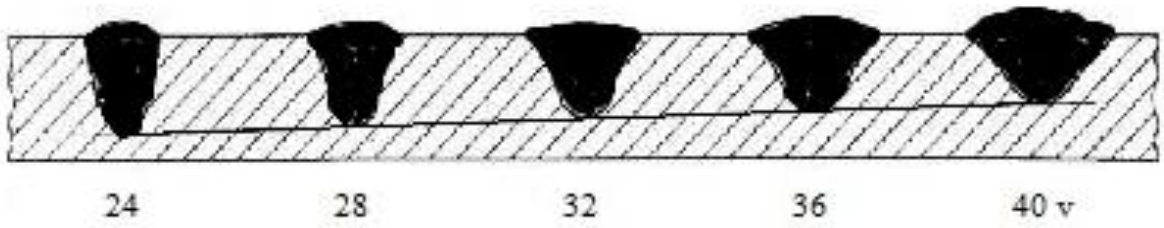

FIGURE 1.7- Effect of variation in welding voltage on weld bead profile [4]

1.4.4 Electrode Stick-out

Electrode stick-out refers to the length of the electrode, between the end of contact tube and the arc, which is subject to resistance heating at the high current densities used in the process. The longer the stick-out, the greater the amount of heating and the higher the deposition rate. Increased electrode stick-out reduces to some extent the energy supplied to the arc, resulting in lower arc voltage and a different bead shape. Hence when the electrode stick-out is increased to obtain higher deposition rate, the voltage setting on the equipment must be increased to maintain correct arc length. [2]

1.4.5 Size of Electrode

As in the case of SAW, the electrode size is selected according to the plate thickness and the desired size of weld. With increase in electrode size, welding current can be increased so as to get higher deposition rates, deeper penetration and increased weld size. At a given welding current, changing over to a larger electrode results in a wider, less penetrating bead shown in Figure 1.8. Hence in joints with poor fit-up, a larger electrode is preferred to a smaller one for bridging the root gap. [2]

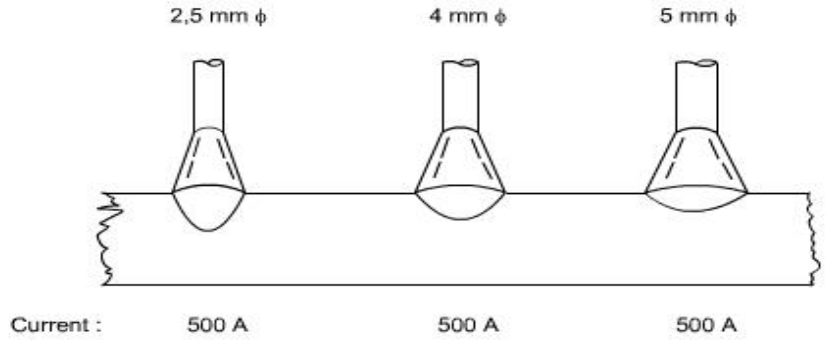

FIGURE 1.8- Effect of variation in electrode size on weld bead profile [4]

1.4.6 Pre-heating of Workpiece & Post-heating of Weldment

Pre-heating of workpiece & post-heating of weldment helps in relaxation of residual and thermal stresses. It also helps in removal of diffusible hydrogen and prevents the work metal from hydrogen cracking. It increases the strength and durability of the weld and reduces stress and eliminates moisture from the plate surface. [4]

1.4.7 Pre-heating of Flux

Pre-heating of flux dries the flux and reduces the thermal shocks arise during welding. It also helps in producing better quality weld and also increases the bead height and width. [4]

1.4.8 Width and Depth of Welding Flux

If the granular layer is too deep, a rough weld is likely to result. The gases generated during welding cannot readily escape and the surface of the molten weld metal is irregularly distorted. If the granular layer is too shallow, the welding zone will not be entirely submerged due to which flashing and spattering will be present also the weld will have a bad appearance and may be porous. [4]

1.5 FLUX

Flux is a chemical cleaning agent which facilitates welding by removing oxidation from the metals to be joined. Common fluxes are: ammonium chloride, rosin, hydrochloric acid, zinc chloride, borax. Different fluxes, based on sodium chloride, potassium chloride, sodium fluoride are used.

In high-temperature metal joining processes (welding, brazing and soldering), the primary purpose of flux is to prevent oxidation of the base and filler materials. Tin-lead solder attaches very well to copper, but poorly to the various oxides of copper, which form quickly at soldering temperatures. Flux is a substance which is nearly inert at room temperature, but which becomes strongly reducing at elevated temperatures, preventing the formation of metal oxides. Flux is normally used in granular form and a sample stock of flux is shown in Figure 1.9.

The functions of the flux are:

- To assist arc striking and stability.
- To form a slag that will protect and shape the weld bead.
- To form a gas shield to protect the molten filler metal being projected across the arc gap.

- To react with the weld pool to provide clean high quality weld metal with the desired properties.
- To deoxidise the weld pool.
- Provide de-oxidants.

FIGURE 1.9- Flux

The most convenient method of classifying, however, is by reference to the **'basicity index' (BI)** of the flux. The index is calculated by dividing the sum of the percentages of the basic constituents by the sum of the acid constituents. Calcium, magnesium, sodium, potassium and manganese oxides, calcium carbonate and calcium fluoride are the basic constituents of a flux, silica and alumina the acid constituents. The basicity of a flux has a major effect on the weld metal properties, most importantly the notch toughness. As a general rule the higher the basicity the higher the notch toughness.

The flux is termed acidic or basic depending on the value of BI. One of the major differences between basic and acidic fluxes is their ability to rid the molten metal of residual sulphur and phosphorus.

Neutral fluxes are designed to have little or no effect on the chemical analysis of the weld metal and therefore on the mechanical properties. They contain low silica, calcium silicate and alumina and do not add significant amounts of silicon and manganese to the weld.

The **acid fluxes** contain substantial amounts of silica, silicates in the form of calcium or manganese silicate and manganese oxide. These fluxes react with the weld pool and will raise both silicon and manganese content of the weld together with high oxygen content. The result of this is that the toughness of the weld is poor but the fluxes will tolerate rusty surfaces, will

detach easily and give a good weld appearance. They are especially useful for single pass high speed welding such as fillet welding of web to flange girder joints.

The **basic fluxes** fill much the same role in submerged arc welding as basic coatings do in manual metal arc welding. They have low silica content and are composed of varying amounts of calcium carbonate and/or fluoride, alumina, calcium, manganese and magnesium oxides.

This combination of compounds gives clean, low sulphur, low oxygen weld metal with good to excellent notch toughness. The transfer of silicon and manganese into the weld metal is also limited. Such fluxes are preferred for the welding of high quality structural steels, pressure vessels, pipe work and offshore structures where either good high or low temperature properties are required.

The BI as adopted by International Institute of Welding is given in terms of the weight percentage of various oxides and fluorides constitutes.

$$\text{Basicity index (BI)} = \frac{\text{Basic oxides}}{\text{Acidic oxides}}$$

The flux is termed acidic or basic depending on the value of BI. One of the major differences between basic and acidic fluxes is their ability to rid the molten metal of residual sulphur and phosphorus. [5] [6]

There are four levels of BI for standardization of flux give as follow [5] [6]:

- Fluxes having basicity index (BI) less than 1 are incapable of controlling the sulphur content of the weld metal effectively. In short BI <1=Acidic.
- Fluxes having basicity index (BI) between 1and 1.5 are capable of controlling the sulphur effectively but not oxygen in the weld metal. In short 1<BI<1.5=Neutral.
- Fluxes having basicity index (BI) between 1.5 and 2.5 are capable of controlling the sulphur and oxygen content effectively and lowering the transition temperature by controlling Si content in the weld metal to a certain extent. In short1.5<BI<2.5=Basic.
- Fluxes having basicity index (BI) above 2.5 are capable of lowering the charpy V-notch transition temperature down to $-40^{O}C$ or even below by controlling the composition and microstructure of weld metal suitably. In short BI>2.5=High Basic.

1.6 TYPES OF FLUXES

SAW flux basically performs the same functions as the coating of a manual electrode. Additionally, it must satisfy certain special conditions demanded by the nature of the process.

The flux protects the molten pool and the arc against atmospheric oxygen and nitrogen by creating an envelope of molten slag. The slag also cleanses the weld metal (i.e. deoxidizes it and removes impurities such as sulphur) modifies its chemical composition and controls the profile of the weld bead. The molten slag also provides favourable conditions for very high current densities, which together with the insulating properties of the flux; concentrate intense heat into a relatively small welding zone. This result in a deeply penetrating arc, which makes narrower and shallower welding grooves practicable, thus reducing the amount of weld metal, required to complete the joint. It also results in higher welding speeds. The properties of the flux enable submerged arc weld to be made over a wide range of welding currents, voltage and speeds, each of which can be controlled independently of the other. Thus one can obtain welded joints of desired shape, chemistry and mechanical and metallurgical properties by using an appropriate welding procedure.

Nowadays, two main types of submerged arc fluxes are available, depending on the method of manufacture i.e**.** fused and agglomerated. [7]

1.6.1 Fused Fluxes

Typical ingredients are quartz, manganese ore or slag, dolomite, potassium feldspar and clay. These minerals are ground and mixed in a definite proportion and melted. Melting is carried out in a magnesia or fireclay crucible, if heating is by gas or in a graphite crucible if electricity is used. Electric melting is started by heating with an arc between the electrode and crucible and continued by resistance heating with the electrode submerged in the molten flux, which is an electrical conductor. After fusion, the melt is solidified rapidly by quenching into water or pouring into cell steel chills to produce small fragments of flux as shown in Figure 1.10 and then these small fragments of flux are dried and crushed to the required size, sieved and packed in bags or drums. [7]

FIGURE 1.10- Fused flux [4]

Fused Flux Features

- Non-hygroscopic
- Fully reacted
- Chemically homogenous
- Contain no metallic deoxidizers
- Glass-like appearance, high grain strength

Fused Flux Benefits

- Particles are non-hygroscopic and do not absorb moisture, therefore only a low temperature (300°F/150°C) drying cycle is required to remove surface moisture/condensation, providing increased protection against hydrogen cracking.
- Provide smooth, stable performance even welding currents (up to 2,000 amps).
- Flux particles are chemically consistent welds.
- Fused fluxes are less susceptible to particle breakdown due to flux recycling, reducing the creation of fine dust particles. [7]

1.6.2 Agglomerated Fluxes

For producing an agglomerated flux, finely powdered ingredients are mixed and ground dry in a mixer. The mix is steadily moistened by spraying with a solution of alkaline silicate and the mixing is continued. The mixer blades are suitably designed to assist agglomeration. The silicate solution initially fills the spaces between the pores of the particles. When subsequently dried, the water evaporates, leaving the binder as bridges between particles. After baking, the flux is graded to a specified granule size by sieving, and packed in water-proof containers as shown in Figure 1.11. [7]

FIGURE 1.11- Agglomerated flux [4]

Agglomerated Flux Features

- Contain metallic deoxidizers
- May contain alloying agents
- Flat, low gloss, or dry particle appearance
- Each flux particle has a unique chemistry.

Agglomerated Flux Benefits

- Presence of deoxidizers provides good performance over rust and mill scale and helps prevent weld porosity.
- Usually provides better peeling properties than fused fluxes.
- Alloying elements can be added to provide improved chemical and mechanical properties.
- Usually exhibit lower flux consumption than a fused flux welded at the same current and voltage. [7]

1.6.3 Sintered Fluxes

They are produced by grinding the dry charge together, pressing into small balls, and heating to 1,000-1,100°C (just below melting point) in gas-fired furnaces. The solid mass produced then has the characteristics of a fused flux. It is crushed to the desired fineness, sieved, sized and packed in suitable containers. [7]

1.7 FLUX STORAGE

To prevent contamination of weld by hydrogen, the flux must be kept dry and free from oils and other hydrocarbons. If flux becomes damp, it must be re-dried. Excessive levels of hydrogen in some steels can cause porosity. In hard able steels, even small amount of hydrocarbon can cause underline cracking. Commercially available dryers are the best method of drying flux. Do not dry flux by using direct flame. This may fuse the flux together; at the same time, the flame produces water that might condense on the flux. [7]

1.8 SOURCES OF DEFECTS IN SAW

The fact that SAW is a high heat input process under a protective blanket of flux greatly decreases the chance of weld defects. However, defects such as lack of fusion, slag entrapment, solidification cracking, hydrogen cracking, or porosity occasionally occur.

1.8.1 Insufficient Fusion and Slag Entrapment

Lack-of-fusion defects and slag entrapment are most commonly caused by improper bead placement or procedure as shown in Figure 1.12. Improper placement can cause the weld metal to roll over and trap slag underneath, or if the weld bead is placed away from the edge to be joined, the liquid metal may not fuse to the base material. A crown-shaped bead caused by low welding voltage may also contribute to slag entrapment and lack of fusion by not allowing the liquid metal to spread out evenly. [1]

FIGURE 1.12- Insufficient penetration and excessive reinforcement, also misaligned [4]

1.8.2 Solidification Cracking

Solidification cracking of saw along the centre of the bead is usually due to bead shape, joint design, or incorrect choice of welding consumables. A convex bead shape with a bead width-to-depth ratio greater than one will decrease solidification cracking tendencies. If weld penetration is too deep, the shrinkage stresses may cause centreline cracking.

Joint design may also contribute to excessive shrinkage stresses, again increasing the risk of solidification cracking as shown in Figure 1.13.

Because cracking is related to stresses in the weld, high-strength materials will have a greater tendency to crack. Therefore, special care must be taken to generate proper bead shape, preheat temperatures, and interpass temperatures, in addition to correct electrode and flux combinations, when welding these materials. [1]

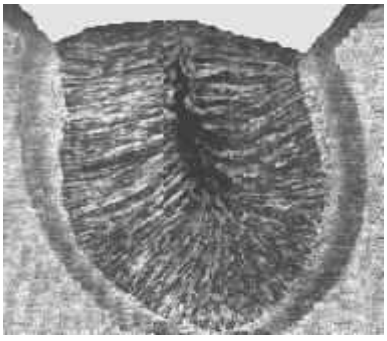

FIGURE 1.13-Solidification cracking [8]

1.8.3 Hydrogen Cracking

Unlike solidification cracking, which appears immediately after welding, hydrogen cracking is a delayed process and may occur from several hours to several days after welding has been completed as shown in Figure 1.14. To minimize hydrogen cracking, all possible sources of hydrogen (for example, water, oil, grease, and dirt) present in the flux, electrode, or joint should be eliminated. The flux, electrode, and plate should be clean and dry.

To prevent moisture pickup, fluxes and electrodes should be stored in moisture resistant containers in dry areas. If a flux or electrode becomes contaminated with moisture, it should be dried according to manufacturer recommendations.

Selection of the consumable, especially when welding high-strength steels that are more susceptible to hydrogen cracking can also play a role in hydrogen cracking.

To further reduce hydrogen related cracking, the joint to be welded should be preheated. Because hydrogen is fairly mobile in steel at temperatures above 95°C, the recommended preheat temperatures should be followed to allow most of the hydrogen to escape and to reduce the risk of hydrogen damage. In thick weldments, maintaining preheat for several hours after welding is completed, will also reduce the risk of hydrogen cracking. [1]

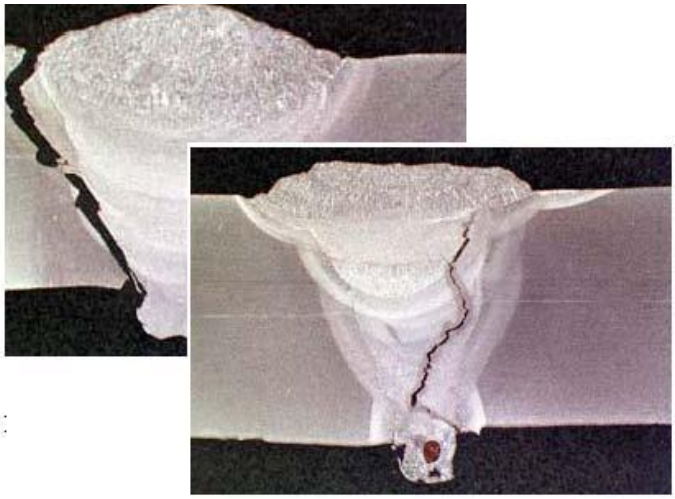

FIGURE 1.14- Hydrogen cracking [9]

1.8.4 Porosity

Porosity caused by trapped gas is uncommon in SAW because of the protection provided by the flux. When porosity does occur, it may be in the form of internal porosity or as depressions on the weld bead surface. The gas bubbles that cause porosity originate either from a lack of protection from the atmosphere or from contaminants such as water, oil, grease, and dirt as shown in Figure 1.15. To reduce porosity in SAW, the weld should have

sufficient flux coverage, and all water, grease, and dirt should be removed from the plate, electrode, and flux. Another cause of porosity in SAW is excessive travel speed. Travel at excessively high speeds will not allow the gas bubbles to escape from the weld, and the bubbles may become trapped in the weld metal at the slag-to-metal interface. [1]

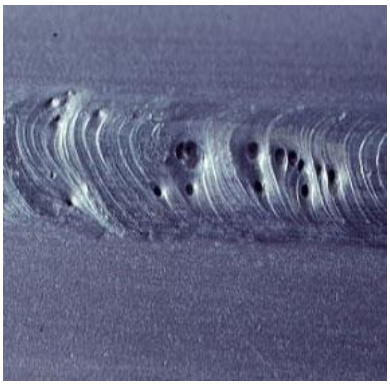

FIGURE 1.15-Porosity [10]

1.9 HIGH STRENGTH LOW ALLOY STEEL

High Strength Low Alloy (HSLA) Steel is a type of alloy steel that provides better mechanical properties or greater resistance to corrosion than carbon steel. HSLA steels vary from other steels in that they aren't made to meet a specific chemical composition, but rather to specific mechanical properties. They have carbon content between 0.05–0.25% to retain formability and weldability. Other alloying elements include up to 2.0% manganese and small quantities of silicon, sulphur, phosphorous, copper, nickel, niobium, vanadium, chromium, molybdenum, titanium, calcium, rare earth elements, or zirconium.

Copper, titanium, vanadium, and niobium are added for strengthening purposes. These elements are intended to alter the microstructure of carbon steels, which is usually a ferrite-pearlite aggregate, to produce a very fine dispersion of alloy carbides in an almost pure ferrite matrix.

This eliminates the toughness-reducing effect of a pearlitic volume fraction, yet maintains and increases the material's strength by refining the grain size, which in the case of ferrite increases yield strength.

The yield strengths vary between 250–655 MPa. Due to their higher strength and toughness HSLA steels usually require 25 to 30% more power to form, as compared to carbon steels.

Copper, silicon, nickel, chromium, and phosphorus are added to increase corrosion resistance. Zirconium, calcium, and rare earth elements are added for sulphide-inclusion shape control which increases formability. These are needed because most HSLA steels have directionally

sensitive properties. Formability and impact strength can vary significantly when tested longitudinally and transversely to the grain.

HSLA steels are also more resistant to rust than most carbon steels, due to their lack of pearlite – the fine layers of ferrite. [11]

1.10 EFFECTS OF ALLOYING ELEMENTS IN STEEL

Steel is basically iron alloyed to carbon with certain additional elements to give the required properties to the finished melt. Listed below is a summary of the effects of various alloying elements in steel.

1.10.1 Carbon

The basic metal, iron, is alloyed with carbon to make steel and has the effect of increasing the hardness and strength by heat treatment but the addition of carbon enables a wide range of hardness and strength.

1.10.2 Manganese

Manganese is added to steel to improve hot working properties and increase strength, toughness and hardenability.

1.10.3 Chromium

Chromium is added to the steel to increase resistance to oxidation. This resistance increases as more chromium is added. When added to low alloy steels, chromium can increase the response to heat treatment, thus improving hardenability and strength.

1.10.4 Nickel

Nickel has a tendency to form austenite which is responsible for a great toughness and high strength at both high and low temperatures. Nickel also improves resistance to oxidation and corrosion. It increases toughness at low temperatures when added in smaller amounts to alloy steels.

1.10.5 Molybdenum

Molybdenum when added to low alloy steels, molybdenum improves high temperature strengths and hardness.

1.10.6 Phosphorus

Phosphorus is usually added with sulphur to improve machinability in low alloy steels, phosphorus, in small amounts, aids strength and corrosion resistance.

1.10.7 Sulphur

Sulphur improves machinability when added in small amount.

1.10.8 Silicon

Silicon is used as a deoxidising (killing) agent in the melting of steel; as a result, most steels contain a small percentage of silicon. Silicon contributes to hardening of the ferritic phase in steels.

1.10.9 Copper

Copper is normally present in stainless steels as a residual element. However it is added to a few alloys to produce precipitation hardening properties. [12]

1.11 HSLA STEEL PROPERTIES

High Strength Low Alloy (HSLA) Steels provide increased strength-to-weight ratios over conventional low-carbon steels for only a modest price premium. Because HSLA alloys are stronger, they can be used in thinner sections, making them particularly attractive for transportation-equipment components where weight reduction is important. HSLA steels are available in all standard wrought forms - sheet, strip, plate, structural shapes, bar-size shapes, and special shapes.

Typically, HSLA steels are low-carbon steels with up to 1.5% manganese, strengthened by small additions of elements, such as columbium, copper, vanadium or titanium and sometimes by special rolling and cooling techniques. Improved-formability HSLA steels contain additions such as zirconium, calcium, or rare-earth elements for sulphide-inclusion shape control.

HSLA steels can have thinner cross sections than equivalent parts made from low-carbon steel; corrosion of HSLA steel can significantly reduce strength by decreasing the load-bearing cross section. While additions of elements such as copper, silicon, nickel, chromium, and phosphorus can improve atmospheric corrosion resistance of these alloys, they also increase cost.

Galvanizing, zinc-rich coatings, and other rust-preventive finishes can help protect HSLA-steel parts from corrosion.

Improved-formability HSLA steels were developed primarily for the automotive industry to replace low-carbon steel parts with thinner cross-section parts for reduced weight without sacrificing strength and dent resistance.

Forming, drilling, sawing, and other machining operations on HSLA steels usually require 25 to 30% more power than do structural carbon steels. They are used to handle large amounts of stress or a good strength-to-weight ratio. HSLA steels are usually 20 to 30% lighter than carbon steel with the same strength. HSLA steels usually have densities of around 7800 kg/m^3.

HSLA alloys have directionally sensitive properties. For some grades, formability and impact strength vary significantly depending on whether the material is tested longitudinally or transversely to the rolled direction. For example, bends parallel to the longitudinal direction are more apt to cause cracking around the outside, tension-bearing surface of the bend. This effect is more pronounced in thick sheets. This directional characteristic is substantially reduced in HSLA steels that have been treated for sulphide shape control. [11]

1.12 APPLICATION OF HSLA STEEL

Improved-formability HSLA steels were developed primarily for the automotive industry to replace low-carbon steel parts with thinner cross-section parts for reduced weight without sacrificing strength and dent resistance. Typical passenger-car applications include door intrusion beams, chassis members, reinforcing and mounting brackets, steering and suspension parts, bumpers, and wheels.

Trucks, construction equipment, off-highway vehicles, mining equipment, and other heavy-duty vehicles use HSLA sheets or plates for chassis components, buckets, grader blades, and structural members outside the body. For these applications, sheets or light-gage plates are specified. Structural forms (alloys from the family of 45,000 to 50,000 psi minimum yield strength HSLA steels) are specified in applications such as offshore oil and gas rigs, single-pole power-transmission towers, railroad cars, and ship construction. [11]

CHAPTER-2
LITERATURE REVIEW

2.1 REVIEW OF LITERATURE

This chapter covers a detailed review of literature on the various aspects of Submerged Arc Welding (SAW) and High Strength Low Alloy (HSLA) Steel. The literature review includes the research carried out on SAW process, effect of weld parameter, flux improvement and effects on HSLA steel. The available literature can be categorized in the following broad classifications.

2.2 CATEGORIZATION OF LITERATURE

The review of literature has been divided into following categories:

- Optimization of SAW process.
- Effect of welding parameters on weld properties.
- Effect of flux improvement on weld properties.
- Study of heat affected zone.
- Effect of weld parameters on HSLA steel.

2.2.1 Optimization of SAW Process

Datta *et al.* [13] in this study optimization was performed to determine the maximum amount of slag–flux mixture that can be used without sacrificing any negative effect on bead geometry, compared to the conventional SAW process, which consumes fresh flux only. Experiments were conducted using welding current, slag-mix percentage and flux Basicity index as process parameters, varied at four different levels.

Patnaik *et al.* [14] studied the SAW process and found wide industrial application due to its easy applicability, high current density and ability to deposit a large amount of weld metal using more than one wire at the same time. It was highly emphasized in manufacturing especially because of its ability to restore worn parts.

SAW was characterized by a large number of process parameters influencing the performance outputs such as deposition rate, dilution and hardness, which subsequently affect weld quality. The relationship between control factors and performance outputs was

established by means of nonlinear regression analysis, resulting in a valid mathematical model.

Moi *et al.* [15] introduced the concept of using slag-mix% as a process variable. The percentage of slag, in the mixture of fused flux and fresh flux, was denoted as slag mix%. The main effect of using slag-mix and interactive effects of process parameters (including slag mix%) on features of bead geometry and HAZ, in terms of bead height, depth of penetration, bead width and HAZ width have been evaluated through analysis of variance (ANOVA) method.

Elsayed & Chen [16] introduced that parameter design, based on the Taguchi method, can optimize the performance characteristic through the setting of process parameters and can reduce the sensitivity of the system performance to sources of variation.

Myers & Montgomery [17] studied that, in submerged arc welding process parameters interact in a complicated manner that influences various features of quality characteristics of the weld bead. Quadratic response surface methodology was an efficient approach to represent these relationships through mathematical equations.

2.2.2 Effect of Welding Parameters on Weld Properties

Ghosh *et al.* [18] derived an analytical solution to predict the transient temperature distribution on the plate during the process of SAW. An analytical solution was derived from the transient three dimensional heat conduction equations. The energy input that was applied on the plate was taken as the volume of heat lost from the electric arc and the kinetic energy of filler droplets specifically driven by gravity, electromagnetic force, arc drag force, carrying mass, momentum and thermal energy. These driving forces periodically impinge onto the base metal, leading to a liquid weld puddle. The electric arc was assumed to be a moving double central conicoidal heat source with a close proximity to a Gaussian distribution. It was observed that the predicted values were in good agreement with the experimental results. HAZ width calculation was also done with the help of the analytical solution of the transient-three dimensional heat conduction equation. Analyses of micro-structural changes were critically investigated to comprehend the HAZ softening and phenomena.

Kumar *et al.* [19] studied the effect of process parameters on micro hardness and microstructure of HAZ in SAW by using Taguchi Experimental Design. Welding current and type of flux were found to be most significant factor leading to change in micro hardness and metallurgical properties. The micro hardness tended to increase significantly with the

increase of welding current from 350A to 450A whereas higher hardness was observed when flux type I (basicity index 0.8) was used. Travel speed and arc voltage were found to be insignificant in relative comparison. The result are as expected as higher ferrite content means less hardness thus correlating the two response to each other.

Prasad & Dwivedi [20] investigated the influence of the SAW process parameters (welding current and welding speed) on the microstructure, hardness, and toughness of HSLA steel weld joints. Attempts were made to analyze the results on the basis of the heat input. The SAW process was used for the welding of 16 mm thick HSLA steel plates. The weld joints were prepared using comparatively high heat input (3.0 to 6.3 KJ/mm) by varying welding current (500–700 A) and welding speed (200–300 mm/min). Results showed that the increase in heat input coarsens the grain structure both in the weld metal and heat affected zone. The hardness was found to vary from the weld centre line to base metal and peak hardness was found in the HAZ. The hardness of the weld metal was largely uniform. The hardness reduced with the increase in welding current and reduction in welding speed (increasing heat input) while the toughness showed mixed trend. The increase in welding current from 500 A to 600 A at a given welding speed (200 mm/min or 300 mm/min) increased toughness and further increase in welding current up to 700 A lowered the toughness.

Gulenc & Kahraman [21] in this study, worn parts were welded using the submerged arc welding process. Various wires and fluxes were used for this purpose. These welded parts were subjected to wear tests under different loads, and changes in the hardness and microstructures were examined. The results showed that the hardest weld metal showed the highest wear resistance, while the least hard weld metal showed the least wear resistance. The weld hardness and wear resistance obtained were found to be dependent on the chemical composition of the weld wire and flux.

Chandel *et al.* [22] observed that many variants of SAW such as twin arc, tandem arc, multiple wire, strip electrodes, etc., are now available and widely used for specific applications. With the use of proper parameters and SAW variant, it is now possible to achieve deposition rates in excess of 50 kg/hr. The increase in deposition rate in most cases was achieved by increasing welding current and hence the heat input, which tends to impair joint toughness.

Pandey & Bharti [23] studied the influence of SAW parameters and flux basicity index on the weld chemistry and transfer of elements namely manganese, silicon, carbon and sulphur were investigated. In this study five fluxes and different values of the welding parameters were used. The welds were produced as a bead on a mild-steel plate. The weld-metal composition showed, gain of silicon and loss of carbon, manganese and sulphur elements. The results showed that welding current and voltage have an appreciable influence on element transfer, as well as on weld composition. On the other hand, the basicity index of the fluxes has minor influence. Weldments properties such as strength, toughness and solidification cracking behaviour were affected by chemical composition.

Devis [24] worked with ten fluxes of different bases, found that the measured and the expected composition were not identical and also studied a three flux system and reported that weld-metal carbon content appeared to be independent of fluxes and reported that the change in silicon content of the weld metal is influenced by the value of basicity index and that degree of influence is greater when the value of basicity index is less than 2.

Troyer & Mikurak [25] had shown that by adding the powder in SAW, a better use of heat can be made. Thus, for a given heat input, the number of passes required to fill a joint can be reduced and therefore, the total energy supplied to the joint can be reduced.
Alternatively, the same bead size or deposition rate can be achieved by lowering heat input per pass. Welds made with lower heat input experience higher cooling rates, and thermal gradients were steeper hence, the width of HAZ is also less. Additionally, the time spent above the peak temperature was reduced the combined effect of the results in a narrow HAZ that cools faster and has smaller grain growth. Weld metals produced under faster cooling rates were also superior in mechanical properties. Thus, the process of powder addition has potential not only for producing welds that were cost effective but metallurgical superior too and they may become attractive for welding HSLA.

2.2.3 Effect of Flux Improvement on Weld Properties

Kumar *et al.* [26] studied that submerged arc welding contributes to approximately 10% of the total welding. Approximately 10% -15% of the flux gets converted into very fine particles termed as flux dust before and after welding, due to transportation and handling. If welding was performed without removing these very fine particles from the flux, the gases generated during welding were not able to escape, thus it may result into surface pitting (pocking) and even porosity. On the other hand, if these fine particles were removed by sieving, the cost of

welding was increased significantly. And if this flux dust was dumped/ thrown, will create the pollution. Therefore to reduce the cost of welding and pollution, several attempts were made to develop the acidic and basic agglomerated fluxes by utilizing wasted flux dust. This study showed that the chemical composition and mechanical properties of the all weld metal prepared from the developed fluxes and the parent fluxes to be in the same range. The welded joints were also found to be radio-graphically sound. Therefore the developed fluxes prepared from the waste flux dust can be used without any compromise in mechanical properties and quality of the welded joint. It will reduce the cost of welding and pollution.

Kanjilal *et al.* [27] studied the combined effect of flux mixture and welding parameters on submerged arc weld metal chemical composition and mechanical properties. Bead-on-plate weld deposits on low carbon steel plates were made at different flux composition and welding parameter combinations. Results show that flux mixture related variables based on individual flux ingredients and welding parameters have individual as well as interaction effects on responses, viz. weld metal chemical composition and mechanical properties. In general, two factor interaction effects were higher than the individual effect of mixture related variables.

Mercado *et al.* [28] investigated the effect of flux composition for the microstructure and tensile properties of a submerged-arc welding. Three flux compositions were used with a low-carbon electrode. A commercial flux composition was used for comparison. The welding conditions were kept the same. Tension tests were pursued at room temperature. Microstructure and macrostructure of welds were observed with light and scanning electron microscopes (SEM). The presence of acicular ferrite was detected for welds of fluxes with the highest content of titanium oxide. The yield and ultimate tensile strengths seem to be influenced by the presence of acicular ferrite. The elongation and area reduction percentages were affected by the inclusion volume percentage. Tensile properties and microstructure were compared with the values predicted by the computer programs.

Eagar [29] observed that the mechanical properties of weld metal were primarily the result of the weld metal chemical composition, microstructure and the cooling rate.

The cooling rate experienced by weld metal deposit was controlled by a combination of heat input and heat extraction. Under identical condition of welding, viz. joint design and plate thickness, heat extraction may be assumed to remain same. Therefore, weld metal chemical composition and heat input controlling microstructure were the governing factors responsible for the mechanical properties of weld metal. The weld metal yield strength (YS), ultimate tensile strength (UTS) and toughness increases with increase in alloying elements, viz. carbon

(up to 0.10 wt%), manganese (up to 1.5 wt%), silicon (up to 0.5 wt%) and nickel (up to 3.5 wt%) by various mechanisms such as (i) solid solution hardening, (ii) grain refinement and (iii) refinement of microstructure, etc. The basic requirements of improved toughness in low alloy steel weld metal are associated with the amount of acicular ferrite in the microstructure.

2.2.4 Study of Heat Affected Zone

Lee *et al.* [30] discussed the effect of welding parameters on the size of the HAZ and its relative size as compared to the weld bead of submerged arc welding. The effect of submerged arc welding parameters on the size of the heat affected zone and HAZ size to bead size ratio has been studied. They concluded that the size of the HAZ is influenced by SAW parameters however different parameters have different degrees of influence. Among the welding parameters, the welding current has the greatest influence on HAZ size and HAZ size to bead size ratio, higher current causes smaller HAZ and HAZ to bead size ratio. Other welding parameters like heat input and polarity also affect HAZ to bead size ratio while voltage, electrode diameter and stick out have no significant effect on it.

Eroglu *et al.* [31] observed high heat input welding processes (submerged arc, shielded metal arc welding and electro slag welding) are commonly used for welding of thick sections. Weld thermal cycles associated with the high heat input processes were known to affect both the macro and microstructure of HAZ and weld metal which in turn influence the mechanical properties of the joint.

2.2.5 Effect of Weld Parameters on HSLA Steel

Beidokhti *et al.* [32] studied the effect of titanium addition on the SAW weld metal microstructure of API 5L-X70 pipeline steel was investigated. The relationship between microstructure and toughness of the weld deposit was studied by means of full metallographic, longitudinal tensile, Charpy-V notch and HIC tests on the specimen cut transversely to the weld bead. The best combination of microstructure and impact properties was obtained in the range of 0.02–0.05% titanium. By further increasing of titanium content, the microstructure was changed from a mixture of acicular ferrite, grain-boundary ferrite and widmanstätten ferrite to a mixture of acicular ferrite, grain-boundary ferrite, bainite and ferrite with M/A micro constituent. Therefore, the mode of fracture also changed from dimpled ductile to quasi-cleavage. The results showed an increase in the titanium content of inclusions with increased titanium levels of weld metal. Titanium-base inclusions improve impact toughness by increasing the formation of acicular ferrite in the microstructure.

Zrilic *et al.* [33] studied that toughness and crack properties of the welded joint, both in the weld metal and the HAZ, were required. Experimental investigations of toughness and crack resistance parameters through static and impact tests of a high-strength, low-alloy steel (HSLA) with a nominal yield strength of 700MPa and its welded joint, were performed on Charpy-sized specimens, V-notched and pre-cracked, of the parent metal, weld metal and HAZ. The selected electrode produced slight under matching and enabled the welded joints to be manufactured without cold cracks. The impact energy and its parts responsible for crack initiation and propagation were determined by toughness evaluation. Crack sensitivity, defined as the ratio of the impact energy for V-notched and for pre-cracked specimens, enabled a comparison of the homogeneous microstructure of the parent metal and the weld metal, and of the heterogeneous microstructure of the HAZ, which indicated a better crack toughness behaviour of the HAZ. The results obtained showed that the toughness and crack resistance of the weld metal were significantly lower than those of the parent metal and the HAZ.

Bhole *et al.* [34] studied the effects of alloy additions of nickel (Ni), molybdenum (Mo), and Ni and Mo together on the impact toughness of API HSLA-70 steel by submerged arc welding in the laboratory were investigated and micro-structural factors which affect the impact toughness were discussed. Ni additions resulted in low impact toughness and an increased fracture appearance transition temperature in weld metal. The above influences of Ni should be attributed to the formation of acicular ferrite suppressed by increasing the Ni content. Conversely, the combined presence of Ni and Mo in the weld metal decreased the volume fractions of grain-boundary ferrite and promoted formation of high toughness of AF. The increase of Mo content created an acicular ferrite-predominant weld metal microstructure with impressively improved toughness. Mo addition of 0.881 wt. % in the weld metal gave the optimal impact toughness at −45 ◦C with a microstructure of 77% AF and 20% granular bainite.

Ravi *et al.* [35] studied that HSLA involve usage of low, even and high strength filler materials (electrodes) than the parent material depending on the application of the welded structures and the availability of the filler materials. In the present investigation, the influences of post weld heat treatment (PWHT) on fatigue life prediction of under matched (UM), even matched (EM) and over matched (OM) weld metals were studied. The base material used in this investigation is HSLA-80 steel of weld-able grade. Shielded Metal Arc Welding (SMAW) process was used to fabricate the single ‘V’ butt joints. Centre Cracked

Tension (CCT) specimen was used to evaluate the fatigue crack growth behaviour of the welded joints. Fatigue crack growth experiments were conducted using servo hydraulic controlled fatigue testing machine at constant amplitude loading. A method was proposed to predict the fatigue life of HSLA steel welds using fracture mechanics approach by incorporating influences of mis-match ratio (MMR) and PWHT.

Ravi *et al.* [36] studied the welding of HSLA involves usage of lower, more even and higher strength filler materials (electrodes) than the parent material depending on the application of the welded structures and the availability of the filler material. In this study an attempt was made to study the influences of MMR, PWHT and notch location on fatigue life of HSLA steel welds. A SMAW process was used to fabricate the butt joints. A CCT specimen was used to evaluate the fatigue life of welded joints. Fatigue experiments were conducted using a servo hydraulic controlled fatigue testing machine at constant amplitude loading (R=0). The design of experiment (full factorial design) concept was used to optimise the number of experimental conditions. Analysis of Variance (ANOVA) method was used to identify the significance of main and interaction effects. A mathematical model was developed to predict the fatigue life of HSLA steel welds using regression analysis.

Tuma & Sedmak [37] showed that any interaction between two adjacent weld metal matrix and soft weld metal inclusions produces local brittle zone (LBZ), causing local unstable fracture behaviour. The formation of a low hardness region was attributed to the multipass welding, reheating process and the self-tempering temperature. The presence of partly solid metallic inclusions with a high content of alloying elements and pro-eutectoid ferrite microstructure were found to be additional causes for the local unstable fracture behaviour of the weld metal. Local strength mis-match induced the yielding and strain hardening in the soft weld metal inclusions, contributing significantly to unstable fracture behaviour.

2.3 LITERATURE SUMMARY

After studying the literature it can be concluded that a lot of work was done in the field of submerged arc welding, in one way or another. Some investigators like [13], [14], [15], [16] and [17] had optimized the submerged arc welding process using the optimisation techniques. These optimisation techniques include Taguchi design of experiment, response surface methodology, grey relational analysis, fuzzy logic etc. Some other researchers [18], [19], [20], [21], [22], [23], [24] and [25] investigated the weld parameter *i.e.* current, voltage, electrode stick out, flux, travel speed, polarity etc. in order to improve the weld property. Some other researchers [26], [27], [28] and [29] investigated different flux composition depending upon the requirement of the weld properties and their effect on the weld was studied. Some investigators like [30] and [31] studied the various responses like bead geometry, width of heat affected zone, hardness etc. Some other researchers [32], [33], [34], [35], [36] and [37] studied the effect of various weld parameters and addition of alloying element on mechanical properties and crack resistance of HSLA Steel. The value and nature of the responses depends upon the range and selection of the input parameters *i.e.* current, voltage, electrode stick out, flux, travel speed, polarity etc. Many studies have been done to improve the surface properties of weld by changing the flux composition and input parameters. The metal loaded in the flux gets mixed with the fused weld metal resulting in betterment of weld joints.

2.4 GAPS IN LITERATURE

After defined literature review regarding the submerged arc welding, it was found that very few comprehensive study has been reported for material with thickness greater than 20 mm and also some, not all, factors such as flux variation, current, voltage, travel speed, wire diameter, edge including angle, preheating of flux, electrode stick-out and preheating and post heating of weldments etc have been studied for the purpose of optimization. Also, it was observed that very few comprehensive studies have been reported for material which was welded with multi-pass submerged arc welding process.

2.5 OBJECTIVE OF THE STUDY

The objective of this study is to evaluate the effects of welding parameters such as welding voltage, current, travel speed, different flux compositions, electrode stick-out, edge preparation, pre-heating of work piece and filler wire diameter on tensile strength, impact strength, microhardness and chemical composition of the weld metal of HSLA work piece

and the results are analysed using analysis of variance (ANOVA) and followed by optimization of the process parameters.

None of the study reported in the literature comprehensively cover all the welding parameters for HSLA material greater than 28 mm thickness.

CHAPTER-3
DESIGN OF EXPERIMENTAL STUDY

The literature review showed that any change in the parameter of submerged arc welding affect the properties of welding. So, in this study it was proposed to find out the effect of changing different welding parameters on tensile strength, toughness, microhardness and change in chemical composition. The high strength low alloy plate of dimension 140 x 125 x 28 mm was used as a work material.

The experiments have been conducted on Submerged Arc Welding Machine i.e. Tornado Saw M-800 transformer and FD 10-200T welding tractor (Make: ADOR Frontech Ltd.) available at Central Workshop, Thapar University, Patiala.

FIGURE 3.1- SAW Machine

(**Courtesy:** Central Workshop, Thapar University, Patiala)

SAW machine used for the experiments is shown in the Figure 3.1. The main parts of the machine are control box panel, electrode wire, wire spool and flux hopper. The welding current, welding voltage and welding speed can be regulated, displayed and preset on the panel of the tractor for the convenience of the operator. The function of inch wire feeding and withdrawing makes it convenient for the welder to preset the operating position of the welding wire. Control is provided on the machine for the movement of the tractor on the platform. The movement can be manual or can be automatic. There is also welding head site adjustment function it make the gun move horizontally and vertically.

Main technical parameters of the tractor are given in Table 3.1.

TABLE 3.1 Main technical parameters of welding tractor

Travel speed	20-60 m/hr
Wire feeding rate	0.5 m/min - 2.5 m/min
Wire diameter	2.4 mm -5 mm
Rated current	800 A
Rated voltage	110 V
Tractor weight	54 kg

3.1 SELECTION OF CONTRIBUTING FACTORS THAT EFFECT WELDING

The determination of contributing factors which needs to be investigated depends on the responses of interest. Pilot study was carried out to identify the factors that affect the responses. There are eight factors to be identified through pilot study that affect the weld characteristics in HAZ of work piece. These are -

- Welding current
- Voltage
- Speed of arc travel
- Electrode stick-out
- Edge including angle
- Pre heating of workpiece
- Different flux composition
- Electrode diameter

A industry expert which uses submerged arc welding of metal greater than 28 mm thickness suggested that optimize result will be achieved when welding current varied in between 350-450 Ampere, welding voltage varied in between 28-32 Volt, speed of arc travel varied in between 15-20 m/hr, electrode stick-out varied in between 20-35 mm, edge including angle varied in between 60-90 degree, preheating of workpiece was maximum up to 150 ^{o}C and electrode diameter varied in between 3.2-4 mm.

In the present experimental setup, there are seven factors varied at 3-level and one factor varied at 2-level were chosen through pilot study. Taguchi design has been used for the design of experiments, because it reduces the number of iterations and used to optimize the

known parameters. The values of the input process parameters and there levels for the SAW are as given below in Table 3.2.

TABLE 3.2 Process parameters and there levels that effects welding

Serial No.	Contributing Factors	Units	Level 1	Level 2	Level 3
1	Welding current	A	350	400	450
2	Voltage	V	28	30	32
3	Speed of arc travel	m/hr	15	18	20
4	Electrode stick-out	mm	20	28	35
5	Edge including angle	degree	60	75	90
6	Pre heating of workpiece	^{O}C	No Preheat	100	150
7	Different flux composition		1	2	3
8	Electrode diameter	mm	3.2	4	---

3.2 FLUX

The three different types of flux was used in this study i.e. AUTOMELT B31, GEE FLUX 544 and GEE FLUX 541 (Make: ADOR Welding Ltd. and GEE Ltd.) which was compatible with EH14 SAW filler wire as shown in Figure 3.2. In which one flux was of neutral in nature and two fluxes were of basic in nature. Table 3.3 shows the basic detail and percent composition of different element present in the fluxes that used in this experiment.

TABLE 3.3 Basic details and percent composition of fluxes

<table>
<tr><th rowspan="2">Sr. No.</th><th rowspan="2">Flux Name</th><th rowspan="2">Flux Type</th><th colspan="6">Flux Composition</th></tr>
<tr><th>SiO_2+TiO_2</th><th>CaO+MgO</th><th>Al_2O_3+MnO</th><th>CaF_2</th><th></th><th></th></tr>
<tr><td>1</td><td>AUTOMELT B31</td><td>Neutral</td><td>15 %</td><td>20 %</td><td>30 %</td><td>35 %</td><td></td><td></td></tr>
<tr><td>2</td><td>GEE FLUX 544</td><td>Basic</td><td>15 %</td><td>35 %</td><td>20 %</td><td>30 %</td><td></td><td></td></tr>
<tr><td rowspan="2">3</td><td rowspan="2">GEE FLUX 541</td><td rowspan="2">Basic</td><td>C</td><td>Mn</td><td>Si</td><td>S</td><td>P</td><td>Cu</td></tr>
<tr><td>0.077</td><td>1.64</td><td>0.33</td><td>0.015</td><td>0.021</td><td>0.12</td></tr>
</table>

FIGURE 3.2- Flux used

3.3 ORTHOGONAL ARRAY

To select an appropriate orthogonal array for experiments, the total degrees of freedom must be computed. The degrees of freedom are defined as the number of comparisons between process parameters that must be made to determine which level is better and, specifically, how much better it is. For example, a two-level process parameter counts for one degree of freedom. The degrees of freedom associated with interaction between two process parameters are given by the product of the degrees of freedom for the two process parameters. In the present study, once the degrees of freedom are known, the next step is to select an appropriate orthogonal array to fit the specific task. The degrees of freedom for the orthogonal array should be greater than, or at least equal to, those for the process parameters. In this study, Taguchi L18 orthogonal array with eight columns and eighteen rows was used. Each welding parameter was assigned to a column and eighteen welding parameter combinations were tested. Therefore, only eighteen experiments were required to study the entire welding parameter space using the L18 orthogonal array. The experimental layout for the welding parameters using the L18 orthogonal array is shown in Table 3.5.

3.3.1 Selection of Orthogonal Array and Factor Assignment

In this experimental study, seven factors were varied to three levels each and one factor at two levels. The degree of freedom (DOF) to a three level parameter is 2 and for two level parameter is 1 (because DOF=number of levels-1), hence total DOF for the experiment is 15. So the Orthogonal Array (OA) which could be used was L18. Degree of freedom allocated to various factors is given in Table 3.4.

TABLE 3.4 DOF allocated to various factor combinations

Serial No.	Parameter	Units	DOF
1	Welding current	Ampere	2
2	Voltage	Volt	2
3	Speed of arc travel	m/hr	2
4	Electrode stick-out	mm	2
5	Edge including angle	degree	2
6	Pre heating of workpiece	^{O}C	2
7	Different flux composition		2
8	Electrode diameter	mm	1
	Total		**15**

3.4 EXPERIMENTAL SET UP

As stated earlier Taguchi L18 array has been selected for the experimentation. The experimental design was completed using the Taguchi's fractional factorial experiments (FFEs). Welding current, Voltage, Speed of arc travel, Electrode stick-out, Edge including angle, Pre heating of workpiece, Different flux composition and Electrode diameter have been chosen as the factors of interest. L18 array with actual factors level is shown in Table 3.5.

TABLE 3.5 Orthogonal array for experimentation

Exp. No.	Electrode Diameter 'Ø' (mm)	Current 'C' (Amp)	Voltage 'V' (Volt)	Electrode Stick-Out 'D' (mm)	Travel Speed 'S' (m/hr)	Preheat Temperature 'T' (^oC)	Flux 'F'	Edge Including Angle 'α' (degree)
1	3.2	350	28	20	15	No Preheat	1	60
2	3.2	350	30	28	18	100	2	75
3	3.2	350	32	35	20	150	3	90
4	3.2	400	28	20	18	100	3	90
5	3.2	400	30	28	20	150	1	60
6	3.2	400	32	35	15	No Preheat	2	75
7	3.2	450	28	28	15	150	2	90
8	3.2	450	30	35	18	No Preheat	3	60
9	3.2	450	32	20	20	100	1	75
10	4	350	28	35	20	100	2	60
11	4	350	30	20	15	150	3	75
12	4	350	32	28	18	No Preheat	1	90
13	4	400	28	28	20	No Preheat	3	75
14	4	400	30	35	15	100	1	90
15	4	400	32	20	18	150	2	60
16	4	450	28	35	18	150	1	75
17	4	450	30	20	20	No Preheat	2	90
18	4	450	32	28	15	100	3	60

3.5 CHEMICAL COMPOSITION OF BASE METAL

Table 3.6 shows the composition of base metal was found by using atomic absorption spectrometer.

FIGURE 3.3- Sample cut out for spectroscopy

TABLE 3.6 Chemical composition of base metal

C	Si	Mn	P	S	Ni	Cu	Cr
0.13	0.25	0.39	0.003	0.01	1.76	0.5	0.41

3.6 FILLER WIRE

The filler wire used in this experiment was EH14 of diameter 3.2 mm and 4 mm. According to American welding standards its AWS code is F7A2-EH14.

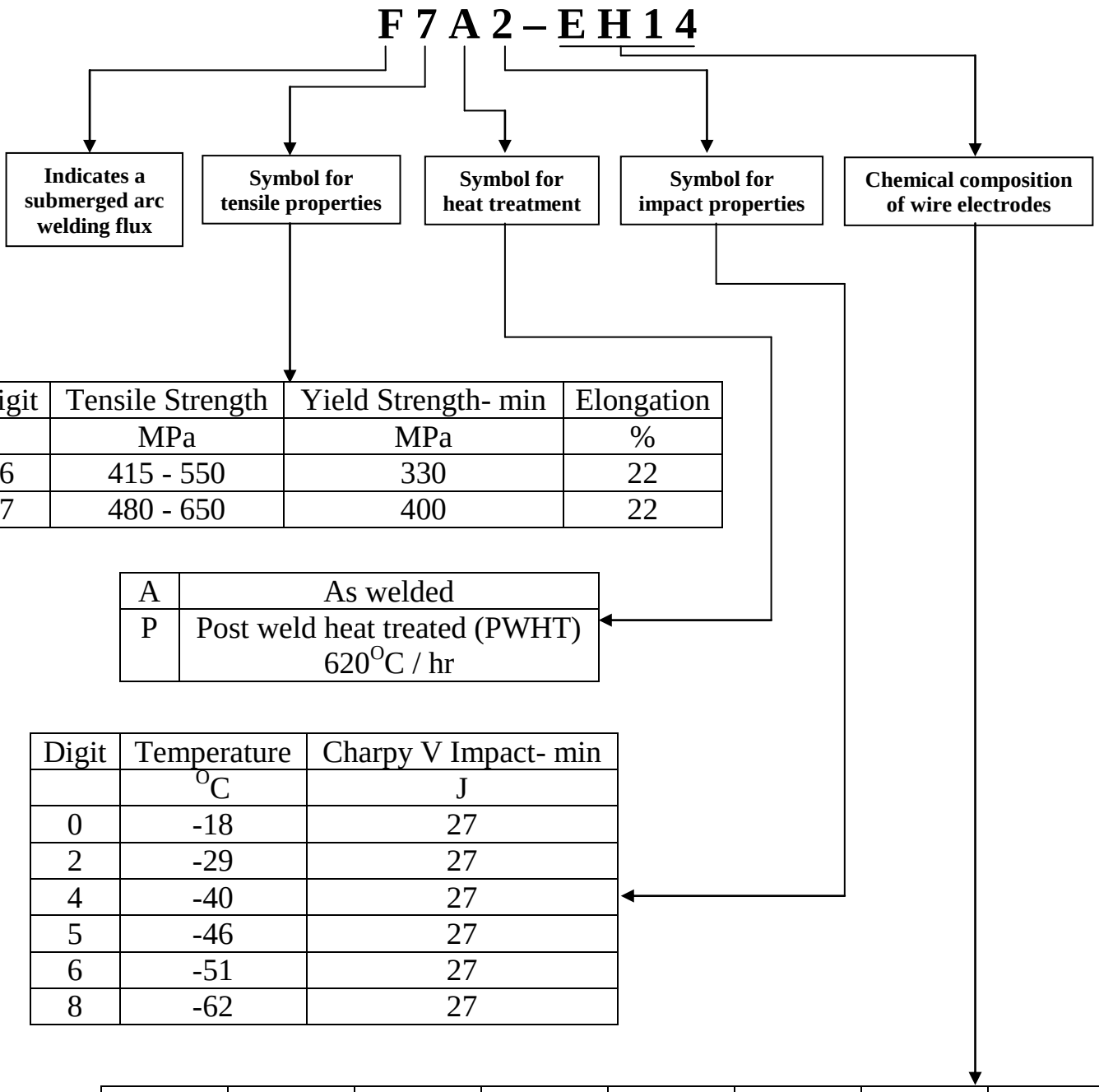

Digit	Tensile Strength	Yield Strength- min	Elongation
	MPa	MPa	%
6	415 - 550	330	22
7	480 - 650	400	22

A	As welded
P	Post weld heat treated (PWHT) 620^{O}C / hr

Digit	Temperature	Charpy V Impact- min
	^{O}C	J
0	-18	27
2	-29	27
4	-40	27
5	-46	27
6	-51	27
8	-62	27

C	Si	Mn	P	S	Ni	Cu	Cr
0.12	0.08	1.88	0.019	0.016	0.03	0.14	0.08

3.7 CUTTING OF STEEL PLATES

The steel plates available for the study were of size 1000 x 500 x 28 mm. These were firstly cut in to strip of size 1000 x 125 x 28 mm through oxy-acetylene gas cutting as shown in Figure 3.4. Then these steel strips were cut to the required size of 140 x 125 x 28 mm with the help of power hacksaw (Make: Jaura, India) as shown in Figure 3.5.

FIGURE 3.4-Cutting of steel plates through oxy-acetylene gas cutting

FIGURE 3.5-Cutting of steel strip through power hacksaw

(**Courtesy:** Central Workshop, Thapar University, Patiala)

3.8 METHOD OF PREPARATION OF STEEL PLATE SPECIMEN

In this study L18 was chosen as the preferred array, 72 plates were cut to size of dimension 140 x 125 x 28 mm for experiment because four plates were required for welding in each trial. Edge preparation was completed on each of the 72 plates as per the requirement of 18 trial condition given by taguchi orthogonal array. The edge preparation of 60^{o}, 75^{o} and 90^{o} was made on 125 mm side as shown in Figure 3.6. Edge preparation was done on shaper as shown in Figure 3.7. Groove between two plates is shown in Figure 3.8. After edge preparation, the plates were tacked through manual arc welding to avoid misalignment as shown in Figure 3.9.

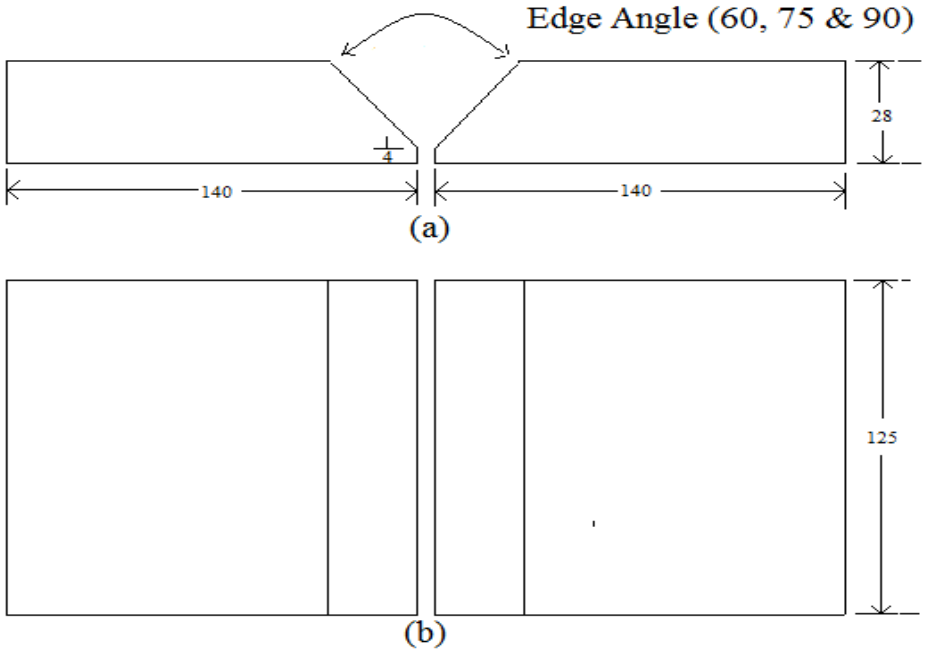

FIGURE 3.6- Groove geometry (a) front view and (b) top view (all dimensions are in mm)

FIGURE 3.7- Making chamfer on corner of plate

(a)

(b)

FIGURE 3.8-Groove between two plates (a) front view (b) top view

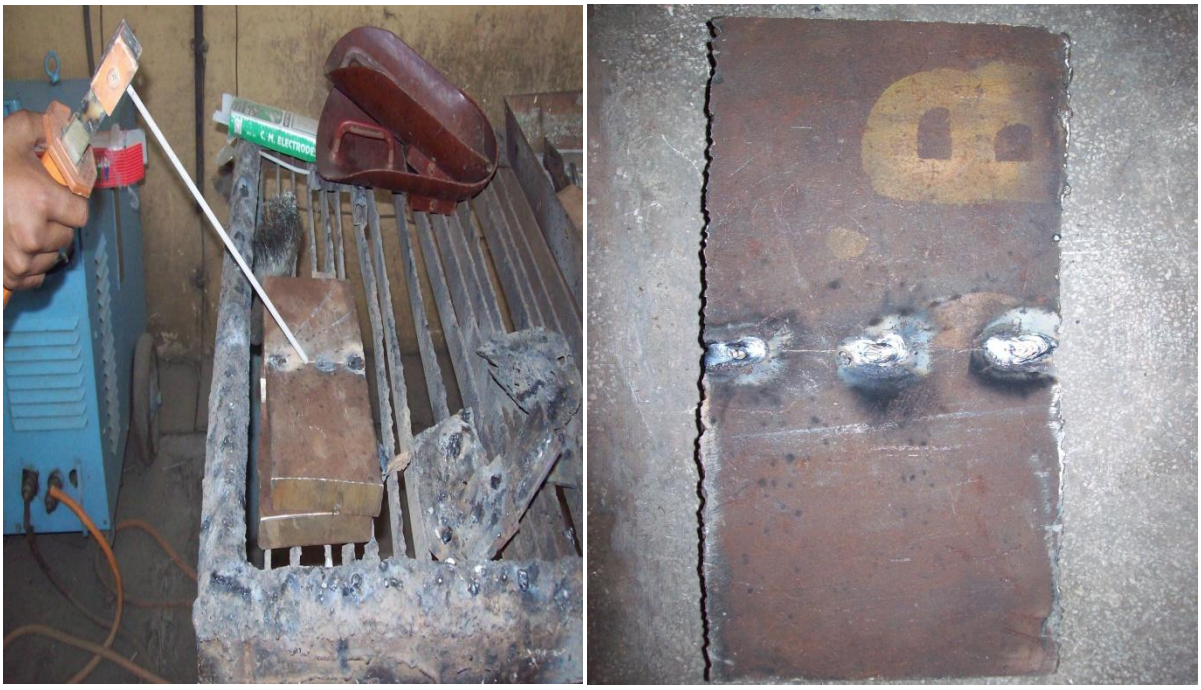

FIGURE 3.9- Tacking on back side of plates

After tacking, root layer was deposited with the help of SMAW (Shielded Metal Arc Welding) as shown in Figure 3.11. The electrode used for SMAW was E7018. Table 3.7 and 3.8 shows the composition of electrode and value of input process parameter for SMAW. Maximum penetration height of root layer was 7 mm. Figure 3.10 shows the schematic diagram of weld bead.

TABLE 3.7 Chemical composition of SMAW Electrode

C	Si	Mn	P	S	Ni	Mo	Cr
0.12	0.75	1.6	0.04	0.03	0.3	0.3	0.2

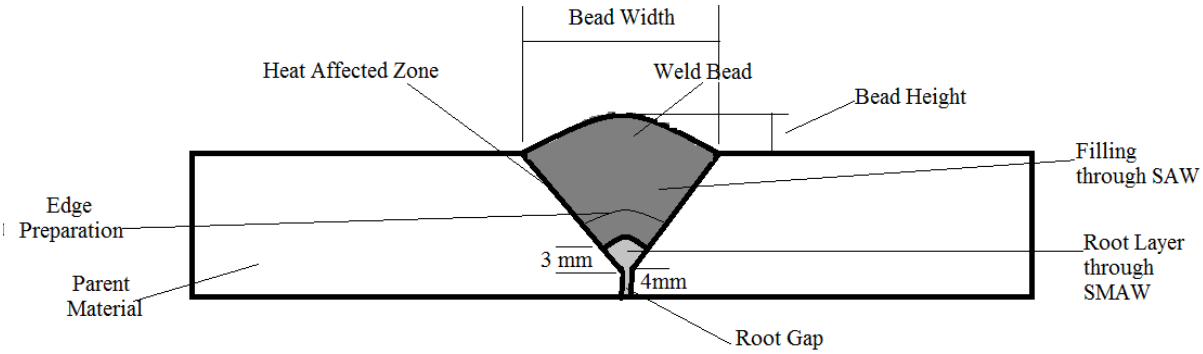

FIGURE 3.10-Schematic diagram of weld bead

TABLE 3.8 Value for input process parameter for SMAW

Serial No.	Parameter	Units	Value
1	Current	Ampere	120
2	Travel Speed	m/hr.	9
3	Electrode Diameter	mm	3.2

FIGURE 3.11-Root layer between grooves of plates through SMAW

After depositing of root layer through SMAW, the plates were welded by SAW. Plates were placed under the electrode for welding and clamped with base plate using ‘C’ clampers. The welding was completed on each part as shown in Figures 3.12, 3.13 and 3.14.

FIGURE 3.12- Submerged arc welding of plates

FIGURE 3.13- Joint of plates after welding

FIGURE 3.14- Welding on plates

After welding the parts were cut to size as per the requirement for tensile test, toughness, microhardness and chemical composition.

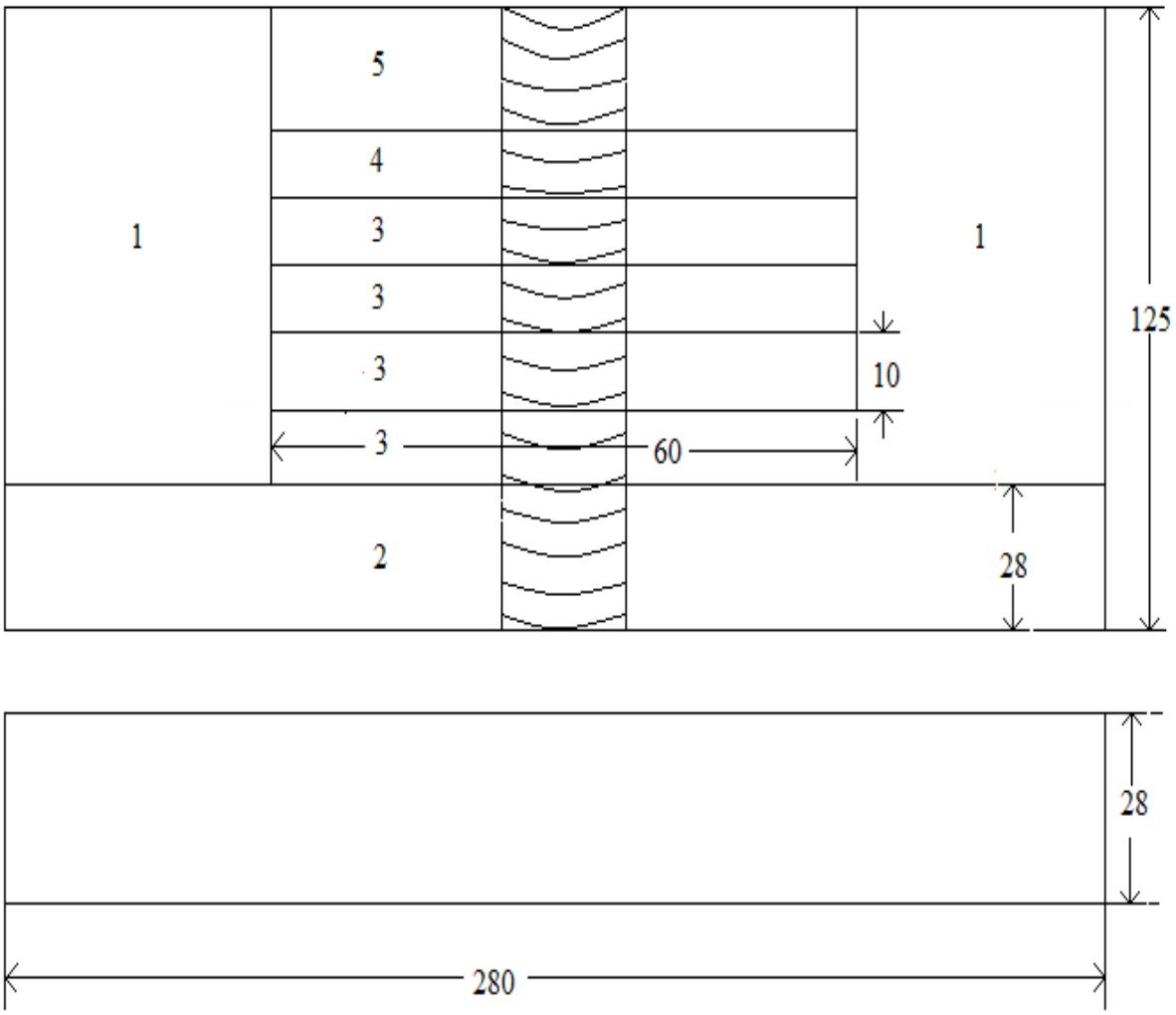

FIGURE 3.15- Cutting of plates after welding

Orientation of cutting of specimens after welding is shown in Figure 3.15, (1) represents waste material, (2) represents tensile test specimen, (3) represents toughness test specimen, (4) represents microhardness test specimen, (5) represents composition test specimen.

Figure 3.16 shows the cutting of plates with the help of surface grinding machine (Make: Himlitz Products, India and motor speed-2800 rpm) and the cutter used for cutting of plates was of dimension 200 X 1.5 X 31.75 mm. Figure 3.17 shows the specimen after cutting through surface grinding machine. Figure 3.18 and 3.19 shows the cutting of weld region with the help of power hacksaw and weld region specimen.

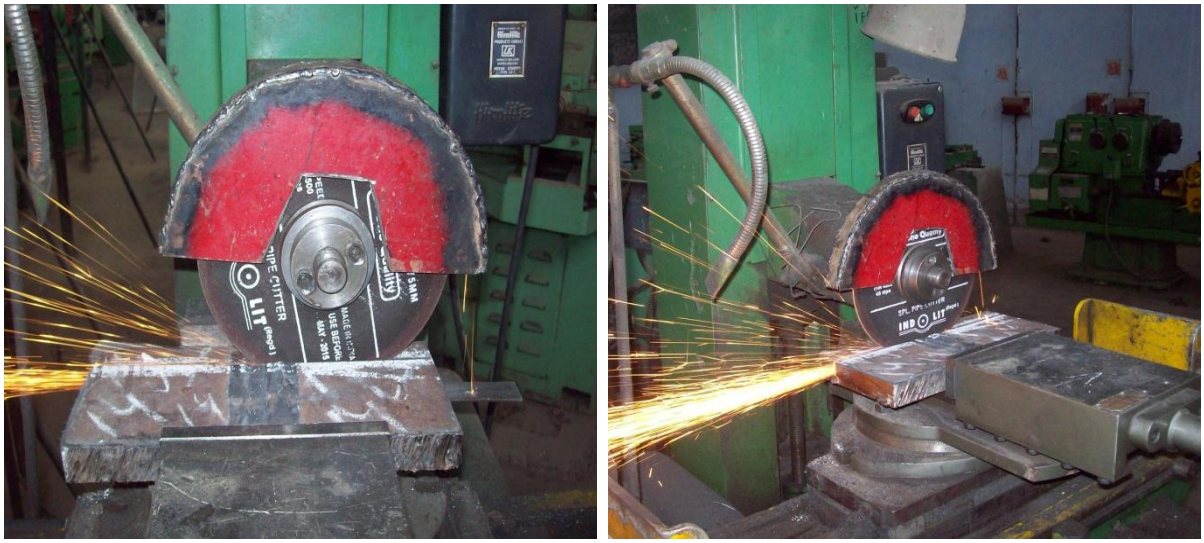

FIGURE 3.16- Cutting of plates according to required size on surface grinding machine

(**Courtesy:** Central Workshop, Thapar University, Patiala)

FIGURE 3.17- Specimen after cutting

FIGURE 3.18- Cutting of weld region

FIGURE 3.19- Weld region

3.9 TESTING OF WELD SPECIMEN

3.9.1 Tensile Test

Ratio of the maximum load a material can support without fracture when being stretched to the original area of a cross section of the material. When stresses less than the tensile strength are removed, a material completely or partially returns to its original size and shape. As the stress approaches that of the tensile strength, a material that has begun to flow forms a narrow, constricted region that is easily fractured. Tensile strengths are measured in units of force per unit area.

Welded specimen made from base metal and fined the tensile strength and stress-strain curves. The testing would be carried on Computerised Universal Testing Machine (Make: Blue Star Ltd.- New Delhi, India, Load capacity-1000 Ton) as shown in Figure 3.20. Figure 3.21 and 3.22 shows the schematic of tensile test specimen and the specimens before machining and the machining was done on lathe (Make: Gujarat Lathe Manufacturing Co. Pvt. Ltd. Rajkot, India) and the tensile test specimen are shown in Figure 3.23.

FIGURE 3.20- Computerised universal testing machine

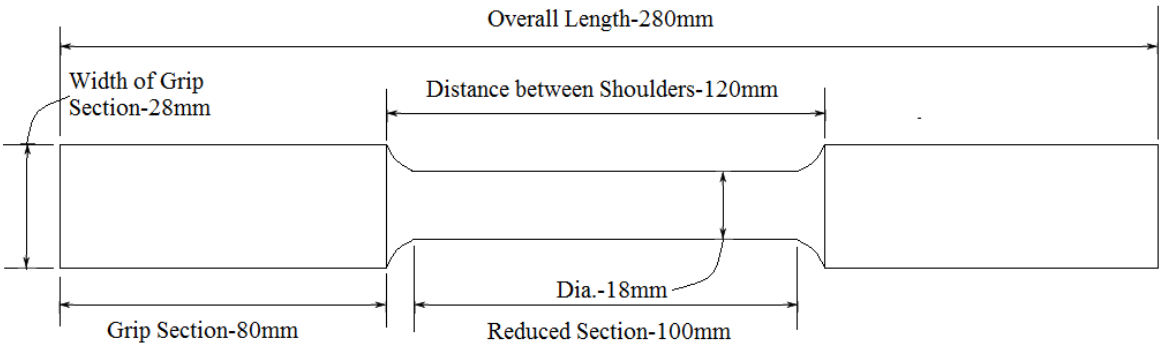

FIGURE 3.21- Schematic diagram for tensile test specimen

(a) **(b)**

FIGURE 3.22- (a) Specimen before machining, (b) Preparation of specimen on lathe (**Courtesy:** Central Workshop, Thapar University, Patiala)

FIGURE 3.23- Specimen for tensile testing

3.9.2 Toughness Test

The ability of a metal to rapidly distribute within itself due to both the stress and strain caused by a suddenly applied load or the ability of a material to withstand shock loading. It is the exact opposite of "brittleness" which carries the implication of sudden failure. A brittle material has little resistance to failure once the elastic limit has been reached.

Figure 3.24 shows the weld region specimen which is of dimension 60 X 90 X 28 mm and the removal of material from both sides of specimen take place on vertical milling machine (Make: HMT Limited, Pinjore India) and after machining the specimen left was of dimension 60 X 90 X 10 mm.

Figure 3.25 shows the specimen with V groove of 45^{o} and 2 mm deep cut on shaping machine (Make: Cooper Engineering Ltd. Satara, India and maximum stroke length is 24 inches) and then cutting of specimens for testing purpose which was to be cut on surface grinding machine.

According to standard as shown in Figure 3.26, 72 specimen were made from each plate of size 10x10x55 mm for charpy test as shown in Figure 3.27, and test all the 72 specimen on charpy toughness test machine as shown Figure 3.28 (Make: Alfred J.Amsler & Co. Schaffhouse, Switzerland) at different temperatures by applying liquid nitrogen i.e. room temperature (37 ^{o}C), -20, -40, -50 ^{o}C as shown in Figure 3.29.

(a) **(b)** **(c)**

FIGURE 3.24- (a) Weld region with 28 mm thickness, (b) Machining on vertical milling machine (**Courtesy:** Central Workshop, Thapar University, Patiala), (c) Weld region with 10 mm thickness

(a) **(b)** **(c)**

FIGURE 3.25- (a) Making of V groove on shaping machine (**Courtesy:** Central Workshop, Thapar University, Patiala), (b) Specimen after V groove, (c) Cutting of specimen for testing on surface grinding machine

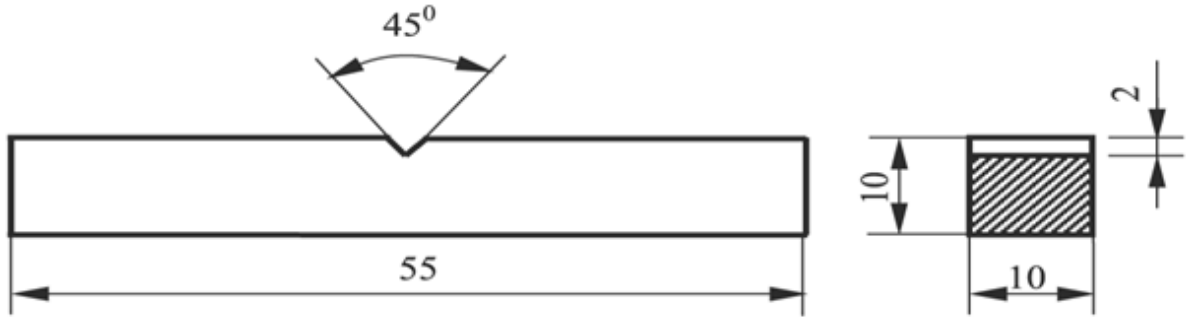

FIGURE 3.26- Standard charpy test specicmen

FIGURE 3.27- Charpy test specimen

FIGURE 3.28- Charpy toughness test machine

(**Courtesy:** Strength of Material Lab, Thapar University, Patiala)

FIGURE 3.29- Apparatus for liquid nitrogen

3.9.3 Microhardness Test

The samples measuring for microhardness were firstly ground on the belt grinder, then rubbed with emery paper size no. 400, 600, 800, 1000 and then polished on polishing wheel (Make: Scientific, India) as shown in Figure 3.30 (a,b,c). Microhardness of the weld region was measured by using the computer interfaced microhardness tester (Make: Metatech Industries, Pune, India) as shown in Figure 3.31. The measurement was dependent on the size of indentation on the samples. The diagonals of the indents formed by a pyramid- shaped

diamond indenter was measured with the help of Quantimet software at 40X magnification, which gave a direct hardness Vickers number (HVN) for microhardness. The hardness values obtained were useful indicators of material properties. The load applied on the indenter was 1 kg and the dwell time was 20 s. Figure 3.32 shows the specimen which was used for microhardness test.

(a) **(b)** **(c)**

FIGURE 3.30- (a) Belt grinder (**Courtesy:** Machine Tool Lab, Thapar University, Patiala), (b) Apparatus with emery paper of grit size 400, 600, 800 and 1000, (c) Polisher (**Courtesy:** Material Science Lab, Thapar University, Patiala)

FIGURE 3.31- Microhardness test machine
(**Courtesy:** Central Workshop, Thapar University, Patiala)

FIGURE 3.32- Microhardness test specimen

3.9.4 Chemical Composition of Weld Metal

The composition of base metal and welded metal was found by using atomic absorption spectrometer (Figure 3.33) in which Argon gas pressure was maintained at 60 litre/min and the software used for finding chemical composition was Worldwide Analytical System (WAS). Figure 3.34 shows the specimen for composition test.

FIGURE 3.33- Atomic absorption spectrometer

(**Courtesy:** Central Workshop, Thapar University, Patiala)

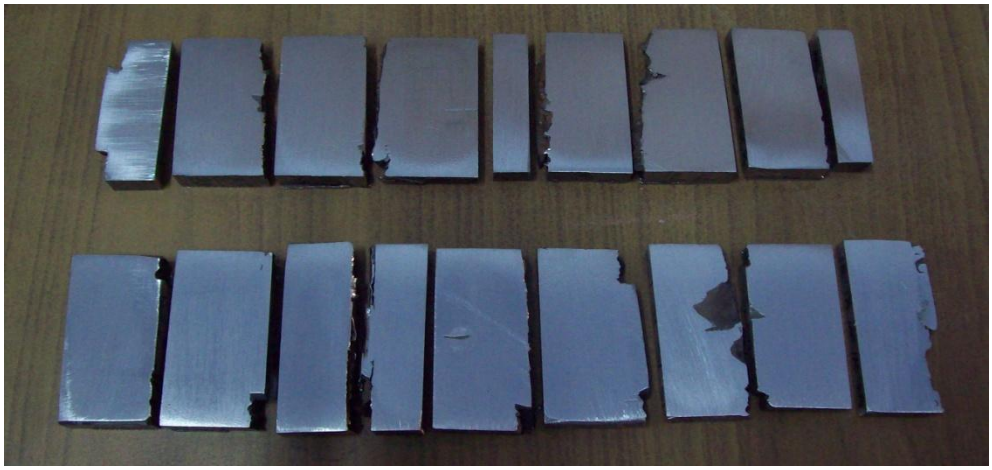

FIGURE 3.34- Specimen for composition test

3.10 ANALYSIS OF RESULTS

Analysis of the results was to be done by using ANOVA for Mean.

3.10.1 Analysis of Variance

ANOVA is a statistical technique which can infer some important conclusions based on analysis of the experimental data. The method is very useful for revealing the level of significance of influence of factor(s) or interaction of factors on a particular response. It separates the total variability of the response (sum of squared deviations about the grand mean) into contributions rendered by each of the parameter/ factor and the error. Thus

$\mathbf{SS_T = SS_F + SS_E}$

Where, $SS_T = \sum_{J=1}^{P} \left(\gamma_j - \gamma_m\right)^2$

Where, SS_T = Total sum of squared deviations about the mean.

γ_j = Mean response for j^{th} experiment.

γ_m = Grand mean of the response.

SS_F = Sum of squared deviations due to each factor.

SS_E = Sum of squared deviations due to error.

In the ANOVA table mean square deviation is defined as:

MS = Mean Square

$$\mathbf{MS = \frac{SS\ (Sum\ of\ squared\ division)}{DOF\ (Degree\ of\ Freedom)}}$$

F-value of Fisher's F ratio (Variance ratio) is defined as:

$$\mathbf{F = \frac{MS\ for\ a\ term}{MS\ for\ the\ error\ term}}$$

Depending on F value, P-value (probability of significance) is then calculated. If P-value for a term appears less than 0.05 (For 95% confidence level) then it can be concluded that the effect of the factors / interaction of factors is significant on the selected response. Significance of all the dependent variables has been completed using statistical software MINITAB 15. These dependent variables studied in this study are (1) Tensile strength (2) Toughness at room temperature (3) Toughness at -40 ^{o}C (4) Microhardness.

In the ANOVA table, the degrees of freedom are used to calculate the mean square (MS). In general, the degrees of freedom measure how much "independent" information is available to calculate each sum of squares (SS).

Total DOF = DOF for all factors + DOF for all interactions + DOF for error

Where n is the total number of observations and,

DOF for factor = $k-1$

Where k is the number of the factor levels.

DOF for Interaction = $(k_1-1) \times (k_2-1)$

Where k_1 is the number of levels of factor one, and k_2 is the number of levels of factor two. The same rule applies to interactions of more than two factors. In the present study, the interaction of factors has not been studied. The sequential sum of squares for each term in the model (factor or interaction) measures the amount of variation in the response that is explained by adding each term to the model sequentially in the order listed under. Thus, the sequential sums of squares for terms are specific to the order of the terms specified in the linear model. The adjusted sum of squares for a term in the model (factor or interaction) measures the amount of additional variation in the response that is explained by the term, given that all the other terms are already in the model. Thus, the values for the adjusted sums of squares do not depend on the order of the terms listed under source. The adjusted mean square for a term is simply the adjusted sum of squares (Adj. SS) divided by the degrees of freedom.

For this experimental work, the following response characteristics have been studied-

1. Response Name : Tensile strength
Response type : Higher-the-better
Units : N/mm^2

2. Response Name : Toughness at room temperature (37 ^{o}C)
Response type : Higher-the-better
Units : Joule

3. Response Name	:	Toughness at -40 ^{o}C
Response type	:	Higher-the-better
Units	:	Joule
4. Response Name	:	Microhardness at weld region
Response type	:	Higher-the-better
Units	:	HVN

CHAPTER-4

RESULTS AND ANALYSIS OF TENSILE TEST

4.1 TENSILE TEST

Ratio of the maximum load a material can support without fracture when being stretched to the original area of a cross section of the material. Specimen after tensile test is shown in Figure 4.1 and 4.2 respectively.

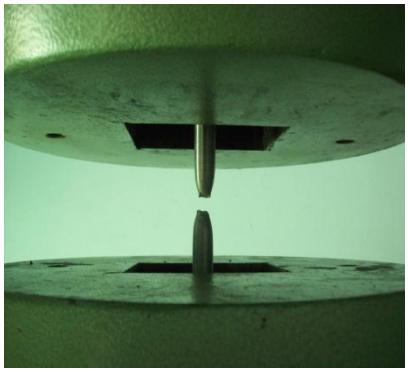

FIGURE 4.1- Specimen after breaking

FIGURE 4.2- Specimen after tensile test

The tensile test details for base metal are shown in Table 4.1 and corresponding tensile test plot is shown in Figure 4.3 for comparison.

TABLE 4.1 Maximum tensile load & strength value of base metal

	Maximum Tensile Load (kN)	**Maximum Tensile Strength (N/mm^2)**
Base Metal	169.7	666.611

Graph- Load vs Displacement

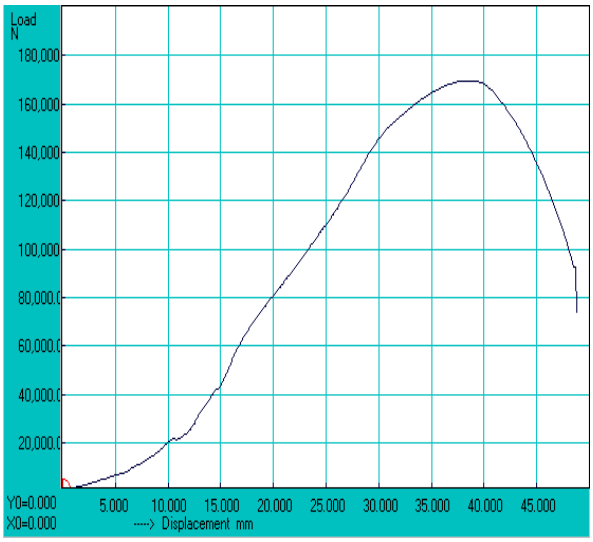

Graph- Stress vs Strain

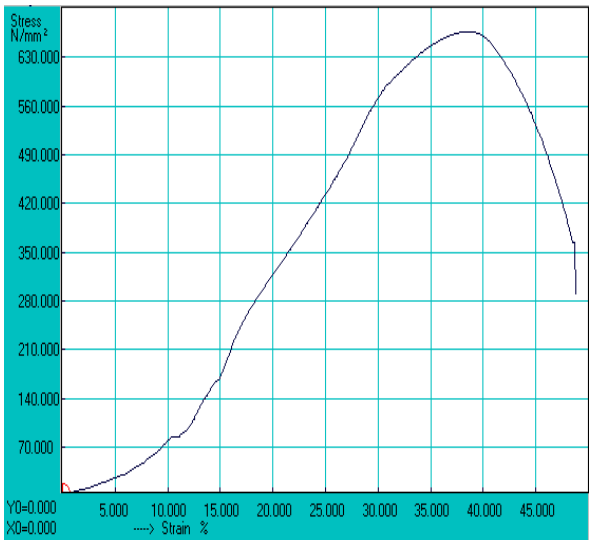

FIGURE 4.3- Load vs displacement and stress vs strain curve base metal

For all the 18 sets of experiment, the tensile test summery is shown in Table 4.2 and corresponding load vs displacement and stress vs strain plots are shown below sequentially in Figure 4.4 (a-r).

TABLE 4.2 Maximum tensile load & strength readings

Experiment No.	Contributing Factors	Maximum Tensile Load (kN)	Maximum Tensile Strength (N/mm^2)
1	Ø1, C1, V1, D1, S1, T1, F1, α1	133.10	522.840
2	Ø1, C1, V2, D2, S2, T2, F2, α2	141.05	554.069
3	Ø1, C1, V3, D3, S3, T3, F3, α3	133.90	525.982
4	Ø1, C2, V1, D1, S2, T2, F3, α3	112.95	443.687
5	Ø1, C2, V2, D2, S3, T3, F1, α1	134.35	527.750
6	Ø1, C2, V3, D3, S1, T1, F2, α2	135.15	530.892
7	Ø1, C3, V1, D2, S1, T3, F2, α3	144.50	567.621
8	Ø1, C3, V2, D3, S2, T1, F3, α1	122.75	482.183
9	Ø1, C3, V3, D1, S3, T2, F1, α2	150.20	590.011
10	Ø2, C1, V1, D3, S3, T2, F2, α1	148.50	583.333
11	Ø2, C1, V2, D1, S1, T3, F3, α2	153.00	601.010
12	Ø2, C1, V3, D2, S2, T1, F1, α3	154.45	606.706
13	Ø2, C2, V1, D2, S3, T1, F3, α2	143.00	561.728
14	Ø2, C2, V2, D3, S1, T2, F1, α3	149.70	588.047
15	Ø2, C2, V3, D1, S2, T3, F2, α1	138.50	544.052
16	Ø2, C3, V1, D3, S2, T3, F1, α2	151.23	594.040
17	Ø2, C3, V2, D1, S3, T1, F2, α3	145.20	570.370
18	Ø2, C3, V3, D2, S1, T2, F3, α1	158.75	623.597

Where,

- Ø1 and Ø2 represents Electrode Diameter vary at two different levels namely (1) 3.2 mm and (2) 4 mm.
- C1, C2 and C3 represents Current vary at three different levels namely (1) 350 Amp, (2) 400 Amp and (3) 450 Amp.
- V1, V2 and V3 represents Voltage vary at three different levels namely (1) 28 volt, (2) 30 volt and (3) 32 volt.
- D1, D2 and D3 represents Electrode Stick-Out vary at three different levels namely (1) 20 mm, (2) 28 mm and (3) 35 mm.
- S1, S2 and S3 represents Travel Speed vary at three different levels namely (1) 15 m/hr, (2) 18 m/hr and (3) 20 m/hr.
- T1, T2 and T3 represents Preheat Temperature vary at three different levels namely (1) No-Preheat, (2) 100 ^{o}C and (3) 150 ^{o}C.
- F1, F2 and F3 represents Flux vary at three different levels namely (1) neutral, (2) basic and (3) basic.
- α1, α2, and α3 represents Edge Including Angle vary at three different levels namely (1) 60^{o}, (2) 75^{o} and (3) 90^{o}.

Graph- Load vs Displacement

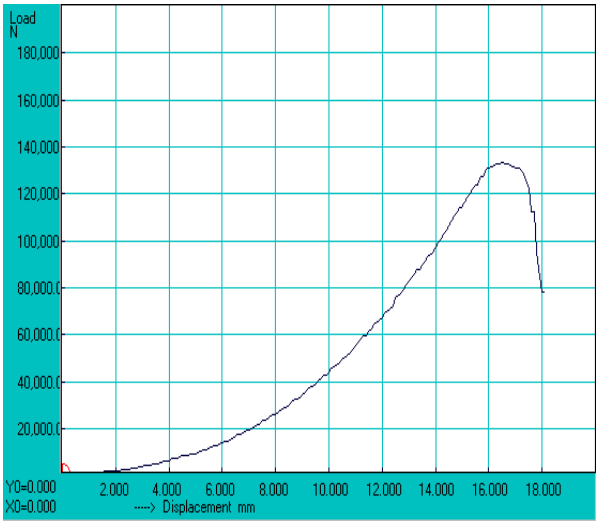

Graph- Stress vs Strain

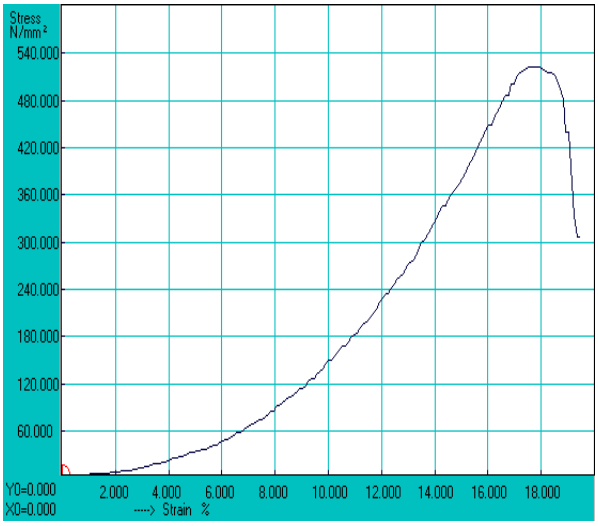

(a) for Trial 01

Graph- Load vs Displacement

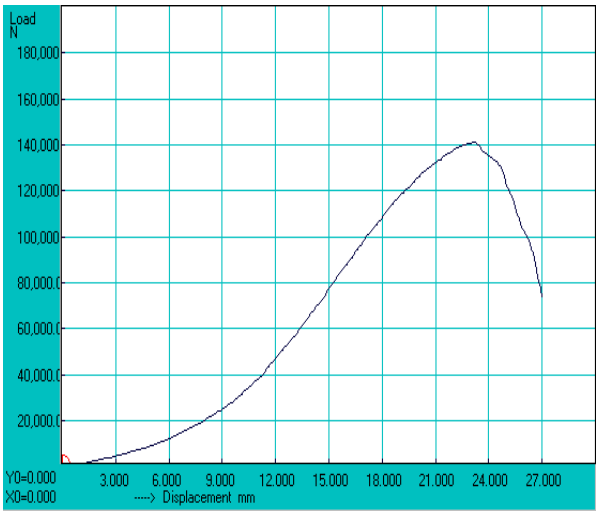

Graph- Stress vs Strain

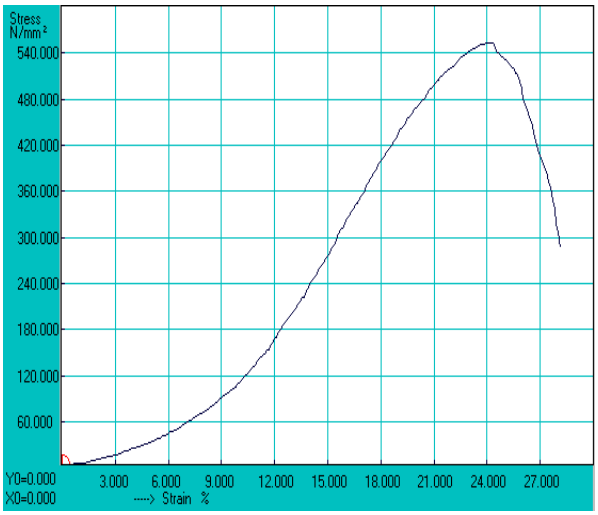

(b) for Trial 02

Graph- Load vs Displacement

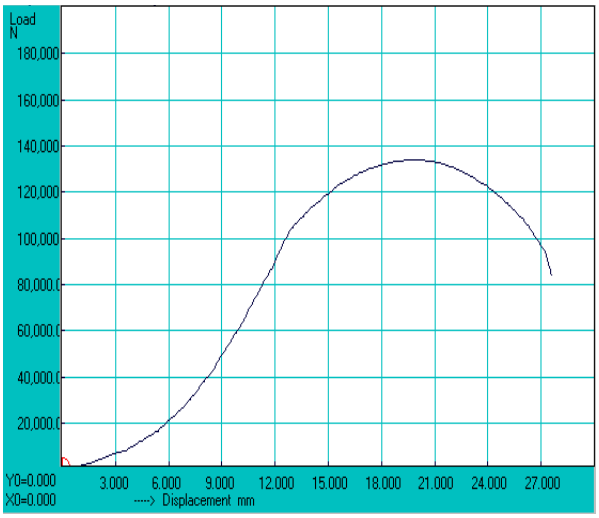

Graph- Stress vs Strain

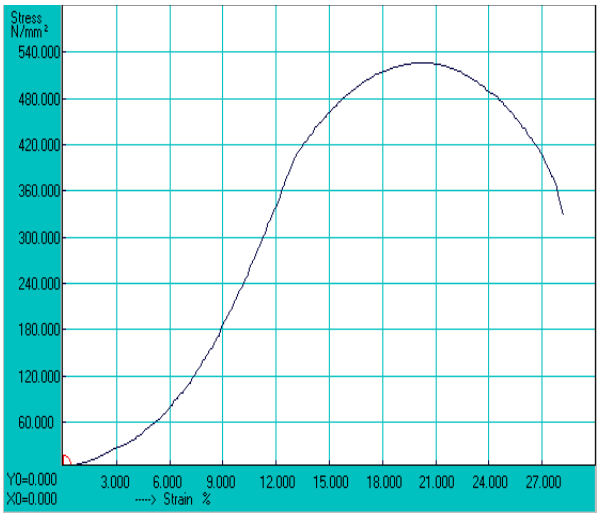

(c) for Trial 03

Graph- Load vs Displacement

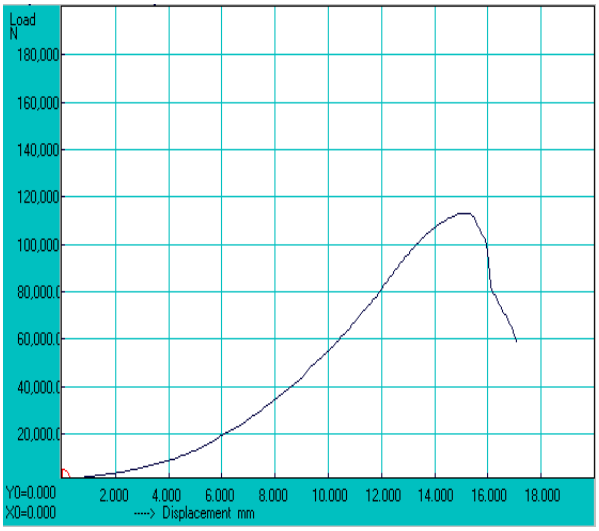

Graph- Stress vs Strain

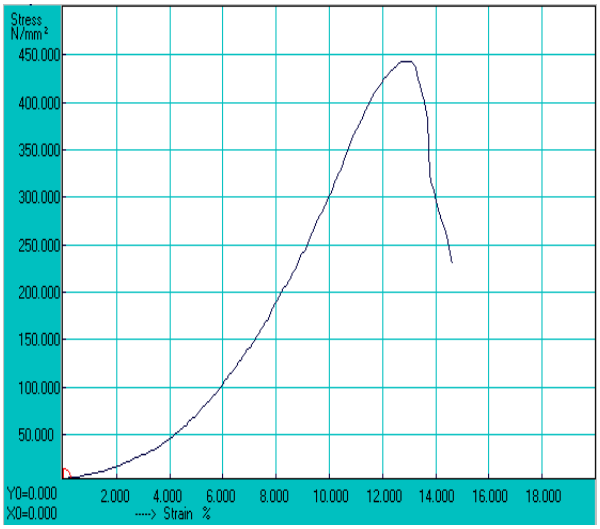

(d) for Trial 04

Graph- Load vs Displacement

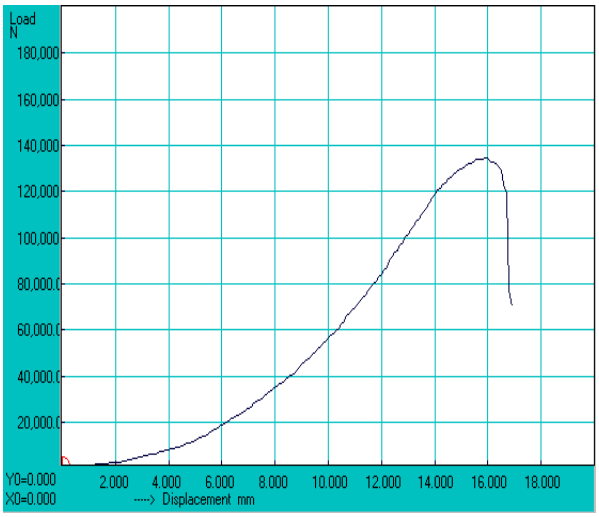

Graph- Stress vs Strain

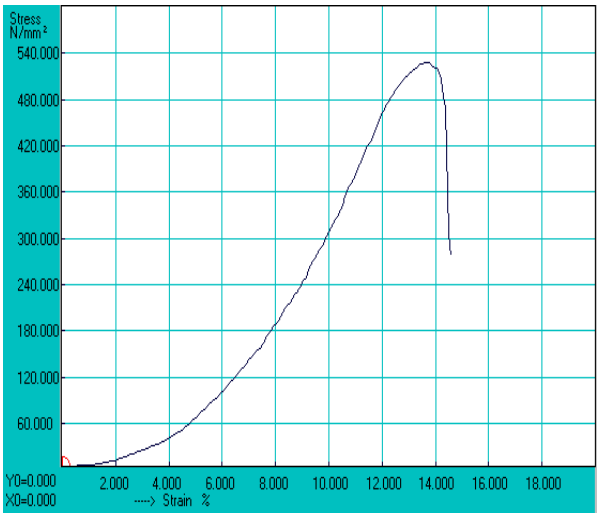

(e) for Trial 05

Graph- Load vs Displacement

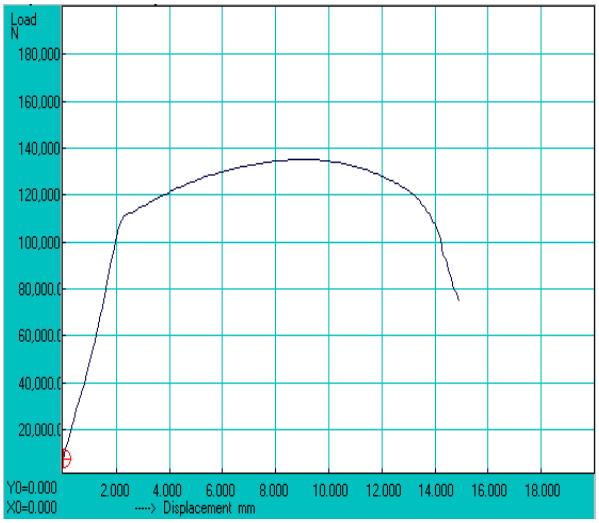

Graph- Stress vs Strain

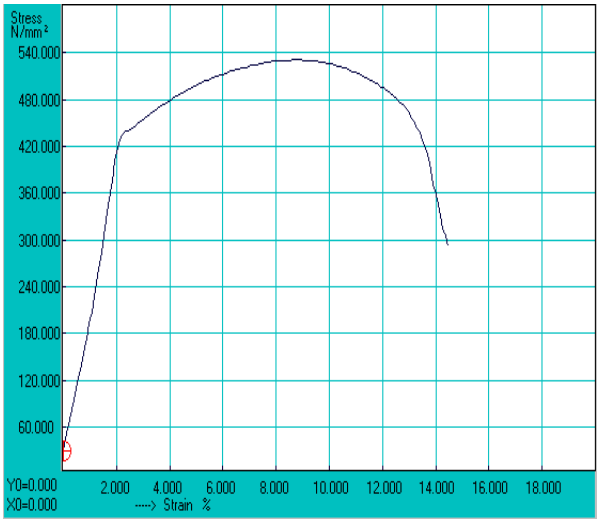

(f) for Trial 06

Graph- Load vs Displacement

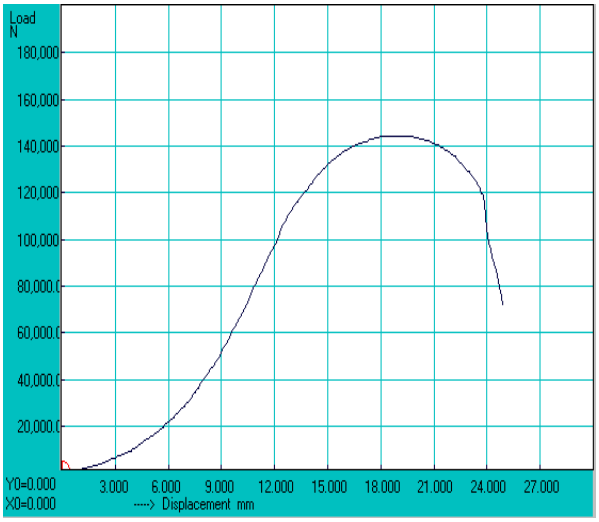

Graph- Stress vs Strain

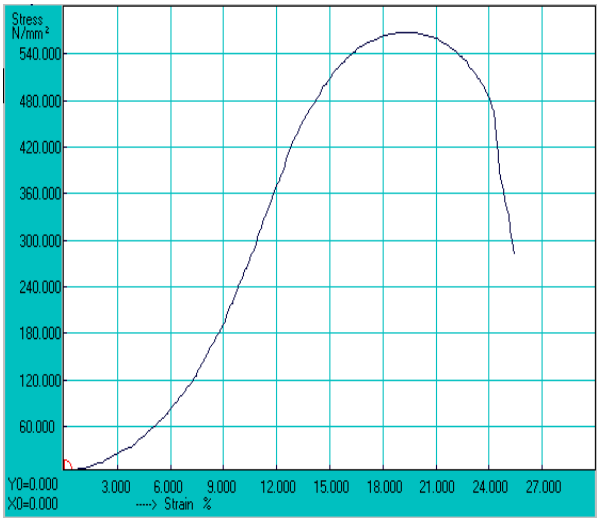

(g) for Trial 07

Graph- Load vs Displacement

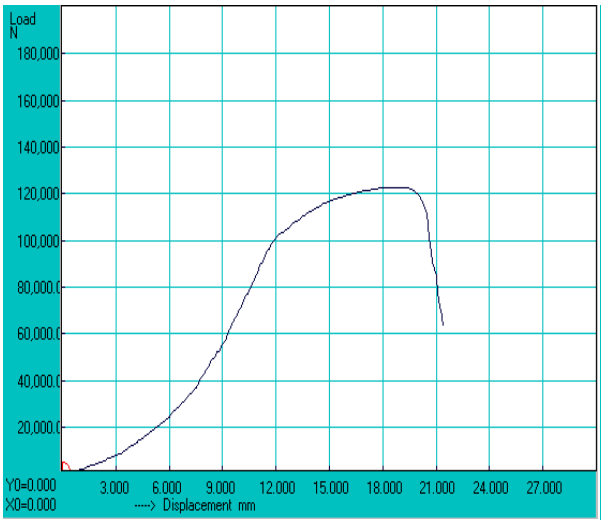

Graph- Stress vs Strain

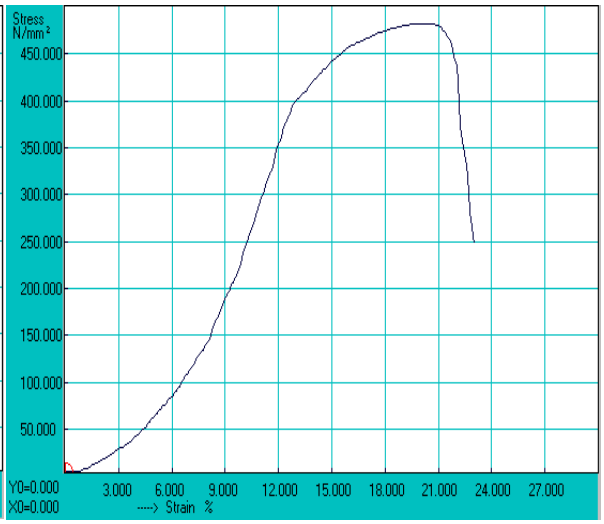

(h) for Trial 08

Graph- Load vs Displacement

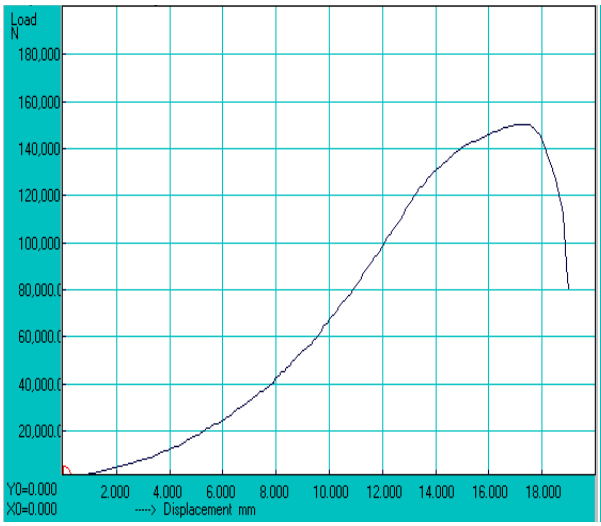

Graph- Stress vs Strain

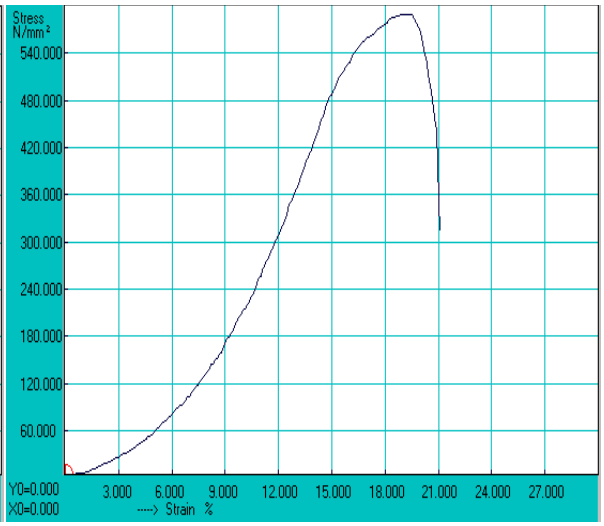

(i) for Trial 09

Graph- Load vs Displacement

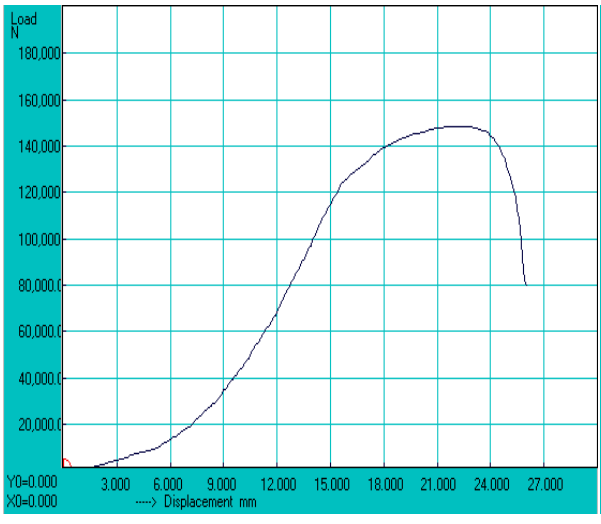

Graph- Stress vs Strain

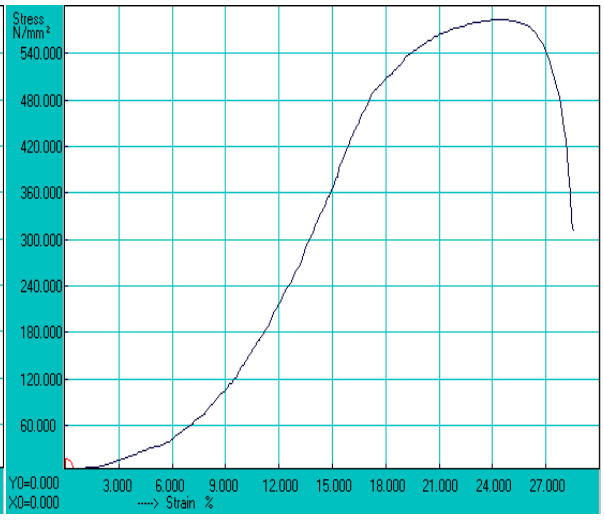

(j) for Trial 10

Graph- Load vs Displacement

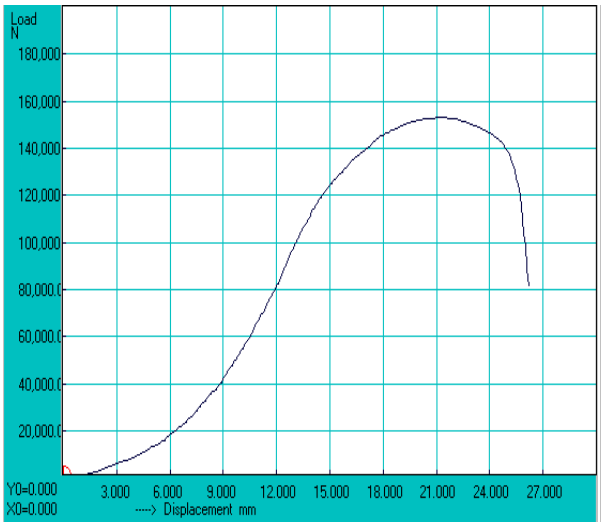

Graph- Stress vs Strain

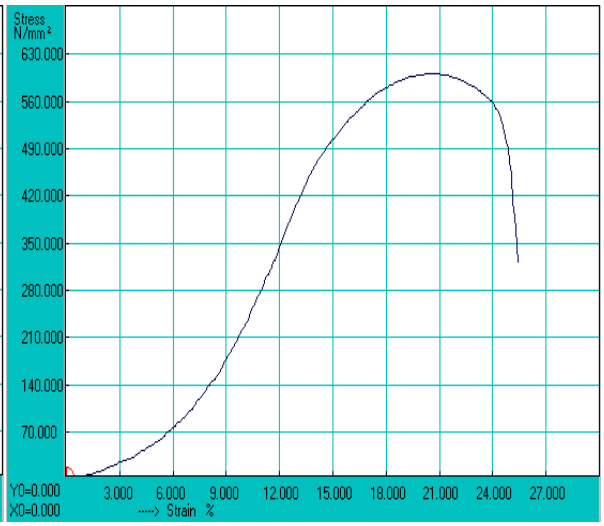

(k) for Trial 11

Graph- Load vs Displacement

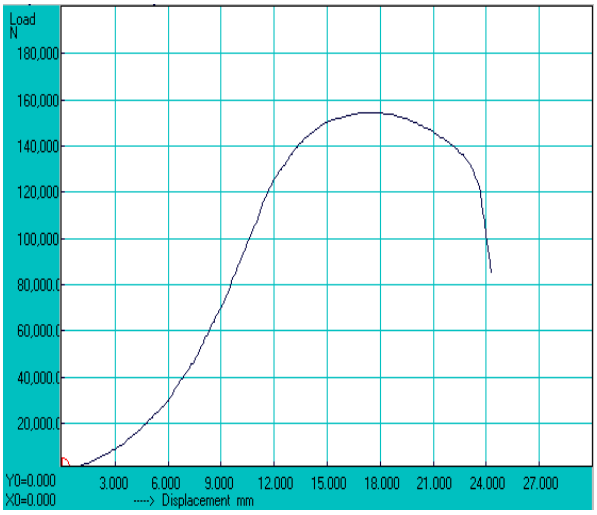

Graph- Stress vs Strain

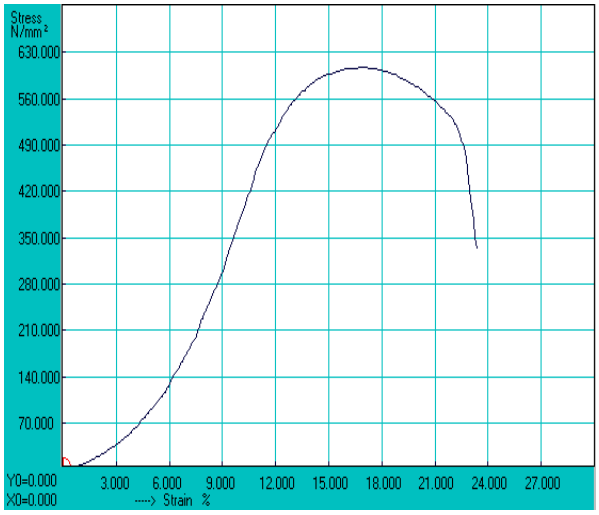

(l) for Trial 12

Graph- Load vs Displacement

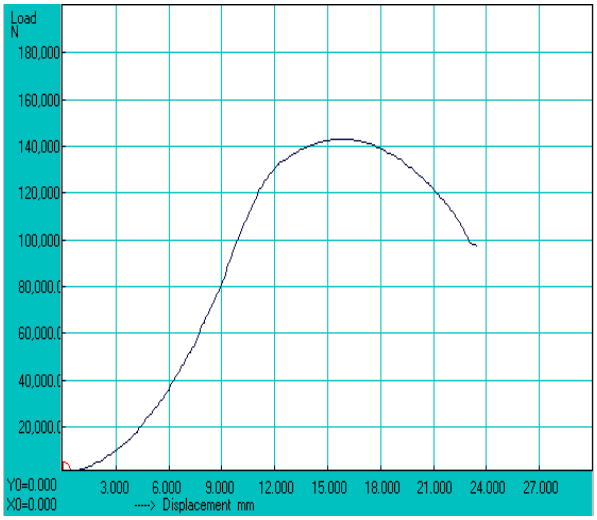

Graph- Stress vs Strain

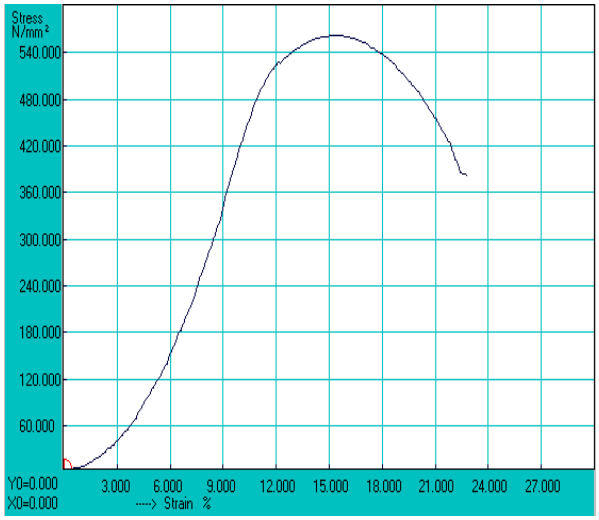

(m) for Trial 13

Graph- Load vs Displacement

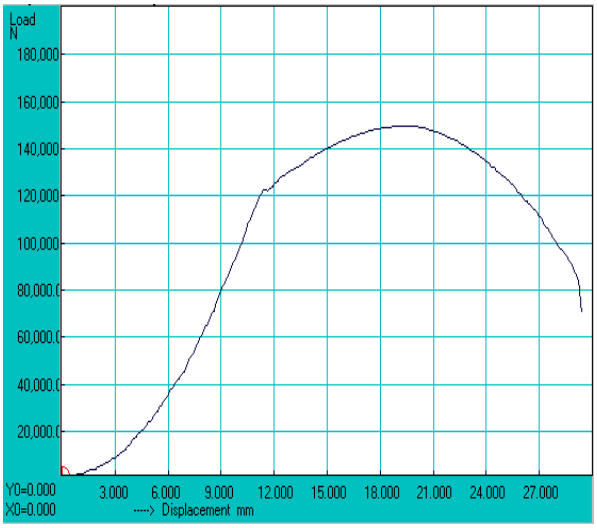

Graph- Stress vs Strain

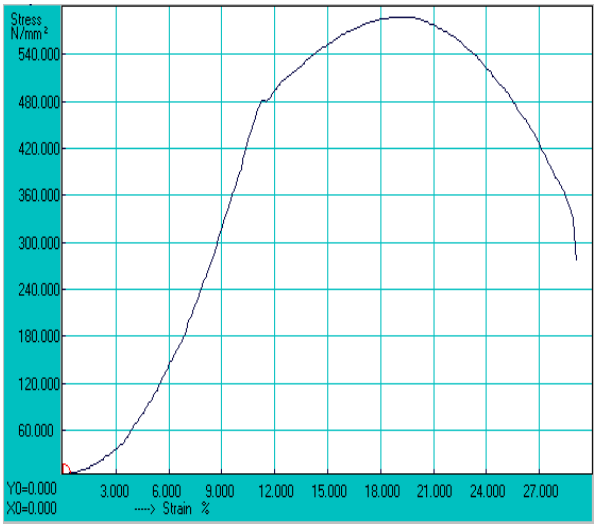

(n) for Trial 14

Graph- Load vs Displacement

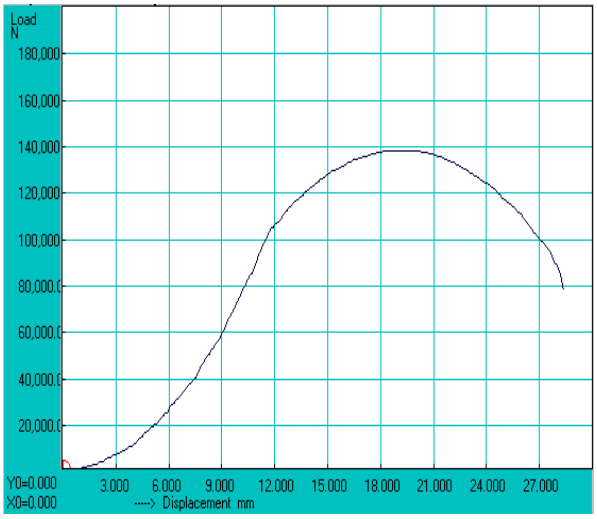

Graph- Stress vs Strain

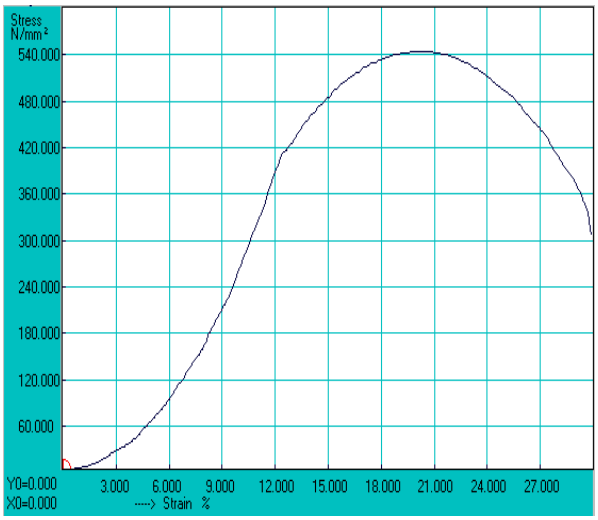

(o) for Trial 15

Graph- Load vs Displacement

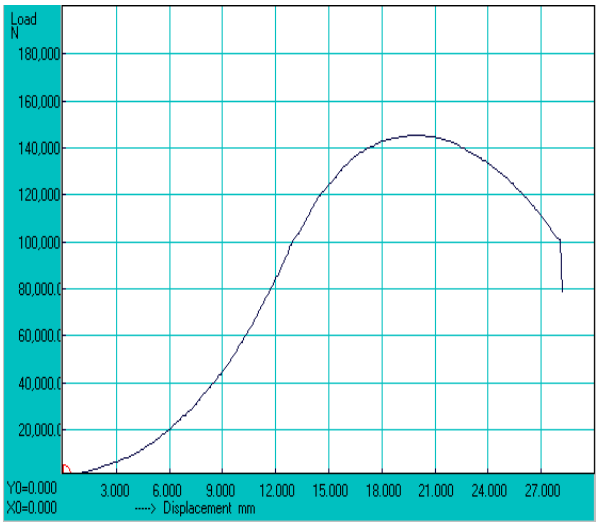

Graph- Stress vs Strain

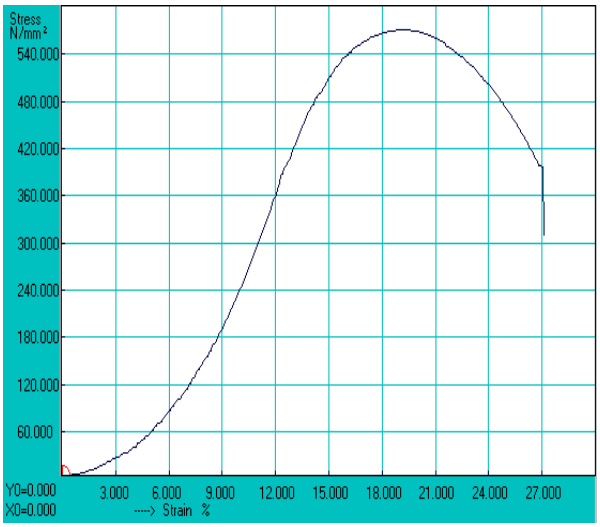

(q) for Trial 17

Graph- Load vs Displacement

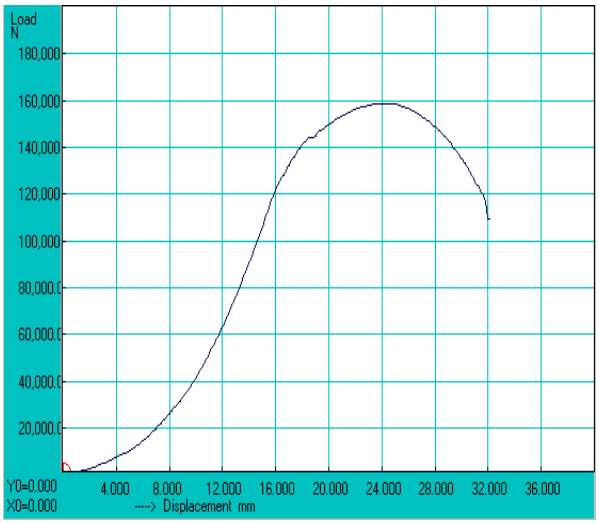

Graph- Stress vs Strain

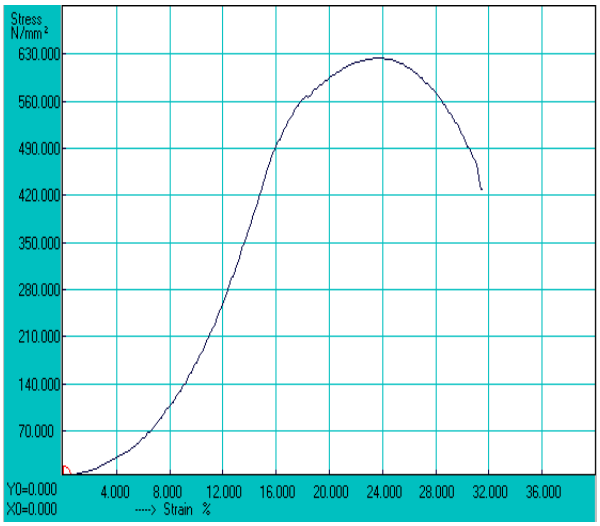

(r) for Trial 18

***** Load vs Displacement and Stress vs Strain curve for tensile test of trial no. 16 was not saved due to power problem.

FIGURE 4.4 (a-r) - Load vs Displacement and Stress vs Strain curve for tensile test for trial no. 1-18

In order to summarize the results of tensile test, for all 18 sets of experiments, the tensile load variation and tensile strength variation is shown in Figure 4.5 & 4.6 respectively. It was observed that maximum tensile load and strength of 158.75 kN and 623.597 N/mm^2 was obtained from specimen no. 18 and minimum tensile load and strength of 112.95 kN and 443.687 N/mm^2 was obtained from specimen no. 4.

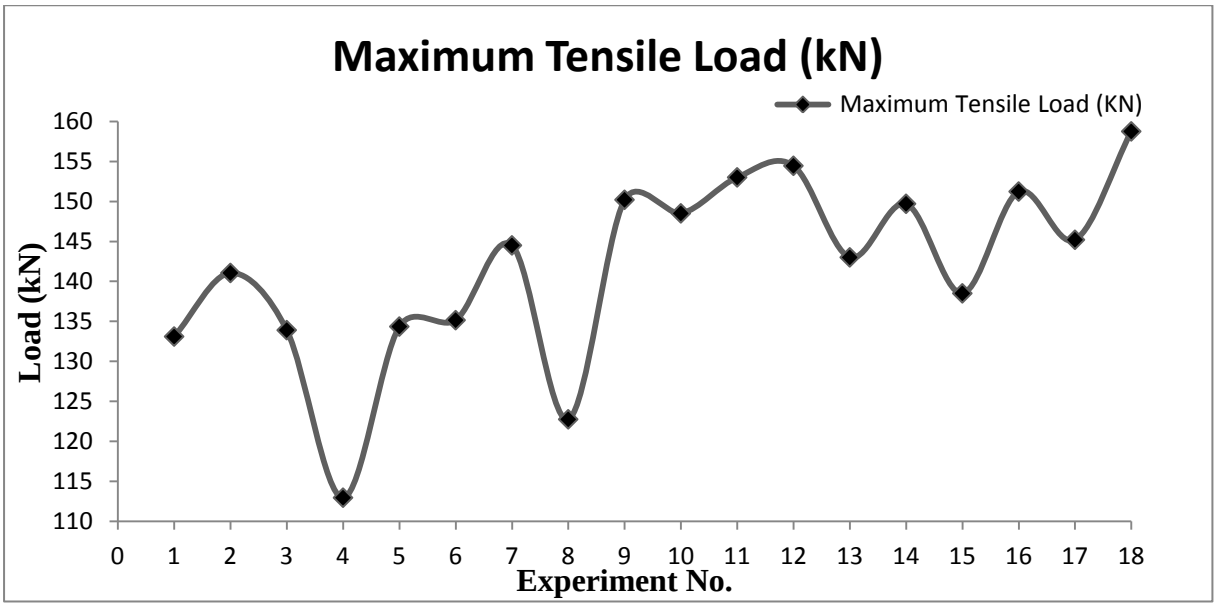

FIGURE 4.5- Variation of maximum tensile load of different trials

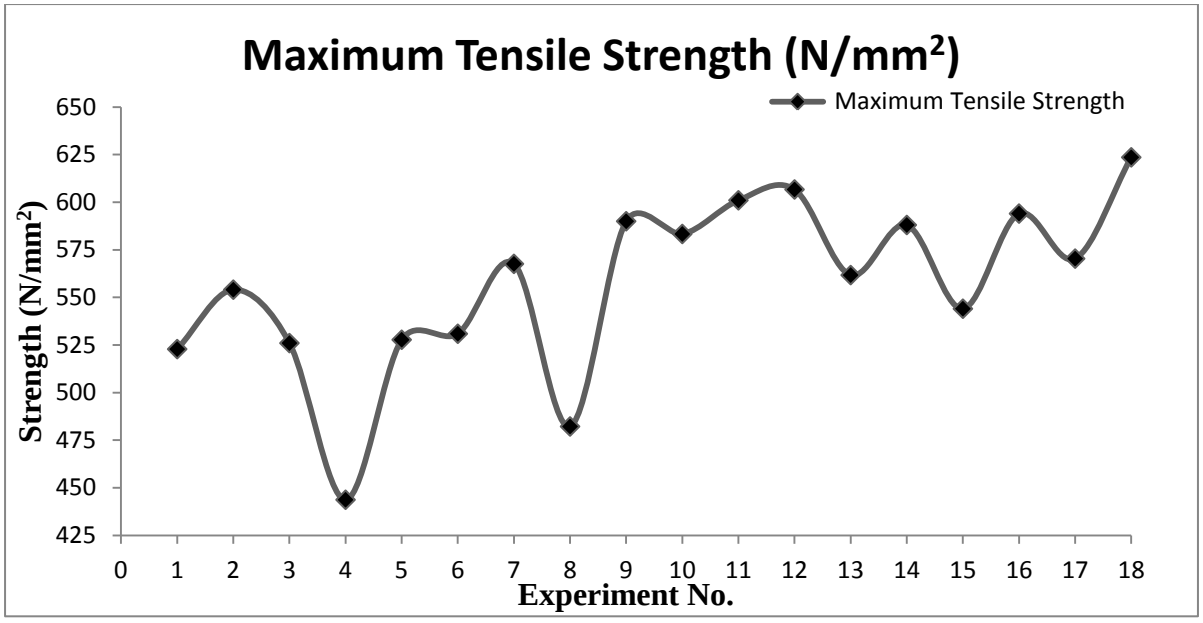

FIGURE 4.6- Variation of maximum tensile strength of different trials

4.2 ANOVA FOR TENSILE STRENGTH

Table 4.2, column no. 4 consists of the values of tensile strength for the eighteen trials. The experimental results for tensile strength were analyzed using ANOVA and is given in the Table 4.3. The p value given in the last column of ANOVA table suggests the significance of the factors on the desired characteristics. The principle behind significance value is that the p value should be lesser than 0.05 (considering confidence level of 95%). The principle of F test is that, the F value should be large compared to e-pooled; larger the F value more is the significance of factor. An ANOVA Table 4.3 show that p value for electrode diameter, current and travel speed is 0.006, 0.036 and 0.049 i.e. less than 0.05 indicates thereby that electrode diameter, current and travel speed are the most significant factor for the tensile strength. The mean value for all eight variables is given in Table 4.4. In last row of Table 4.4 ranks have been given to various factors. Higher is the rank, higher is the significance. In Table 4.4 electrode diameter with the highest rank 1 and is the most significant factor and preheat temperature with its lowest rank is least significant in affecting the tensile strength. Main effect plots are shown in Figure 4.7 shows the variation in the tensile strength with the change in the input factors i.e. electrode diameter, current, voltage, electrode stick-out, travel speed, preheat temperature, flux and edge including angle. It could be seen from the Figure 4.7 that electrode diameter causes the most significant change in the tensile strength with change in electrode diameter value. The change in current and travel speed also has some

effect on the variation in the tensile strength. Voltage and electrode stick-out, preheat temperature, flux and edge including angle have very low effect on tensile strength.

TABLE 4.3 Analysis of variance for means tensile strength

Source	DF	Seq SS	Adj SS	Adj MS	F	P
Electrode Diameter (mm)	1	15479.1	15479.1	15479.1	159.95	**0.006**
Current (Ampere)	2	5218.6	5218.6	2609.3	26.96	**0.036**
Voltage (Volt)	2	1888.1	1888.1	944.1	9.76	0.093
Electrode Stick-Out (mm)	2	2697.5	2697.5	1348.7	13.94	0.067
Travel Speed (m/hr)	2	3748.2	3748.2	1874.1	19.37	**0.049**
Preheat Temperature (^{o}C)	2	1084.3	1084.3	542.1	5.60	0.151
Flux	2	3077.1	3077.1	1538.5	15.90	0.059
Edge Including Angle (degree)	2	2165.5	2165.5	1082.7	11.19	0.082
Residual Error	2	193.5	193.5	96.8		
Total	17	35551.9				

TABLE 4.4 Response table for means of tensile strength

Level	Electrode Diameter (mm)	Current (amp)	Voltage (volt)	Electrode Stick-Out (mm)	Travel Speed (m/hr)	Preheat Temperature (^{o}C)	Flux	Edge Including Angle (degree)
1	527.2	565.7	545.5	545.3	572.3	545.8	571.6	547.3
2	585.9	532.7	553.9	573.6	537.5	563.8	558.4	572.0
3		571.3	570.2	550.7	559.9	560.1	539.7	550.4
Delta	58.6	38.6	24.7	28.3	34.9	18.0	31.9	24.7
Rank	**1**	**2**	**7**	**5**	**3**	**8**	**4**	**6**

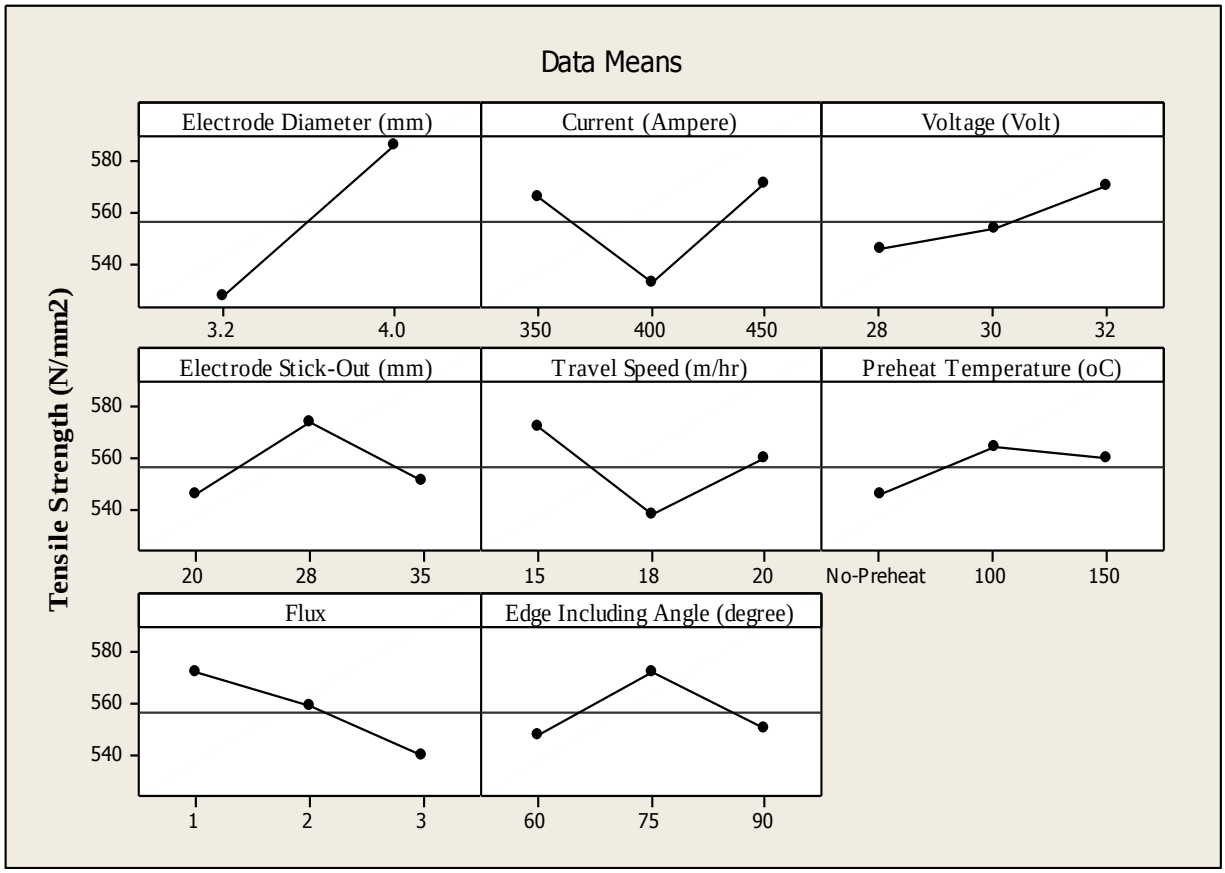

FIGURE 4.7- Main effect plot for tensile strength

4.3 OPTIMAL DESIGN FOR TENSILE STRENGTH

In this experimental analysis, the main effect plot in Figure 4.7 has been used to estimate the tensile strength in optimal conditions. From Table 4.3, it can be concluded that electrode diameter, current and travel speed are three significant factors. In order to obtain maximum tensile strength, the electrode diameter should be 4 mm, welding current should be 450 Ampere and travel speed should be 15 m/hr has been chosen. Confidence interval predict with 95 % confidence so that value of tensile strength at optimal design conditions would be 616.398 ± 38.26 N/mm^2

Mean value of tensile strength is given by-

$\mu_{\emptyset_2 C_3 S_1} = \overline{\emptyset_2} + \overline{C_3} + \overline{S_1} - 2\overline{T}$

$= 585.9 + 571.3 + 572.3 - 2 \times 556.551$

$= 616.398$ N/mm^2

Confidence Interval around the estimated mean tensile strength

$$C.I. = \sqrt{\frac{f\alpha{:}v1{:}v2 \; X \; Ve}{neff}}$$

α = risk (0.05) confidence = 1-α

v1 = DOF for mean (which is always 1)

v2 = DOF for error = 12

Where $f\,\alpha{:}v1{:}v2 = f\,0.05{:}1{:}12$ = F ratio = 4.7472

Variance = $Ve = \frac{SS\ of\ e\ pooled}{DOF\ of\ e\ pooled} = \frac{11106}{12} = 925.5$

n_{eff} = number of tests performed using participating factors

$n_{eff} = \frac{18}{1+\mathrm{DOF}_{\emptyset_2 C_3 S_1}} = 3$

C.I. = 38.26

So, the confidence interval around tensile strength is given by 616.398 ± 38.26 N/mm^2.

4.4 DISCUSSION OF TENSILE TEST RESULTS

The effect of various process parameters i.e. current, voltage, travel speed, electrode diameter, flux composition, pre heating of workpiece, electrode stick-out and angle of edge preparation on ultimate tensile load and ultimate tensile strength of the welded joint were examined. From Figure 4.5-4.6, it appears that maximum tensile load and strength was observed for specimen no 18 i.e. 158.75 kN and 623.597 N/mm^2 and for specimen no. 11 and 12 values obtained were nearly equal to specimen no. 18. And the lowest tensile load and strength was observed for specimen no. 4 i.e. 112.95 kN and 443.687 N/mm^2 and for specimen no. 8 values obtained were nearly equal to specimen no. 4 and the mean tensile strength using the optimal condition would be 616.398 ± 38.26 N/mm^2 with electrode diameter should be 4 mm, welding current should be 450 Ampere and travel speed should be 15 m/hr.

CHAPTER-5

RESULTS AND ANALYSIS OF TOUGHNESS TEST

5.1 TOUGHNESS TEST

The ability of a metal to rapidly distribute within itself due to both the stress and strain caused by a suddenly applied load or the ability of a material to withstand shock loading. It is the exact opposite of "brittleness" which carries the implication of sudden failure. The tested specimen after toughness test is shown in Figure 5.1 for 18 sets of experiment.

FIGURE 5.1- Specimen after toughness test

The toughness test details for base metal are shown in Table 5.1 and corresponding plot is shown in Figure 5.2 for comparison.

TABLE 5.1 Toughness values of base metal

Base Metal	**Charpy Test at -50 ^{o}C (Joule)**	**Charpy Test at -40 ^{o}C (Joule)**	**Charpy Test at -20 ^{o}C (Joule)**	**Charpy Test at Room Temp. (Joule)**
	49	118	177	216

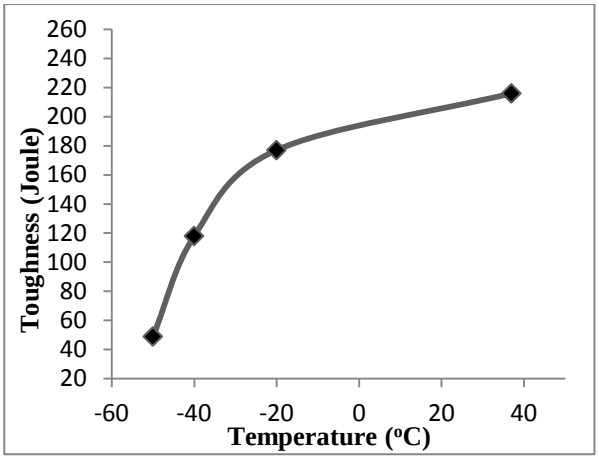

FIGURE 5.2- Toughness value of base metal at different temperature

For all the 18 sets of experiment, the toughness test summery is shown in Table 5.2 and corresponding plots at different temperature i.e. -50 ºC, -40 ºC, -20 ºC and room temperature are shown below sequentially in Figure 5.3 (a-r).

TABLE 5.2 Toughness values

Exp. No.	Contributing Factors	Charpy Test at -50 ºC (Joule)	Charpy Test at -40 ºC (Joule)	Charpy Test at -20 ºC (Joule)	Charpy Test at Room Temp. (Joule)
1	Ø1, C1, V1, D1, S1, T1, F1, α1	44	98	172	201
2	Ø1, C1, V2, D2, S2, T2, F2, α2	47	123	190	250
3	Ø1, C1, V3, D3, S3, T3, F3, α3	41	128	175	255
4	Ø1, C2, V1, D1, S2, T2, F3, α3	31	108	147	172
5	Ø1, C2, V2, D2, S3, T3, F1, α1	49	121	167	242
6	Ø1, C2, V3, D3, S1, T1, F2, α2	51	113	191	221
7	Ø1, C3, V1, D2, S1, T3, F2, α3	34	123	211	245
8	Ø1, C3, V2, D3, S2, T1, F3, α1	35	128	206	235
9	Ø1, C3, V3, D1, S3, T2, F1, α2	39	119	177	196
10	Ø2, C1, V1, D3, S3, T2, F2, α1	46	110	181	204
11	Ø2, C1, V2, D1, S1, T3, F3, α2	59	116	183	231
12	Ø2, C1, V3, D2, S2, T1, F1, α3	39	103	186	206
13	Ø2, C2, V1, D2, S3, T1, F3, α2	54	123	161	191
14	Ø2, C2, V2, D3, S1, T2, F1, α3	34	93	128	177
15	Ø2, C2, V3, D1, S2, T3, F2, α1	45	114	152	186
16	Ø2, C3, V1, D3, S2, T3, F1, α2	49	120	169	199
17	Ø2, C3, V2, D1, S3, T1, F2, α3	44	111	149	181
18	Ø2, C3, V3, D2, S1, T2, F3, α1	54	131	191	233

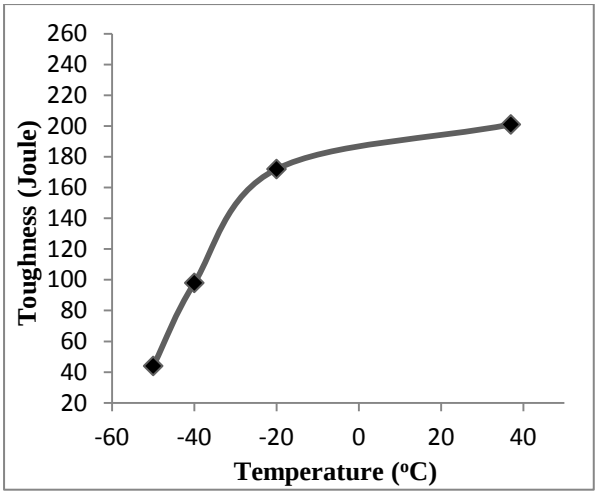

(a) for Trial 01

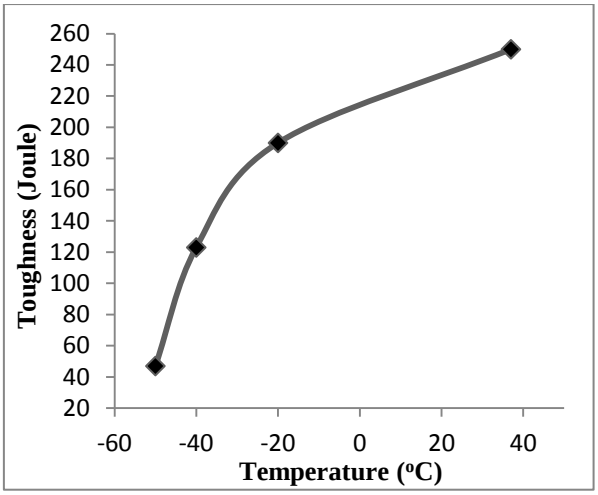

(b) for Trial 02

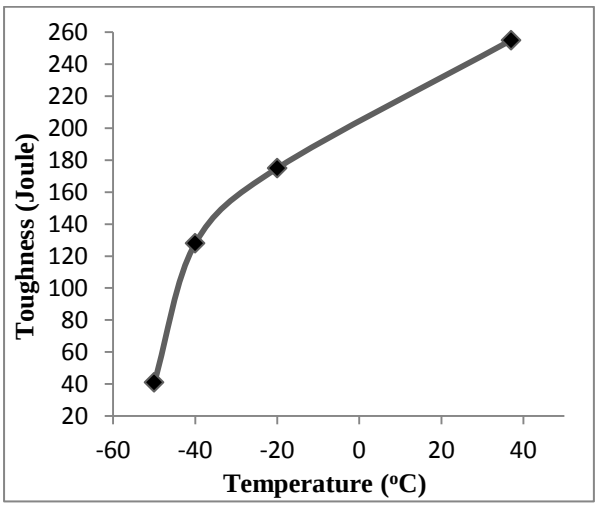

(c) for Trial 03

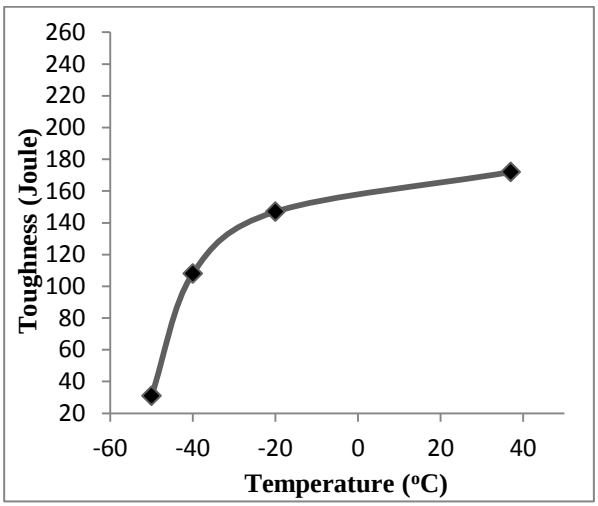

(d) for Trial 04

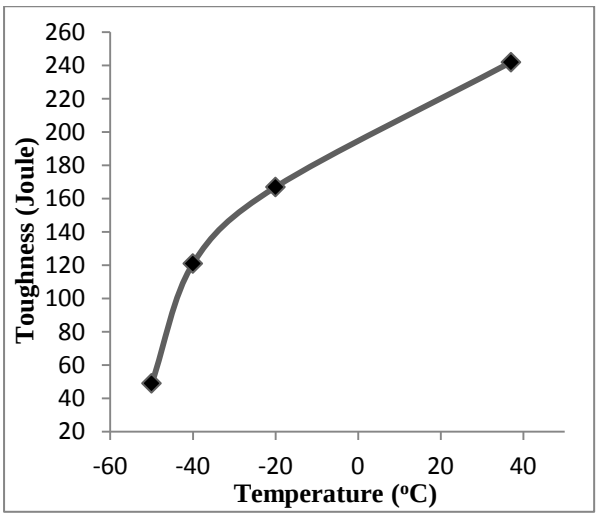

(e) for Trial 05

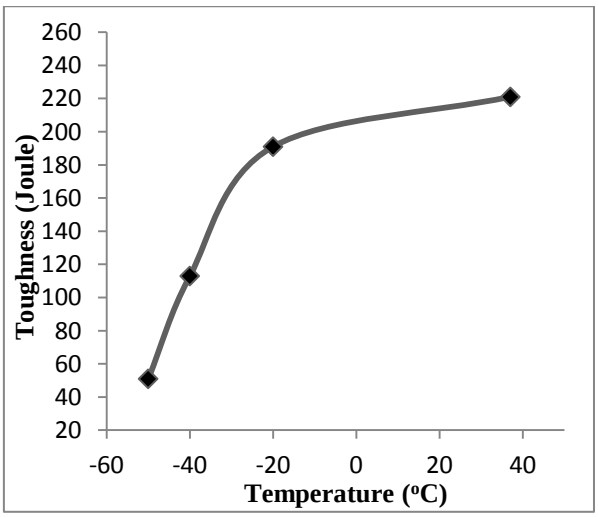

(f) for Trial 06

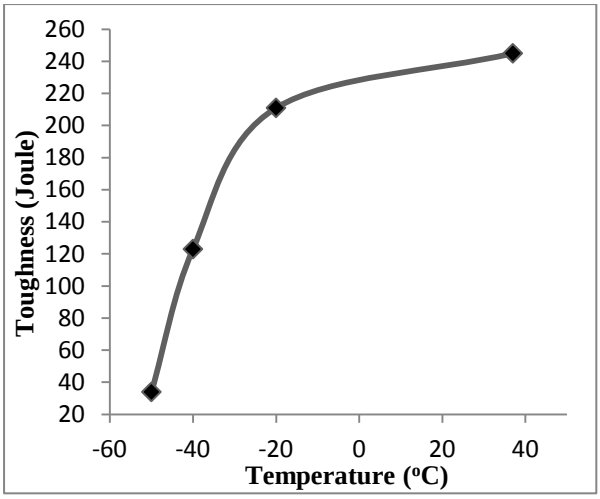

(g) for Trial 07

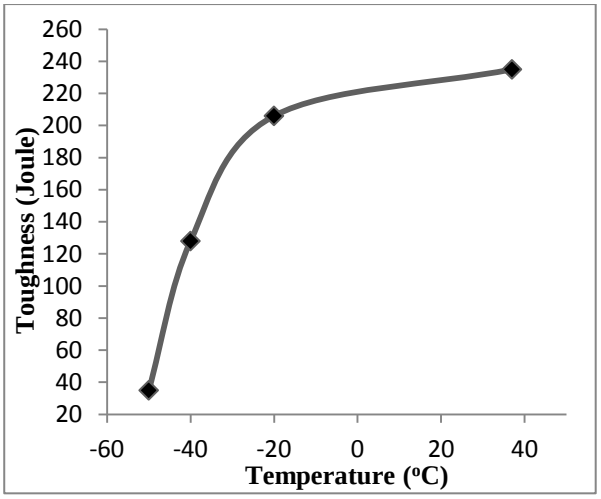

(h) for Trial 08

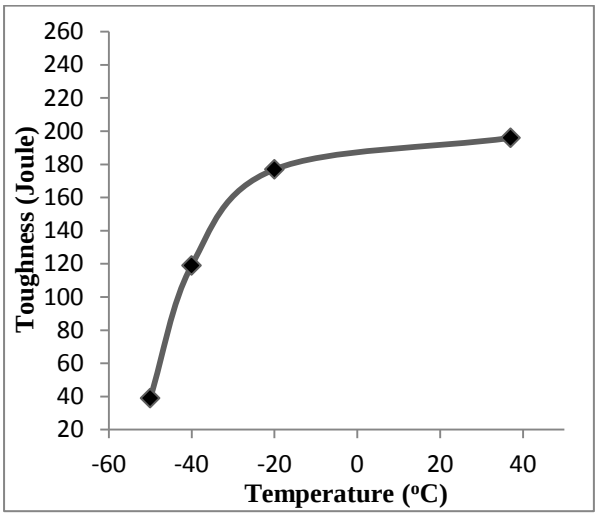

(i) for Trial 09

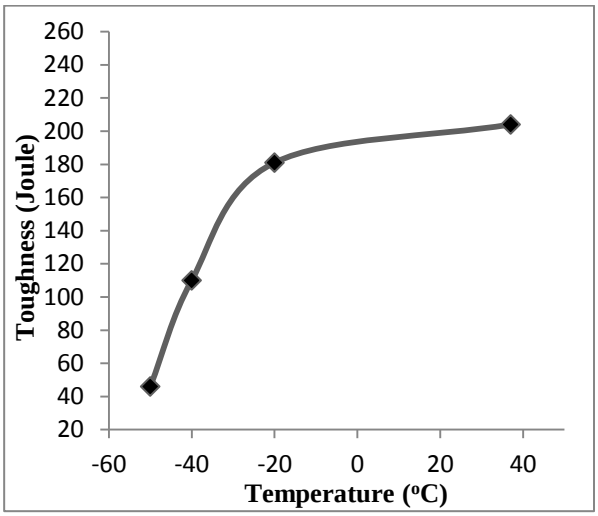

(j) for Trial 10

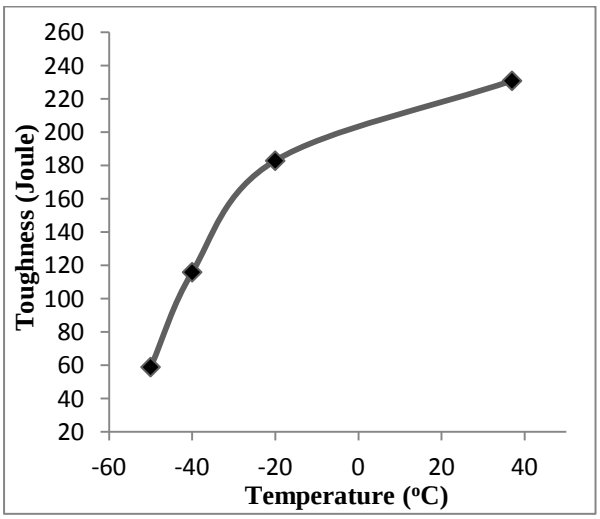

(k) for Trial 11

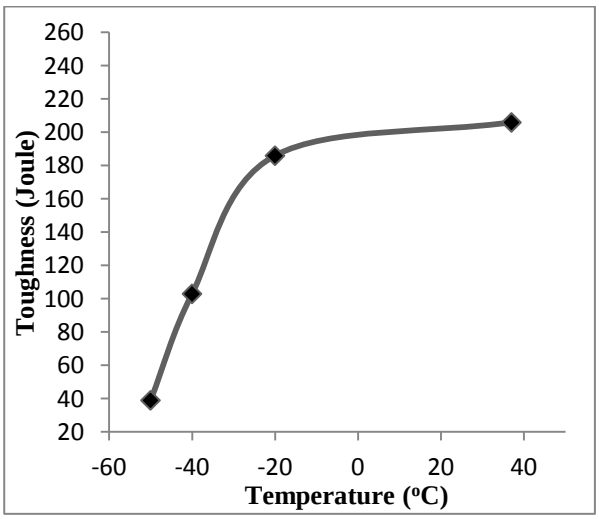

(l) for Trial 12

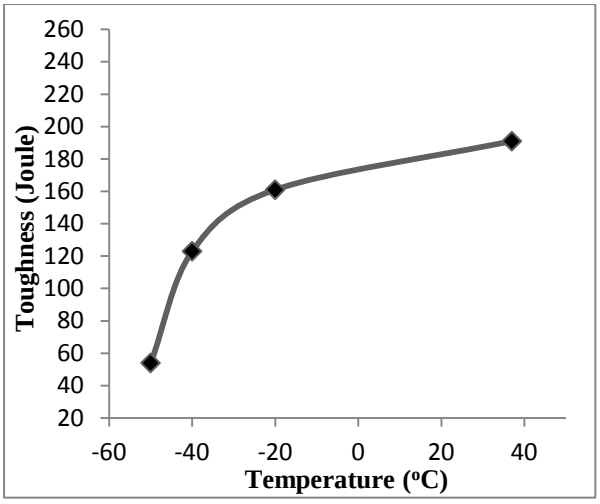

(m) for Trial 13

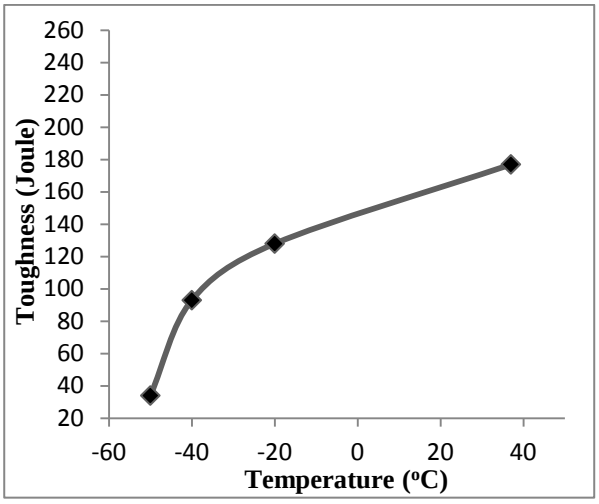

(n) for Trial 14

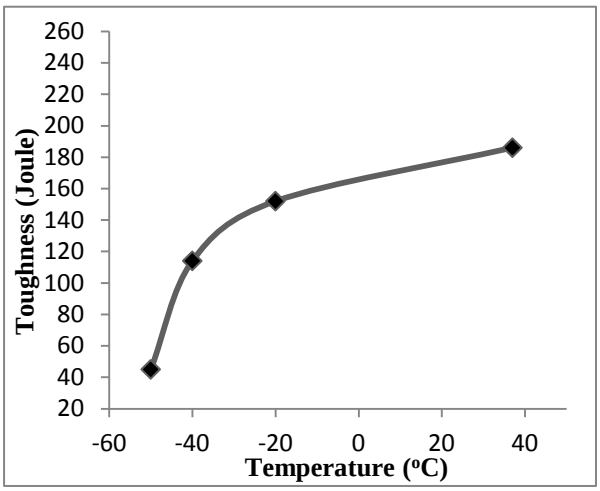

(o) for Trial 15

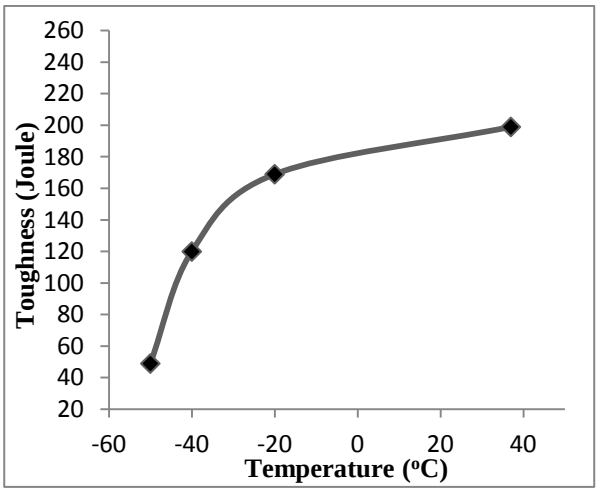

(p) for Trial 16

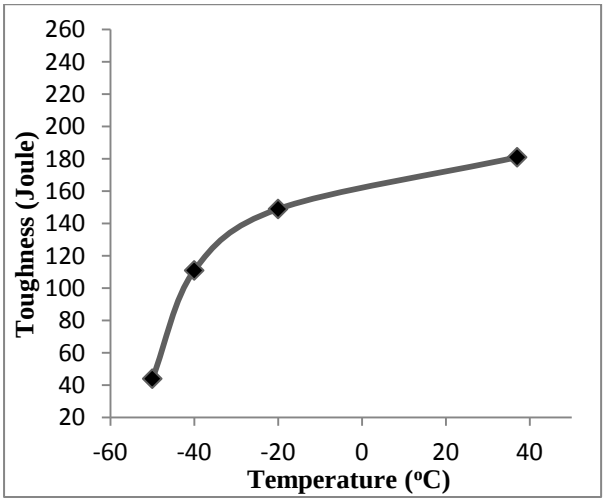

(q) for Trial 17

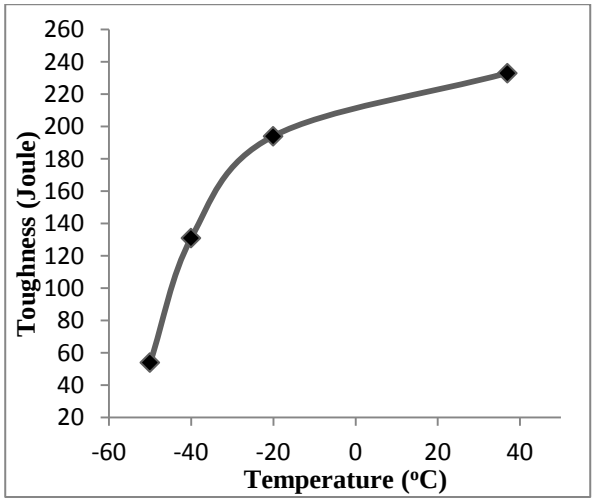

(r) for Trial 18

FIGURE 5.3 (a-r) – Variation of toughness of trial no. 1-18 at different temperature

In order to summarize the results of toughness test, for all 18 sets of experiments, the toughness variation at different temperature i.e. room temperature, -20 ºC, -40 ºC and -50 ºC is shown in Figure 5.4, 5.5, 5.6 & 5.7 respectively.

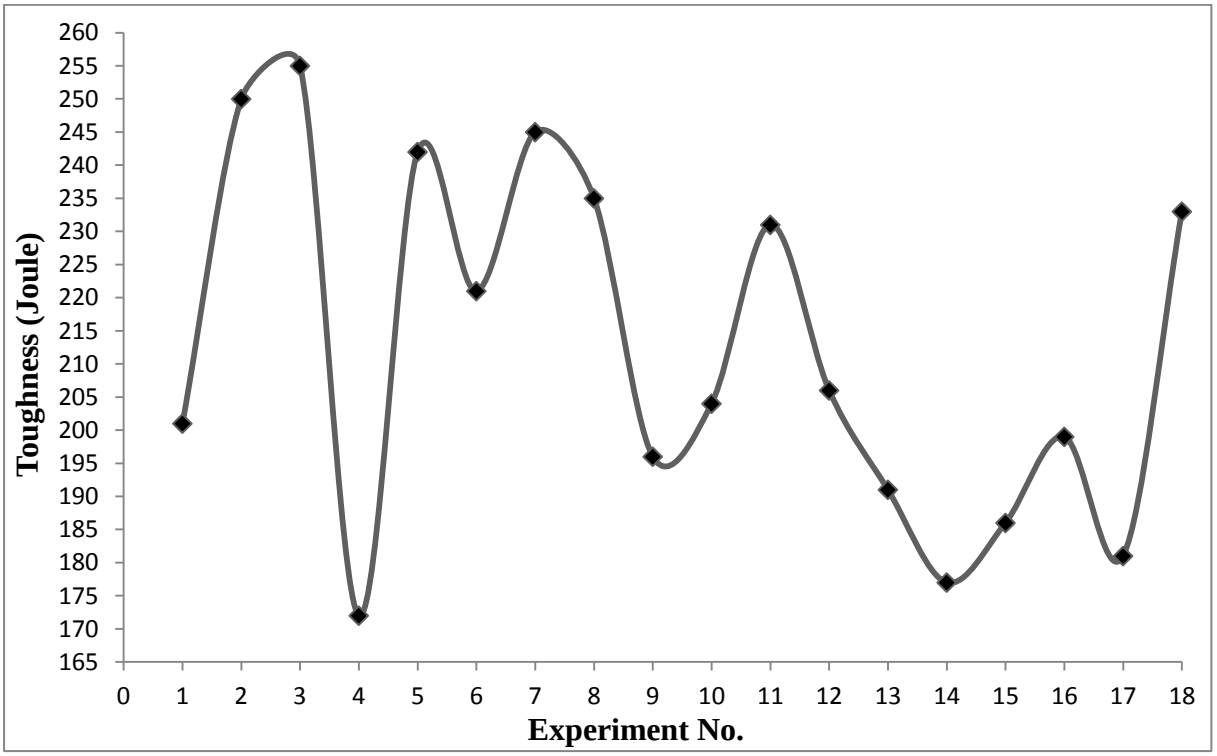

FIGURE 5.4- Variation in toughness at room temperature

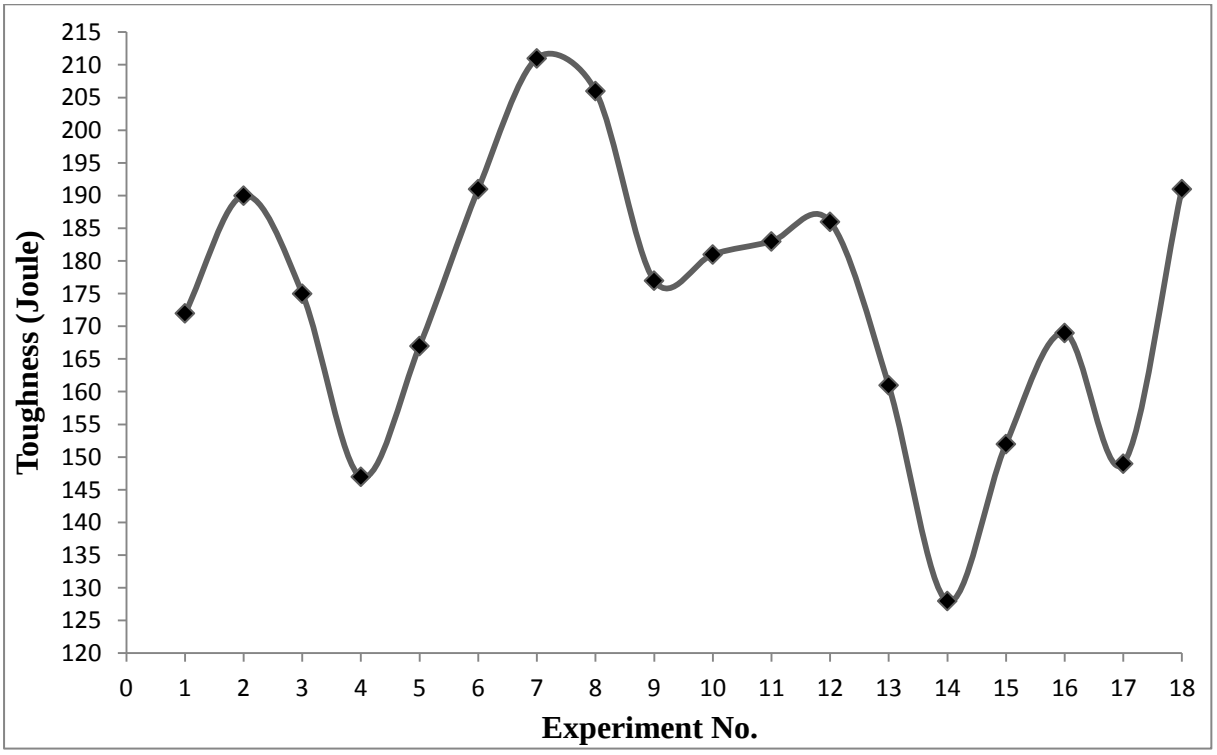

FIGURE 5.5- Variation in toughness at -20 ^{o}C

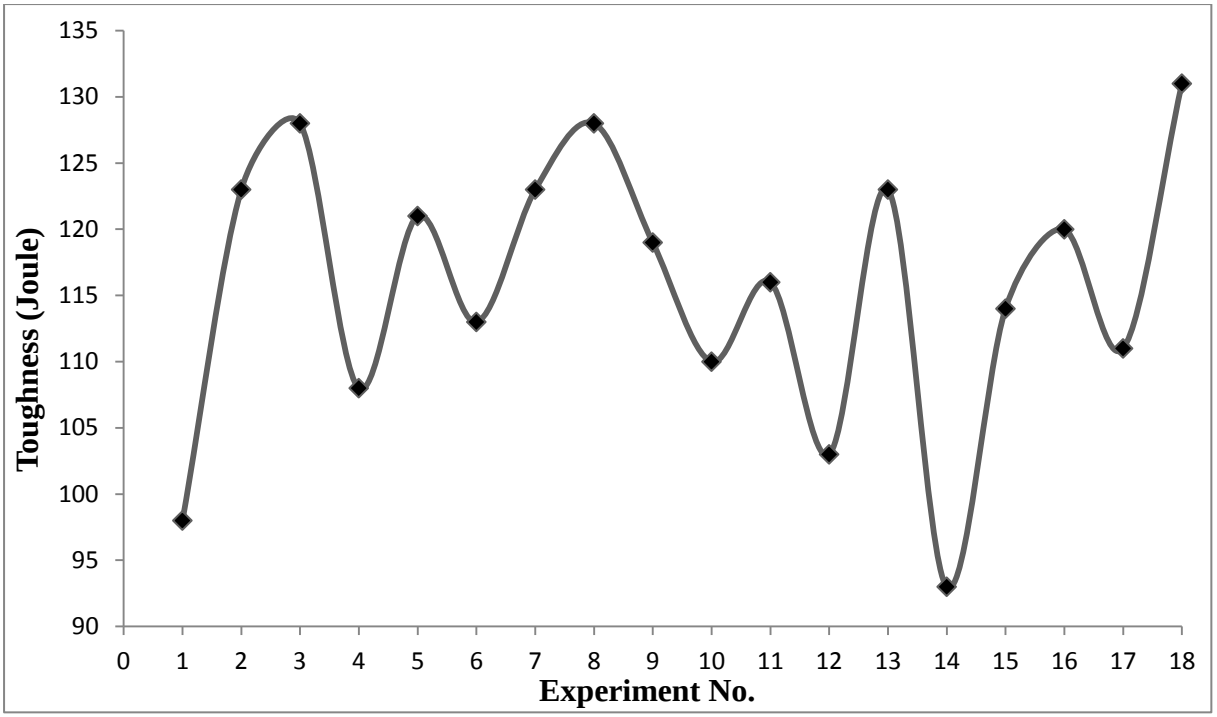

FIGURE 5.6- Variation in toughness at -40 ^{o}C

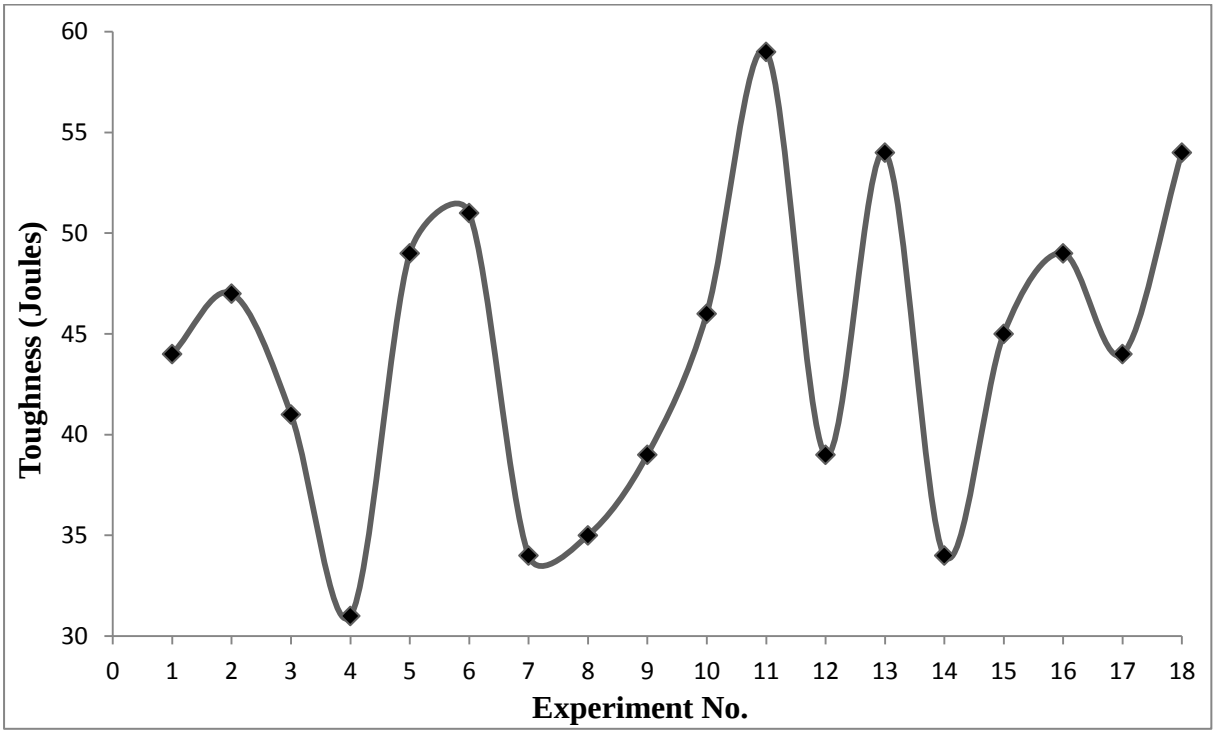

FIGURE 5.7- Variation in toughness at -50 ^{o}C

5.2 ANOVA FOR TOUGHNESS AT ROOM TEMPERATURE

Table 5.2, column no. 6 consists of the values of toughness at room temperature for the eighteen trials. The experimental results for toughness are analyzed using ANOVA and is given in the Table 5.3. An ANOVA Table 5.3 show that p value for electrode diameter,

electrode stick-out, current, preheat temperature, voltage and flux is 0.007, 0.009, 0.015, 0.018, 0.031 and 0.039 respectively are the most significant factor for the toughness at room temperature. In Table 5.4 electrode stick-out with the highest rank 1 and is the most significant factor and travel speed with its lowest rank is least significant in affecting the toughness at room temperature. Main effect plots are shown in Figure 5.8 shows the variation in the toughness at room temperature with the change in the input factors i.e. electrode diameter, current, voltage, electrode stick-out, travel speed, preheat temperature, flux and edge including angle. It could be seen from the Figure 5.8 that electrode diameter causes the most significant change in the toughness. The change in current, electrode stick-out, preheat temperature, voltage and flux also has some effect on the variation in the toughness at room temperature. Edge including angle and travel speed does not have any significant effect on toughness at room temperature.

TABLE 5.3 Analysis of variance for means toughness at room temperature

Source	DF	Seq SS	Adj SS	Adj MS	F	P
Electrode Diameter (mm)	1	2426.7	2426.72	2426.72	149.59	**0.007**
Current (Ampere)	2	2129.3	2129.33	1064.67	65.63	**0.015**
Voltage (Volt)	2	1022.3	1022.33	511.17	31.51	**0.031**
Electrode Stick-Out (mm)	2	3397.3	3397.33	1698.67	104.71	**0.009**
Travel Speed (m/hr)	2	309.0	309.00	154.50	9.52	0.095
Preheat Temperature (^{o}C)	2	1723.0	1723.00	861.50	53.11	**0.018**
Flux	2	804.0	804.00	402.00	24.78	**0.039**
Edge Including Angle (degree)	2	394.3	394.33	197.17	12.15	0.076
Residual Error	2	32.4	32.44	16.22		
Total	17	12238.5				

TABLE 5.4 Response table for means of toughness at room temperature

Level	Electrode Diameter (mm)	Current (amp)	Voltage (volt)	Electrode Stick-Out (mm)	Travel Speed (m/hr)	Preheat Temperature (^{o}C)	Flux	Edge Including Angle (degree)
1	224.1	224.5	202.0	194.5	218.0	205.3	203.5	216.8
2	200.9	198.2	219.3	227.8	208.0	226.3	214.5	214.7
3		214.8	216.2	215.2	211.5	205.8	219.5	206.0
Delta	23.2	26.3	17.3	33.3	10.0	21.0	16.0	10.8
Rank	**3**	**2**	**5**	**1**	**8**	**4**	**6**	**7**

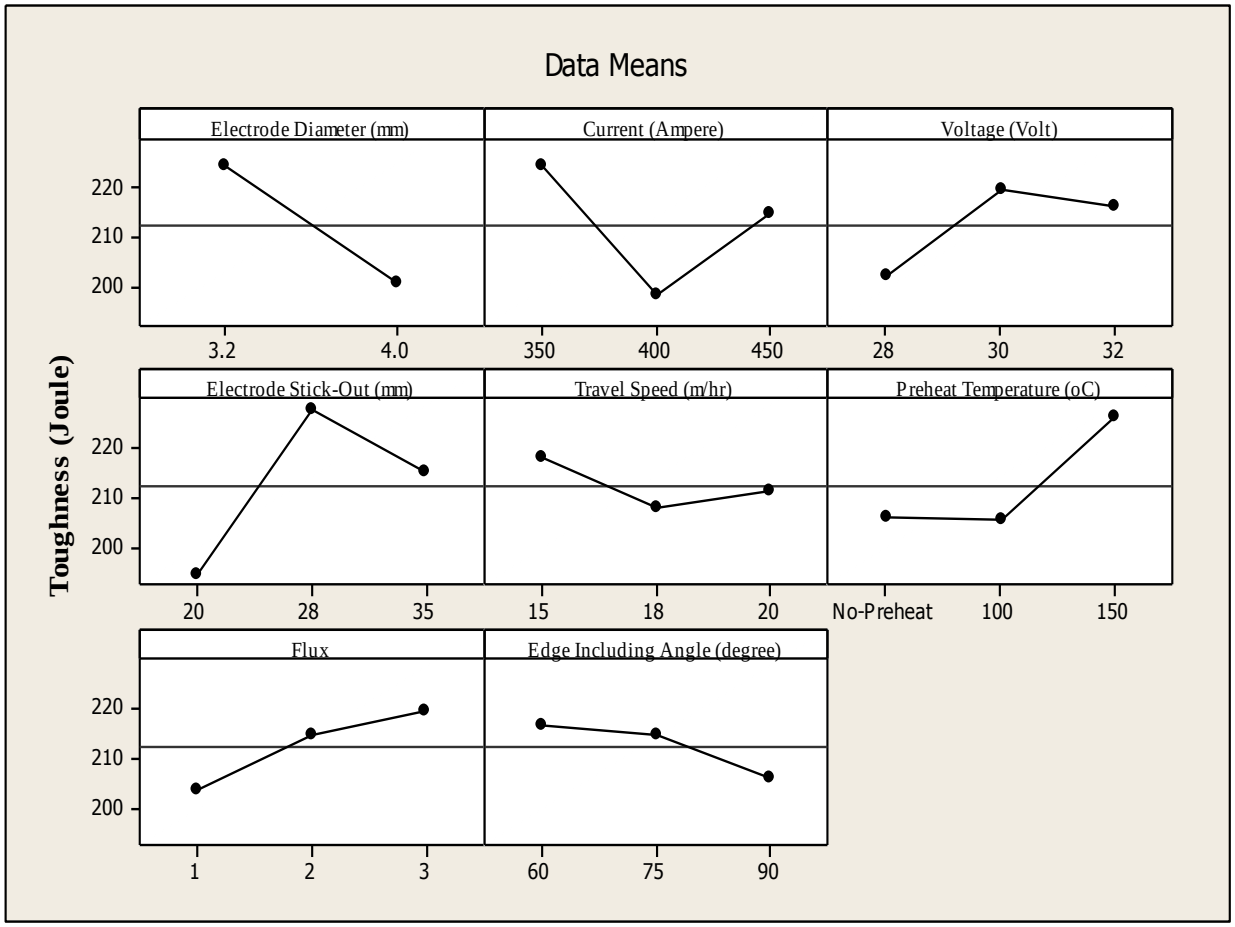

FIGURE 5.8- Main effect plot for toughness at room temperature

5.3 OPTIMAL DESIGN FOR TOUGHNESS AT ROOM TEMPERATURE

In this experimental analysis, the main effect plot in Figure 5.8 has been used to estimate the toughness in optimal conditions. From Table 5.3, it can be concluded that electrode diameter, electrode stick-out, current, preheat temperature, voltage and flux are the most significant

factors. In order to obtain maximum toughness at Room Temperature, the electrode diameter should be 3.2 mm, electrode stick-out should be 28 mm, welding current should be 350 Ampere, preheat temperature should be 150 ^{o}C and welding voltage should be 30 Volts and flux should be of type 3 i.e. GEEFLUX 541 (Basic) has been chosen. Confidence interval predict with 95 % confidence so that value of toughness at room temperature at optimal design conditions would be 279 ± 22.13 Joule.

Mean value of toughness at Room Temperature is given by-

$\mu_{\emptyset_1 D_2 C_1 T_2 V_2 F_3} = \overline{\emptyset_1} + \overline{D_2} + \overline{C_1} + \overline{T_2} + \overline{V_2} + \overline{F_3} - 5\overline{T}$

$= 224.1 + 227.8 + 224.5 + 226.3 + 219.3 + 219.5 – 5 \times 215.5$

$= 279$ Joule

C.I. $= \sqrt{\frac{f\alpha:v1:v2\ X\ Ve}{neff}}$

v2 = DOF for error = 11

Where $f\,\alpha{:}v1{:}v2 = f\,0.05{:}1{:}6 = 5.9874$

Variance = $Ve = \frac{735.7}{6} = 122.61$

$n_{eff} = \frac{18}{1+\mathrm{DOF}_{\emptyset_1 D_2 C_1 T_2 V_2 F_3}} = 1.5$

C.I. = 22.13

So, the confidence interval around toughness at room temperature is given by 279 ± 22.13 Joule.

5.4 ANOVA FOR TOUGHNESS AT -40 ^{O}C

Table 5.2, column no. 4 consists of the values of toughness at -40 ^{o}C for the eighteen trials. The experimental results for toughness were analyzed using ANOVA and is given in the Table 5.5. An ANOVA Table 5.5 show that p value for flux is 0.023, current is 0.033 and value of electrode stick-out is 0.042 i.e. less than 0.05 indicates thereby that flux, current and electrode stick-out are the most significant factor for the toughness at -40 ^{o}C. In last row of Table 5.6 ranks have been given to various factors. In Table 5.6 flux with the highest rank 1 and is the most significant factor and voltage with its lowest rank is least significant in affecting the toughness at -40 ^{o}C. Main effect plots are shown in Figure 5.9 shows the variation in the toughness at -40 ^{o}C. It could be seen from the Figure 5.9 that flux causes the most significant change in the toughness with change in flux. The change in current and

electrode stick-out also has some effect on the variation in the toughness at -40 ^{o}C. Electrode diameter, edge including angle, voltage, preheat temperature and travel speed have very low effect on toughness at -40 ^{o}C.

TABLE 5.5 Analysis of variance for means toughness at -40 ^{o}C

Source	DF	Seq SS	Adj SS	Adj MS	F	P
Electrode Diameter (mm)	1	88.89	88.89	88.889	14.29	0.063
Current (Ampere)	2	364.00	364.00	182.00	29.25	**0.033**
Voltage (Volt)	2	57.33	57.33	28.667	4.61	0.178
Electrode Stick-Out (mm)	2	281.33	281.33	140.667	22.61	**0.042**
Travel Speed (m/hr)	2	121.33	121.33	60.667	9.75	0.093
Preheat Temperature (^{o}C)	2	201.33	201.33	100.667	16.18	0.058
Flux	2	533.33	533.33	266.667	42.86	**0.023**
Edge Including Angle (degree)	2	208.00	208.00	104.00	16.71	0.056
Residual Error	2	12.44	12.44	6.222		
Total	17	1868.00				

TABLE 5.6 Response table for means of toughness at -40 ^{o}C

Level	Electrode Diameter (mm)	Current (amp)	Voltage (volt)	Electrode Stick-Out (mm)	Travel Speed (m/hr)	Preheat Temperature (^{o}C)	Flux	Edge Including Angle (degree)
1	117.9	113.0	113.7	111.0	112.3	114.0	109.0	117.0
2	113.4	112.0	115.3	120.7	116.0	120.3	115.7	119.0
3		122.0	118.0	115.3	118.7	112.7	122.3	111.0
Delta	4.4	10.0	4.3	9.7	6.3	7.7	13.3	8.0
Rank	**7**	**2**	**8**	**3**	**6**	**5**	**1**	**4**

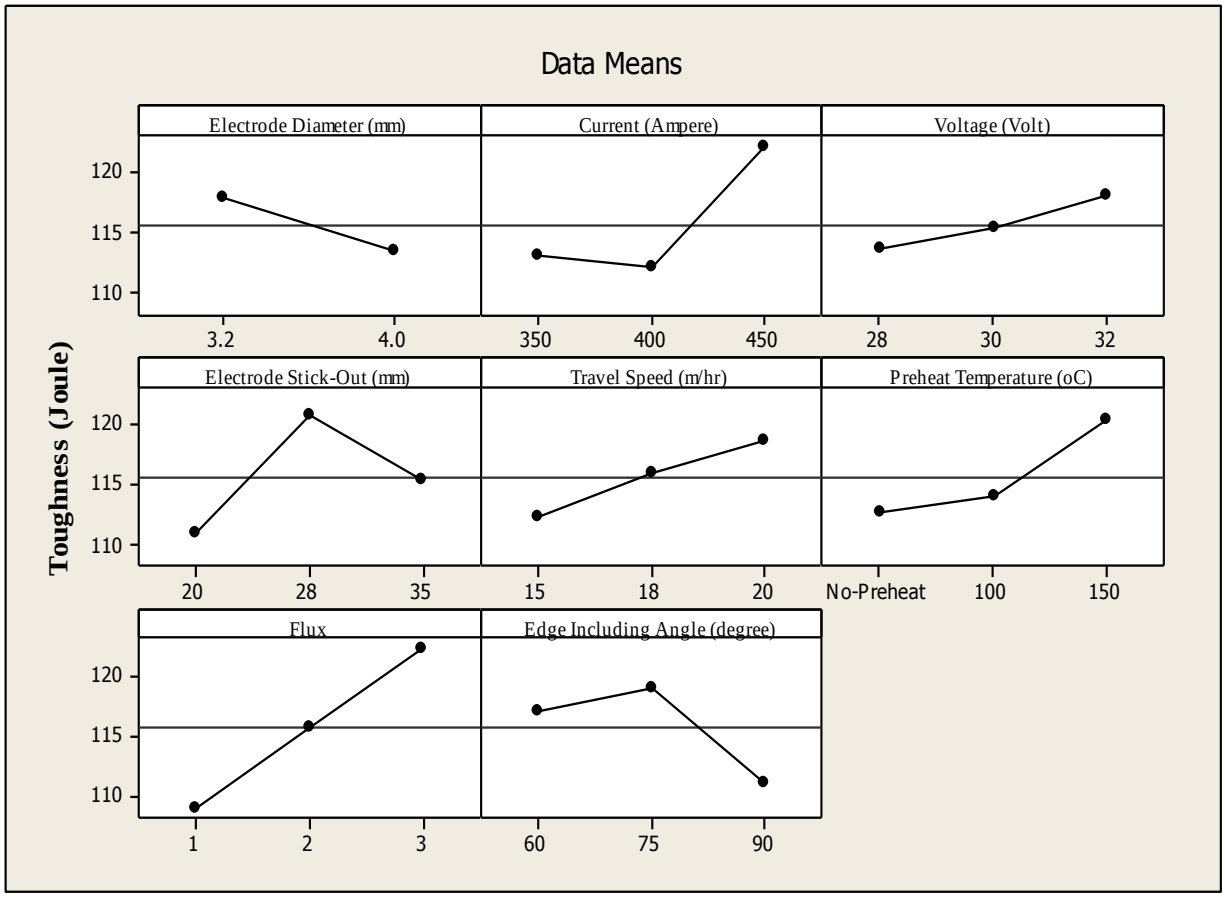

FIGURE 5.9 - Main effect plot for toughness at -40 ^{o}C

5.5 OPTIMAL DESIGN FOR TOUGHNESS AT -40 ^{O}C

In this experimental analysis, the main effect plot in Figure 5.9 has been used to estimate the toughness in optimal conditions. From Table 5.5, it can be concluded that flux, current and electrode stick-out are the three most significant factors. In order to obtain maximum toughness at -40 ^{o}C, the flux should be of type 3 i.e. GEEFLUX 541 (Basic), current should be 450 Ampere and electrode stick-out should be 28 mm has been chosen. Confidence interval predict with 95 % confidence so that value of toughness at -40 ^{o}C at optimal design conditions would be 133.666 ± 10.87 Joule.

Mean value of toughness at -40 ^{o}C is given by-

$\mu_{F_3C_3D_2} = \overline{F_3} + \overline{C_3} + \overline{D_2} - 2\overline{T}$

$= 122.3 + 122.0 + 120.7 - 2 \times 115.667$

$= 133.666$ Joule

Confidence Interval around the estimated mean toughness

C.I. = $\sqrt{\frac{f\alpha:v1:v2\ X\ Ve}{neff}}$

v2 = DOF for error = 11

Where $f\,\alpha{:}v1{:}v2 = f\,0.05{:}1{:}11$ = 4.8443

Variance = $Ve = \frac{689.32}{11}$ = 62.66

$n_{eff} = \frac{18}{1+\mathrm{DOF}_{F_3C_3D_2}}$ = 2.57

C.I. = 10.87

So, the confidence interval around toughness at -40 ^{o}C is given by 133.666 ± 10.87 Joule.

5.6 DISCUSSION OF TOUGHNESS TEST RESULTS

It is clear from Figure 5.4 that maximum toughness at room temperature is obtained from specimen no. 3 i.e. 255 Joule. It is concluded that at room temperature specimen no. 3 enhances toughness value. The mean toughness at room temperature using the optimal condition would be 279 ± 22.13 Joule with electrode diameter should be 3.2 mm, electrode stick-out should be 28 mm, welding current should be 350 Ampere, preheat temperature should be 150 ^{o}C and welding voltage should be 30 Volts and flux should be of type 3 i.e. GEEFLUX 541 (Basic).

It is clear from Figure 5.5 that maximum toughness at -20 ^{o}C is obtained from specimen no. 7 i.e. 211 Joule. It is concluded that at room temperature specimen no. 7 enhances toughness value.

It is clear from Figure 5.6 that maximum toughness at -40 ^{o}C is obtained from specimen no. 18 i.e. 131 Joule. It is concluded that at room temperature specimen no. 18 enhances toughness value. The mean toughness at -40 ^{o}C using the optimal condition would be 133.666 ± 10.87 Joule with flux should be of type 3 i.e. GEEFLUX 541 (Basic), current should be 450 Ampere and electrode stick-out should be 28 mm.

It is clear from Figure 5.7 that maximum toughness at -50 ^{o}C is obtained from specimen no. 11 i.e. 59 Joule. It is concluded that at room temperature specimen no. 11 enhances toughness value.

CHAPTER-6

RESULTS AND ANALYSIS OF MICROHARDNESS TEST

6.1 MICROHARDNESS TEST

The microhardness test details for base metal are shown in Table 6.1 and corresponding plots is shown in Figure 6.1 for comparison.

TABLE 6.1 Microhardness values of base metal at different region

Base Metal	Indent Load (gm)	Dwell Time (sec)	Hardness Value at -20 mm from Centre (HVN)	Hardness Value at -10 mm from Centre (HVN)	Hardness Value at Centre (HVN)	Hardness Value at 10 mm from Centre (HVN)	Hardness Value at 20 mm from Centre (HVN)
	1000	20	77.42	76.61	78.45	77.05	76.33

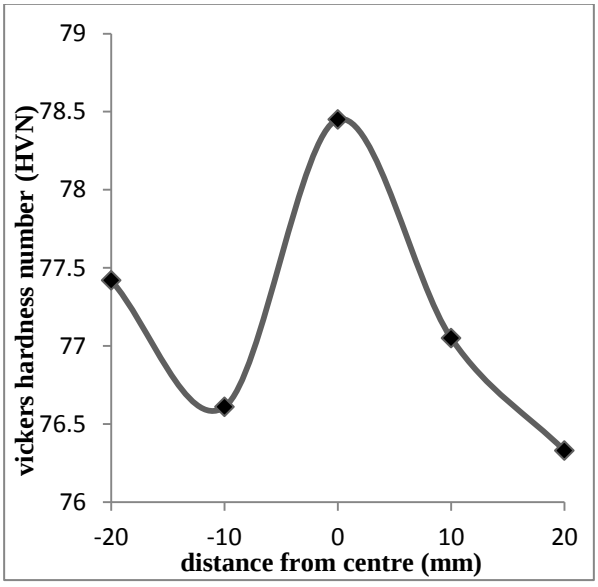

FIGURE 6.1- Microhardness of base metal

For all the 18 sets of experiment, the microhardness test summery is shown in Table 6.2 and corresponding plots at different region are shown below sequentially in Figure 6.2 (a-r).

TABLE 6.2 Microhardness values at weld region (indent load 1 kg and dwell time 20 s)

Exp No.	Contributing Factors	Hardness Value at -20 mm from Weld Centre (HVN)	Hardness Value at -10 mm from Weld Centre (HVN)	Hardness Value at Weld Centre (HVN)	Hardness Value at 10 mm from Weld Centre (HVN)	Hardness Value at 20 mm from Weld Centre (HVN)
1	Ø1, C1, V1, D1, S1, T1, F1, α1	71.57	71.28	70.9	65.62	70.44
2	Ø1, C1, V2, D2, S2, T2, F2, α2	67.68	60.02	62.24	69.28	70.75
3	Ø1, C1, V3, D3, S3, T3, F3, α3	68.19	66.53	60.57	69.41	72.34
4	Ø1, C2, V1, D1, S2, T2, F3, α3	71.88	66.98	62.49	60.9	65.01
5	Ø1, C2, V2, D2, S3, T3, F1, α1	71.72	75.54	71.27	73.65	68.74
6	Ø1, C2, V3, D3, S1, T1, F2, α2	67.26	69.93	72.09	63.49	63.64
7	Ø1, C3, V1, D2, S1, T3, F2, α3	65.08	63.62	65.02	72.96	72.12
8	Ø1, C3, V2, D3, S2, T1, F3, α1	78.93	73.59	94.42	79.84	70.44
9	Ø1, C3, V3, D1, S3, T2, F1, α2	78.28	74.77	74.18	69.34	71.97
10	Ø2, C1, V1, D3, S3, T2, F2, α1	70.96	69.2	61.14	74.72	69.48
11	Ø2, C1, V2, D1, S1, T3, F3, α2	77.9	69.05	61.27	72.71	65.18
12	Ø2, C1, V3, D2, S2, T1, F1, α3	67.68	67.12	62.86	67.26	75.7
13	Ø2, C2, V1, D2, S3, T1, F3, α2	76.67	65.68	61.88	73.75	76.91
14	Ø2, C2, V2, D3, S1, T2, F1, α3	68.34	67.68	72.43	70.44	75.16
15	Ø2, C2, V3, D1, S2, T3, F2, α1	62.74	74.77	67.49	67.03	67.68
16	Ø2, C3, V1, D3, S2, T3, F1, α2	60.31	74.51	76.08	82.04	66.08
17	Ø2, C3, V2, D1, S3, T1, F2, α3	62.99	62.12	60.43	60.55	68.62
18	Ø2, C3, V3, D2, S1, T2, F3, α1	69.05	75.66	68.91	71.5	72.12

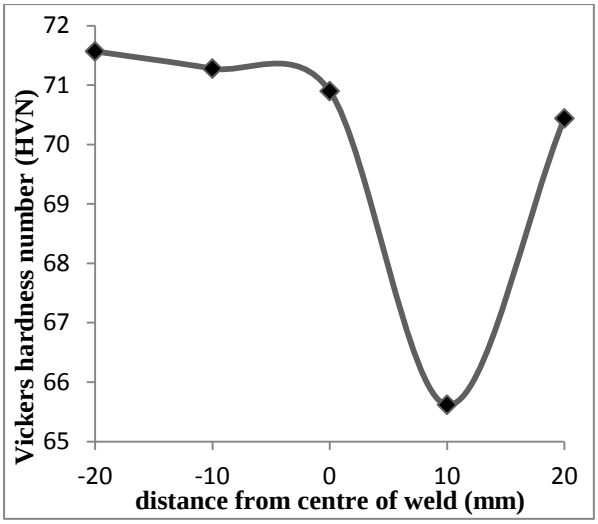

(a) for Trial 01

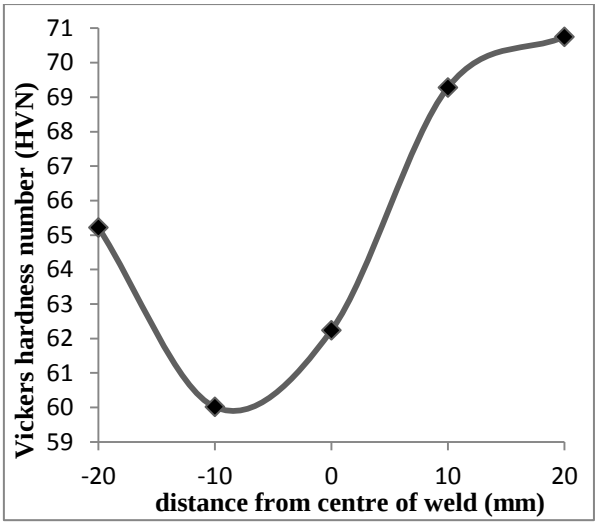

(b) for Trial 02

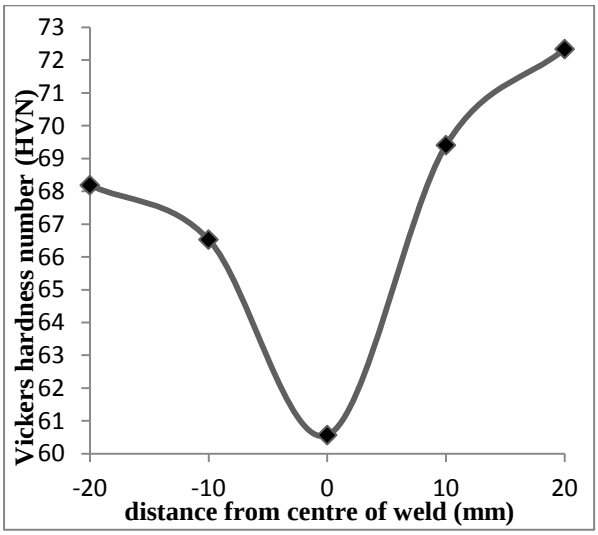

(c) for Trial 03

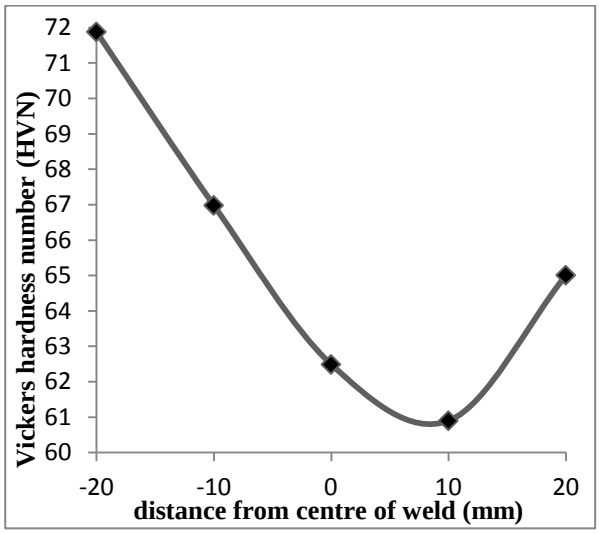

(d) for Trial 04

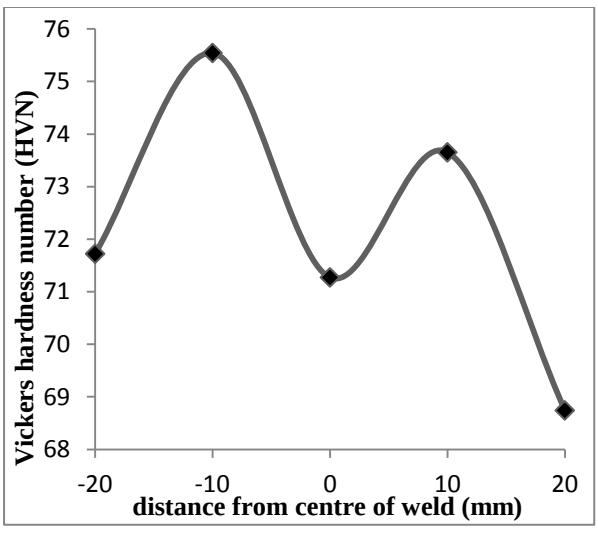

(e) for Trial 05

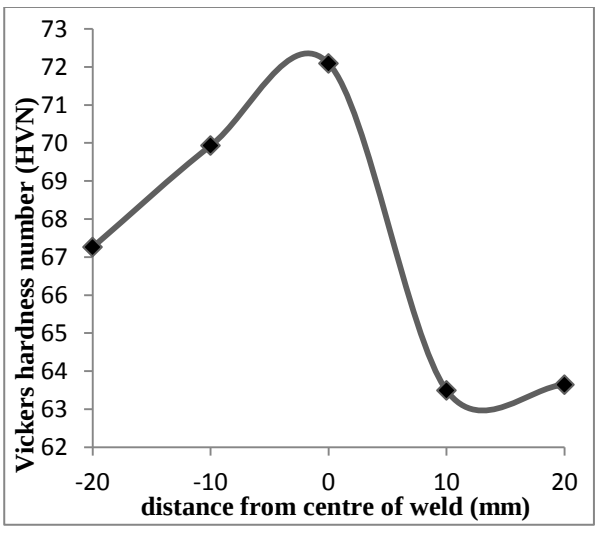

(f) for Trial 06

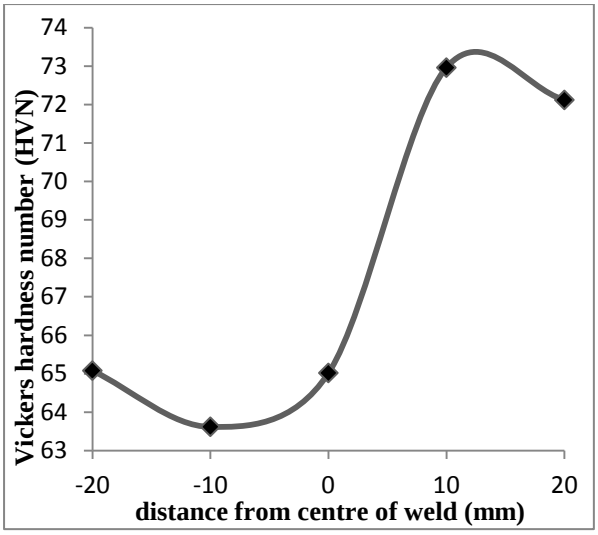

(g) for Trial 07

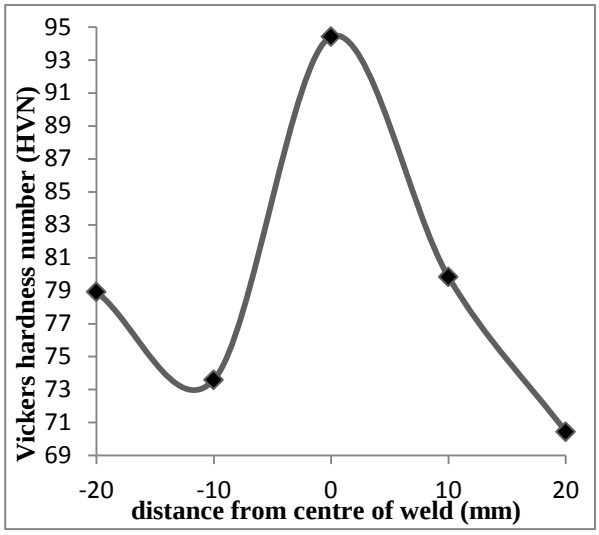

(h) for Trial 08

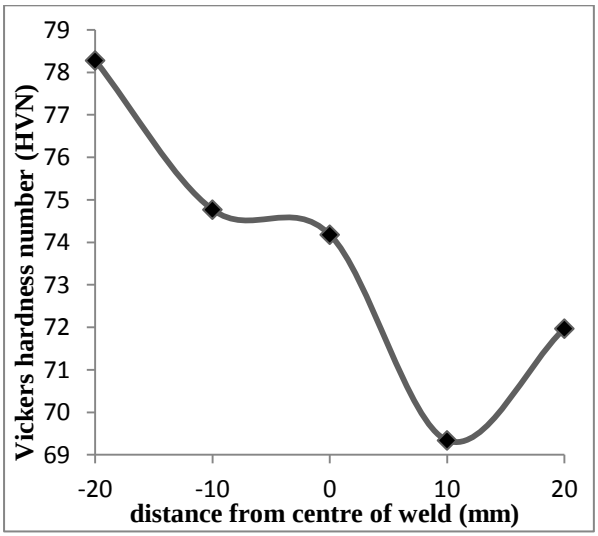

(i) for Trial 09

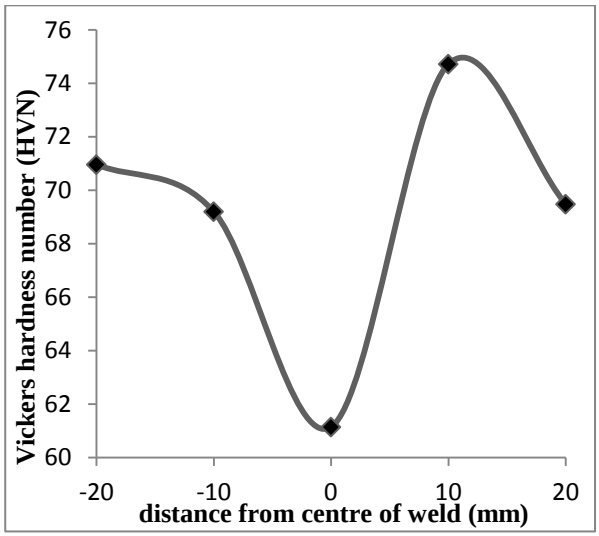

(j) for Trial 10

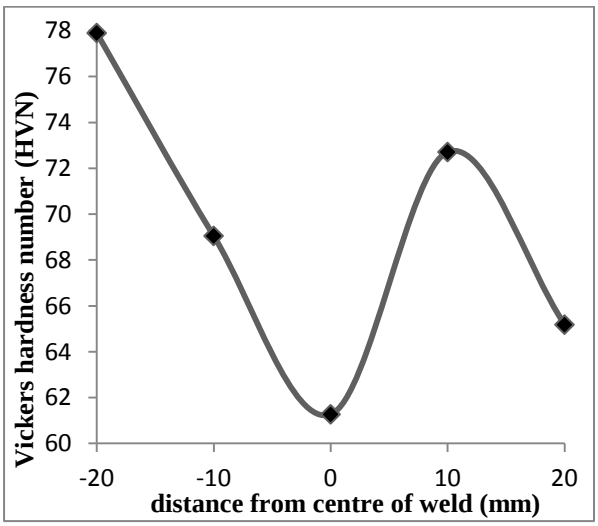

(k) for Trial 11

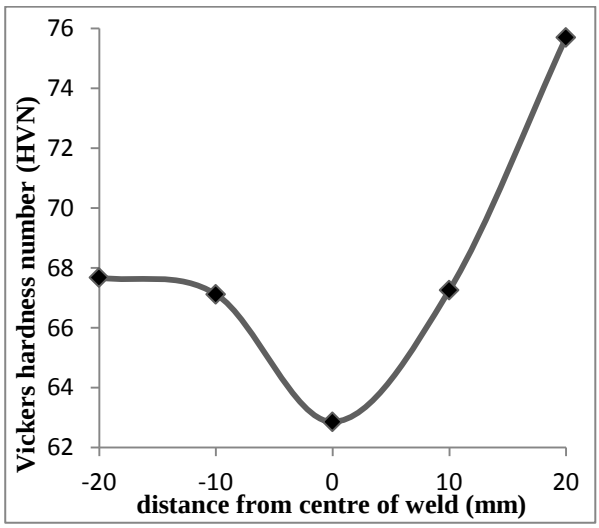

(l) for Trial 12

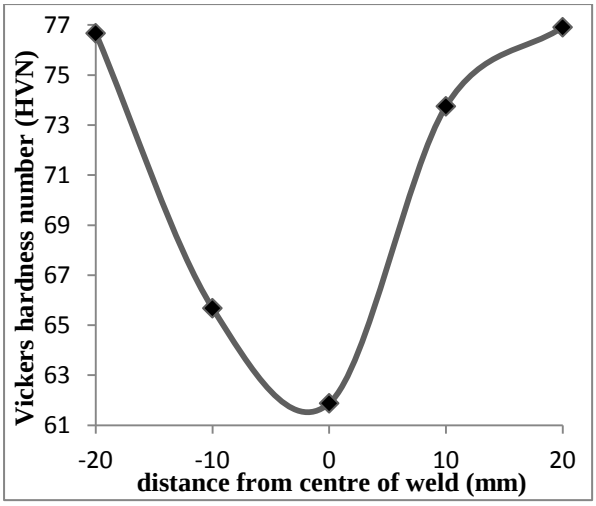

(m) for Trial 13

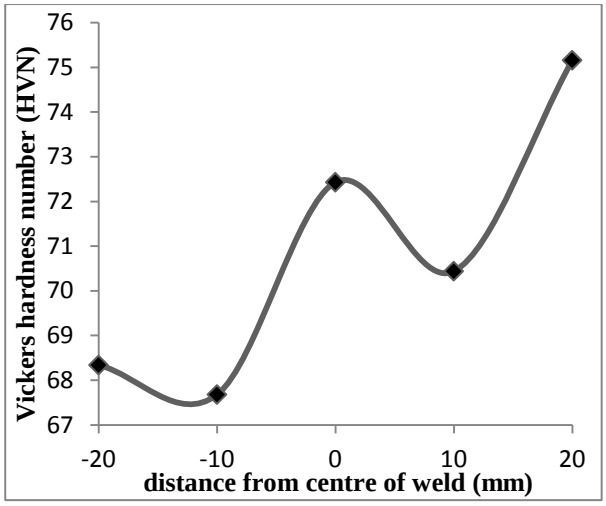

(n) for Trial 14

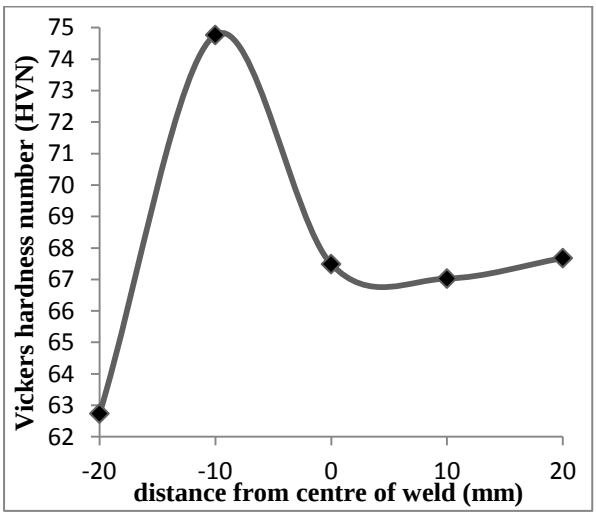

(o) for Trial 15

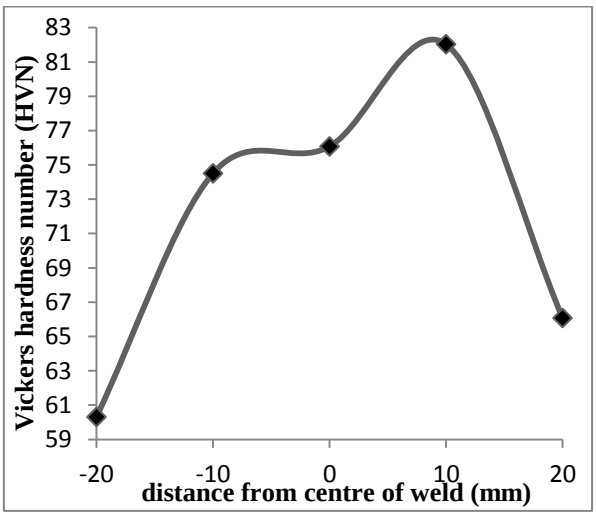

(p) for Trial 16

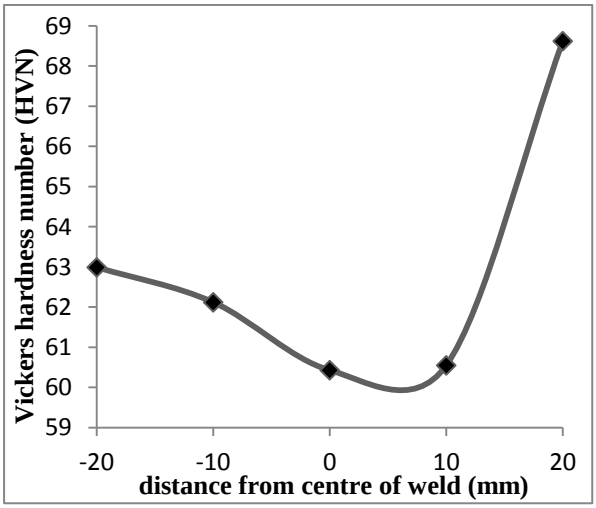

(q) for Trial 17

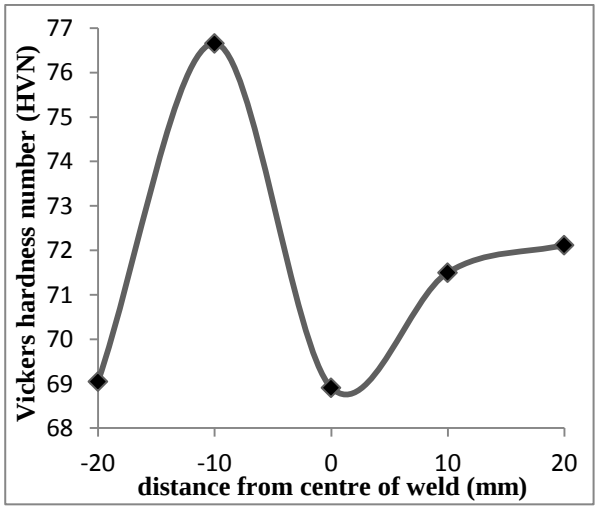

(r) for Trial 18

FIGURE 6.2 (a-r) – Variation of microhardness of different trials at weld region

In order to summarize the results of microhardness test, for all 18 sets of experiments, the variation in microhardness value at centre, 10 mm, -10 mm, 20 mm and -20 mm from weld centre is shown in Figure 6.3.

From Figure 6.3, it was observed that

- At weld centre, maximum microhardness of 94.42 HVN was obtained from specimen no. 8 and minimum microhardness of 60.43 HVN was obtained from specimen no. 17.
- At 10 mm from weld centre, maximum microhardness of 82.04 HVN was obtained from specimen no. 16 and minimum microhardness of 60.55 HVN was obtained from specimen no. 17.
- At -10 mm from weld centre, maximum microhardness of 75.66 HVN was obtained from specimen no. 18 and minimum microhardness of 60.02 HVN was obtained from specimen no. 2.
- At 20 mm from weld centre, maximum microhardness of 76.91 HVN was obtained from specimen no. 13 and minimum microhardness of 63.64 HVN was obtained from specimen no. 6.
- At -20 mm from weld centre, maximum microhardness of 78.93 HVN was obtained from specimen no. 8 and minimum microhardness of 60.31 HVN was obtained from specimen no. 16.

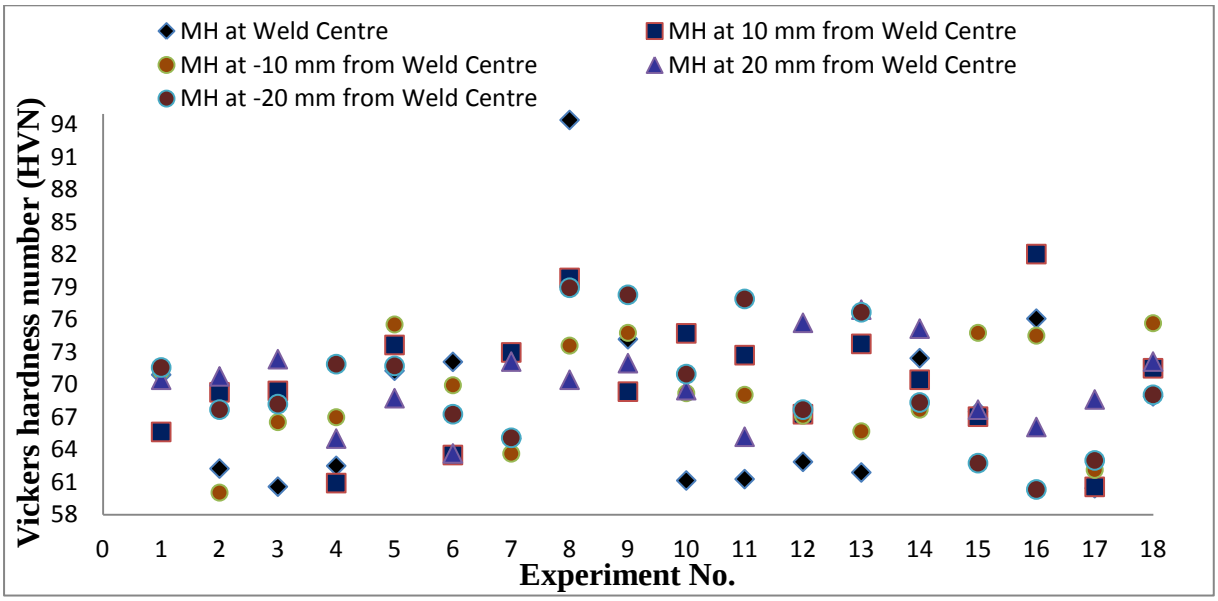

*MH represents Microhardness

FIGURE 6.3- Variation in microhardness at centre, 10 mm, -10 mm, 20 mm and -20 mm from weld centre

6.2 ANOVA FOR MICROHARDNESS AT WELD CENTRE

Table 6.2, column no. 5 consists of the values of microhardness at weld region for the eighteen trials. The experimental results for microhardness were analyzed using ANOVA and the mean value for all eight variables is given in Table 6.3. In Table 6.3 welding current with the highest rank 1 and is the most significant factor and preheat temperature with its lowest rank is least significant in affecting the microhardness. Main effect plots are shown in Figure 6.4 shows the variation in the microhardness with the change in the input factors i.e. electrode diameter, current, voltage, electrode stick-out, travel speed, preheat temperature, flux and edge including angle. It could be seen from the Figure 6.4 that welding current causes the most significant change in the microhardness with change in current. As the welding current increases from 350 Ampere to 450 Ampere, microhardness will also increase. As the edge including angle increases from 60 to 90 degree, microhardness will decrease. The change in flux and electrode stick-out also has some effect on the variation in the microhardness. Electrode diameter, voltage, preheat temperature and travel speed have very low effect on microhardness.

TABLE 6.3 Response table for mean of microhardness at weld centre

Level	Electrode Diameter (mm)	Current (amp)	Voltage (volt)	Electrode Stick-Out (mm)	Travel Speed (m/hr)	Preheat Temperature (^{o}C)	Flux	Edge Including Angle (degree)
1	70.35	63.16	66.25	66.13	68.44	70.43	71.29	72.35
2	65.83	67.94	70.34	65.36	70.93	66.90	64.73	67.96
3		73.17	67.68	72.79	64.91	66.95	68.26	63.97
Delta	4.52	10.01	4.09	7.42	6.02	3.53	6.55	8.39
Rank	**6**	**1**	**7**	**3**	**5**	**8**	**4**	**2**

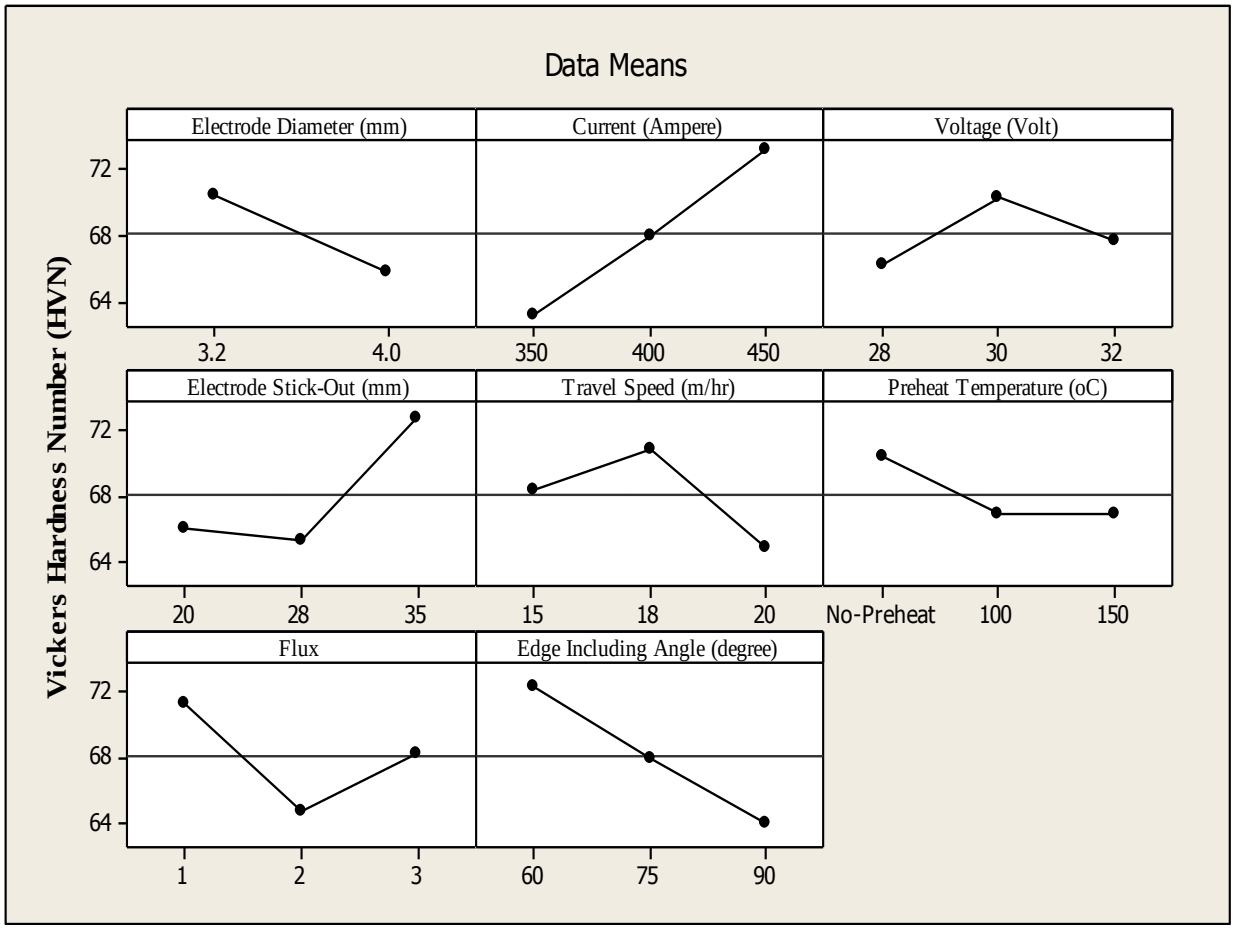

FIGURE 6.4- Main effect plot for microhardness at weld centre

6.3 DISCUSSION OF MICROHARDNESS

Microhardness measurement was taken at the weld pool interface. Five readings at different location were taken and analysis was done at the weld centre. It is clear from Figure 6.4 that maximum microhardness (Vickers hardness number) in weld centre is obtained from specimen no. 8 i.e. 94.42 HVN. The microhardness would be maximum when edge including angle should be 60 degree, flux should be of type 1 i.e. AUTOMELT B31 (Neutral), current should be 450 Ampere and electrode stick-out should be 35 mm. The increase in microhardness at the welding interface is generally due to oxidation processes which took place during welding processes.

CHAPTER-7

RESULTS AND DISCUSSIONS OF CHEMICAL COMPOSITION

7.1 CHEMICAL COMPOSITION OF WELD METAL

The composition of welded metal was found by using atomic absorption spectrometer. The specimen after spectroscopy are shown in Figure 7.1

FIGURE 7.1- Specimen after checking composition

Figure 7.2 (a-h) shows the variation in %age composition of different elements i.e. carbon, silicon, manganese, phosphorus, sulphur, nickel, copper and chromium.

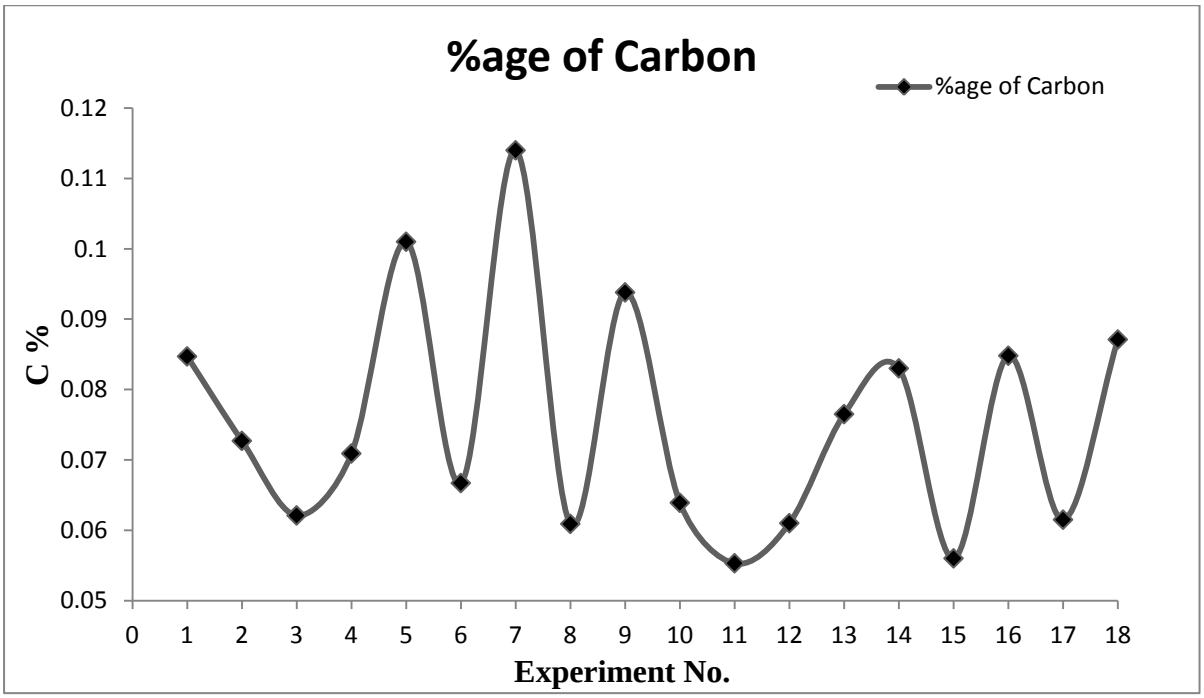

FIGURE 7.2 (a) – Variation in %age composition of carbon at weld centre

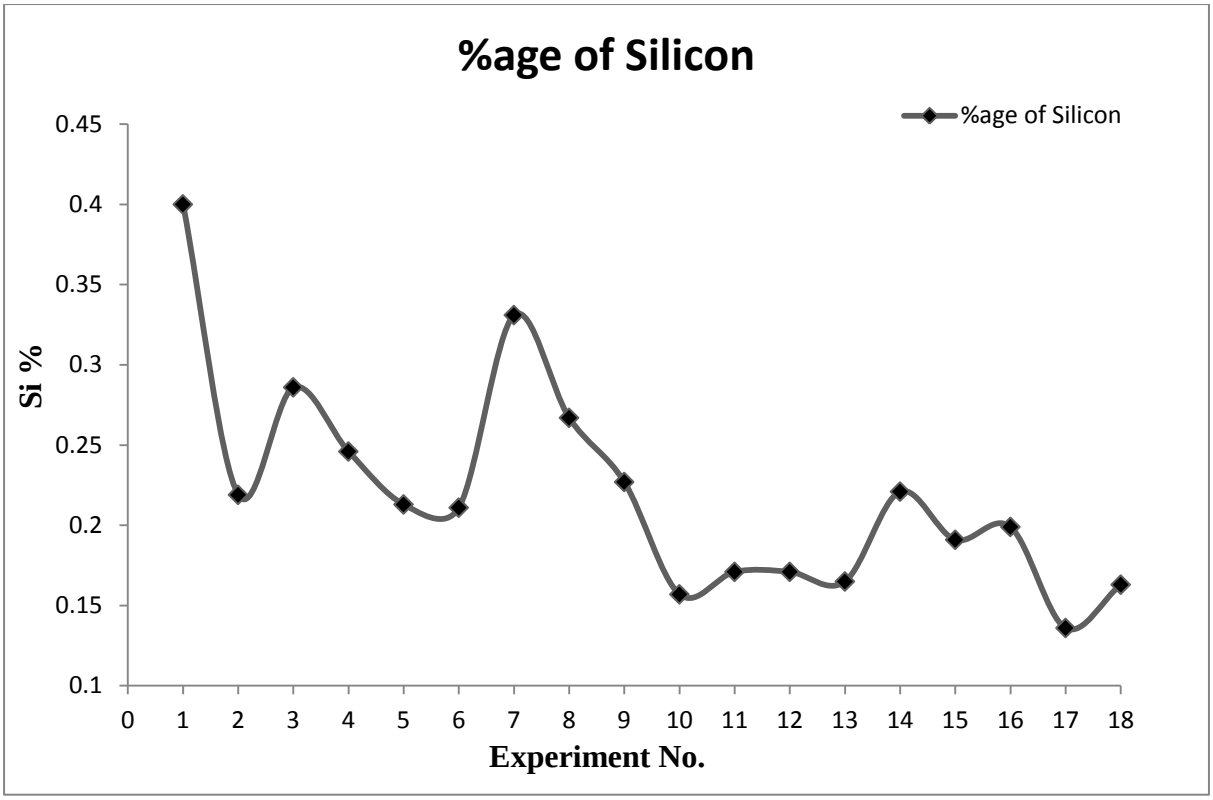

FIGURE 7.2 (b) - Variation in %age composition of silicon at weld centre

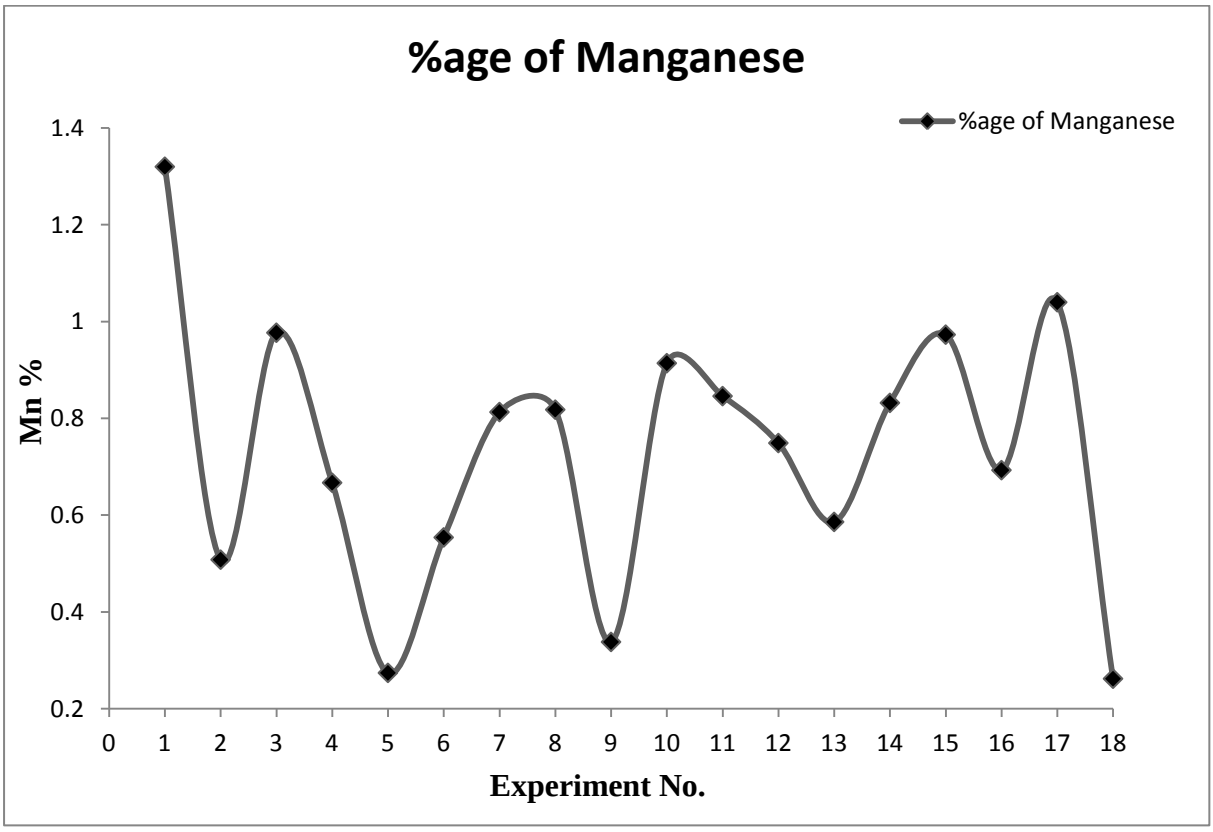

FIGURE 7.2 (c) - Variation in %age composition of manganese at weld centre

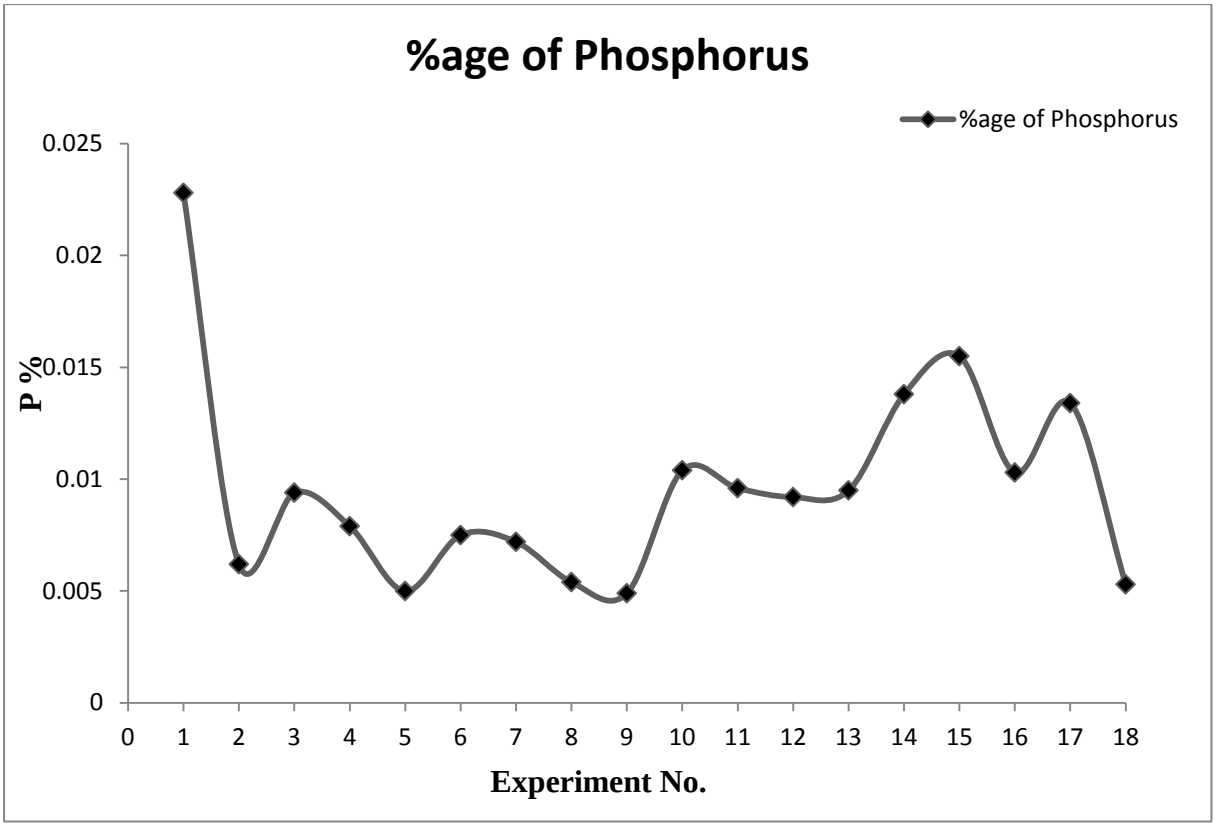

FIGURE 7.2 (d) - Variation in %age composition of phosphorus at weld

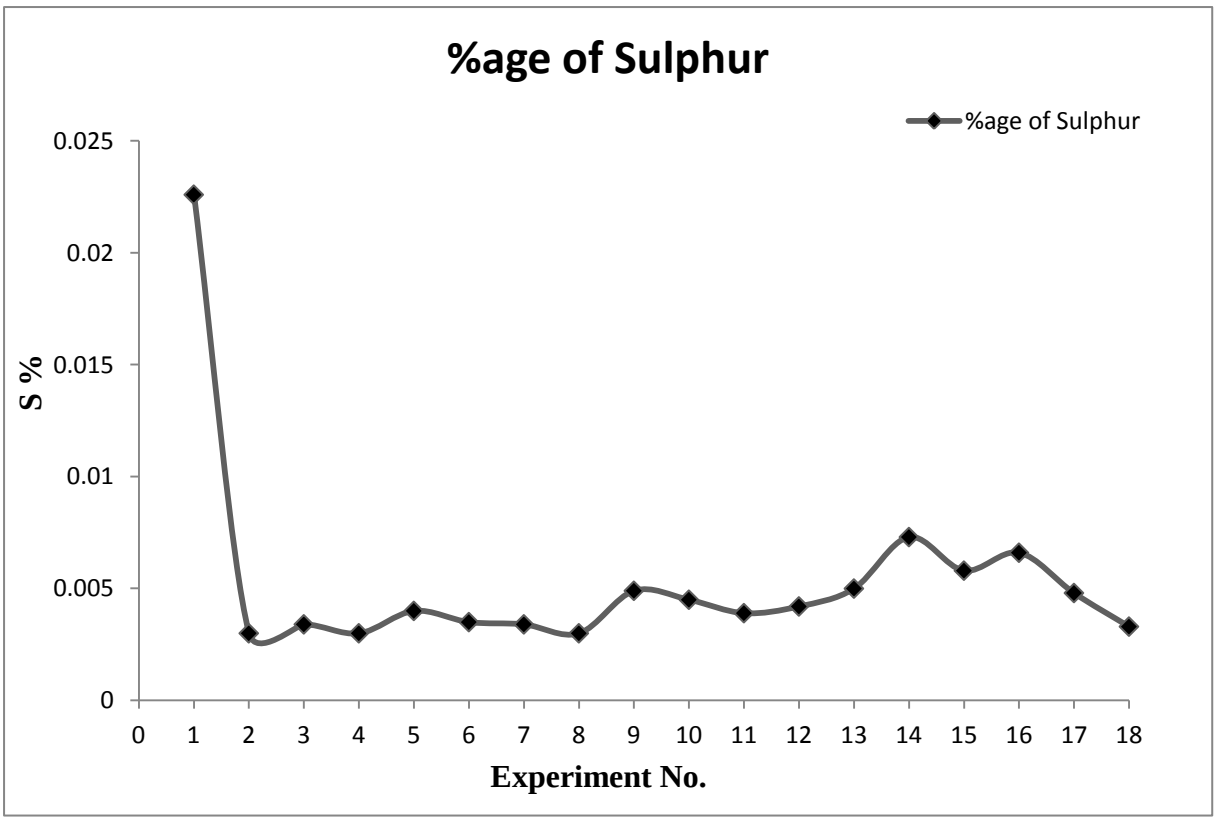

FIGURE 7.2 (e) - Variation in %age composition of sulphur at weld centre

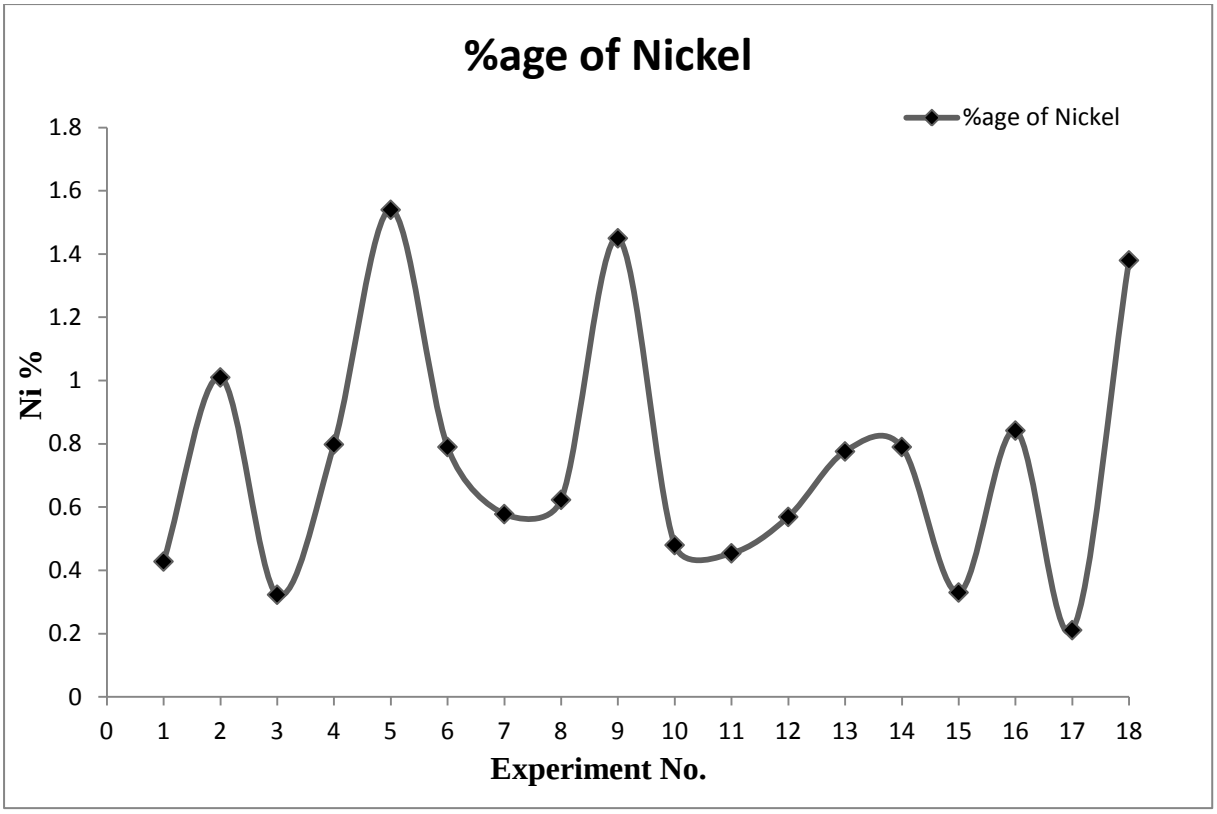

FIGURE 7.2 (f) - Variation in %age composition of nickel at weld centre

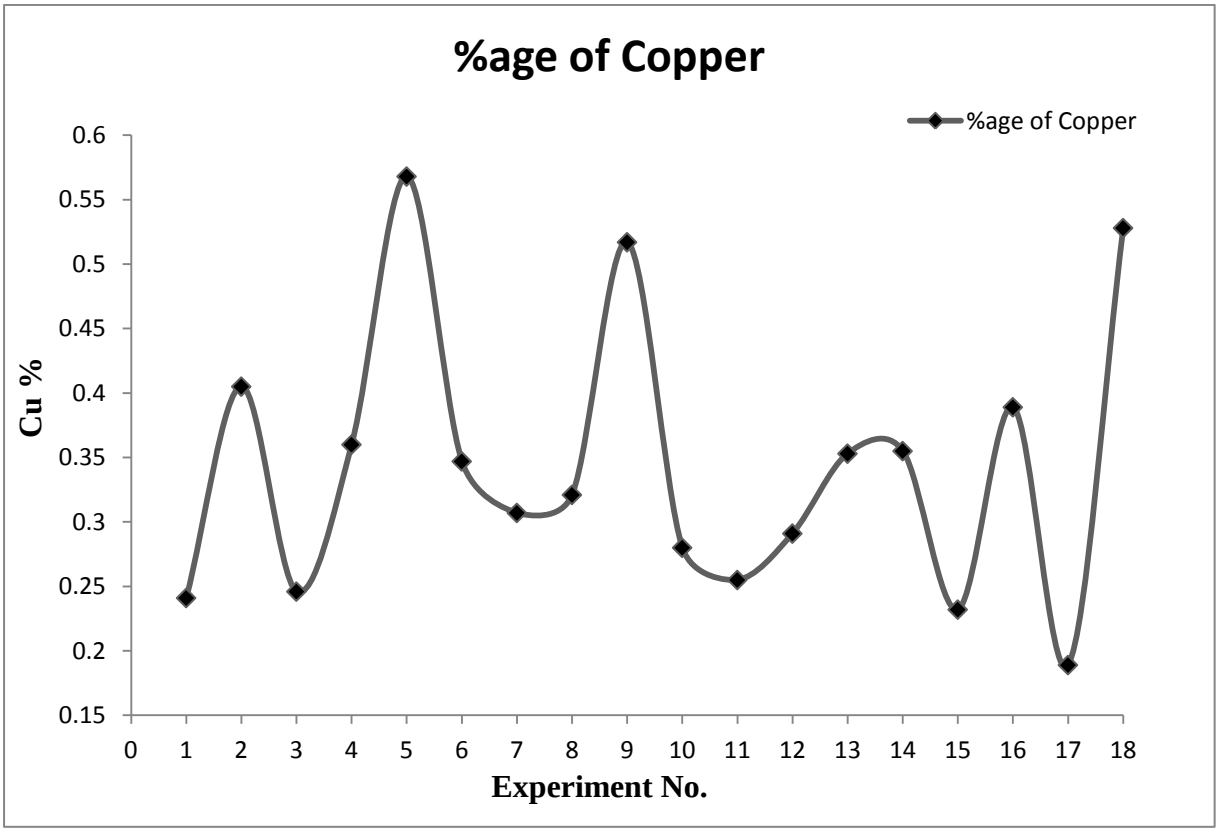

FIGURE 7.2 (g) - Variation in %age composition of copper at weld centre

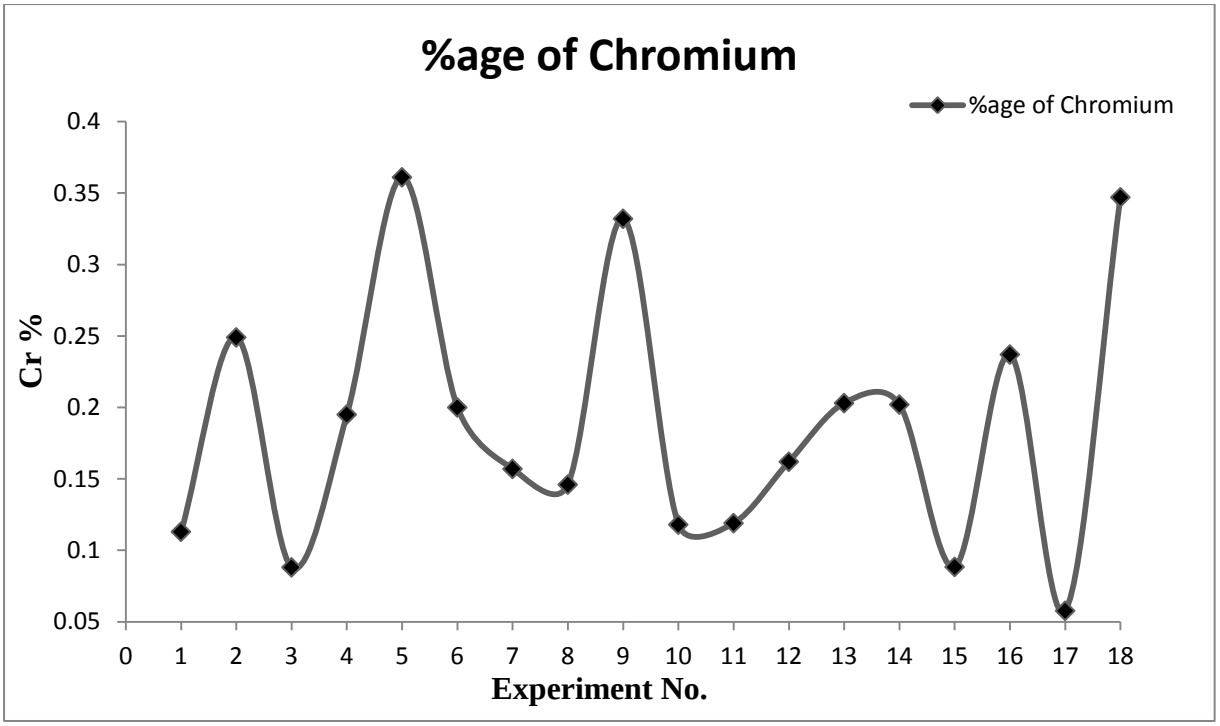

FIGURE 7.2 (h) - Variation in %age composition of chromium at weld centre

7.2 PERCENTAGE CHANGE IN CHEMICAL COMPOSITION

The Table 7.1-7.4 shows the %age difference in chemical contents after spectroscopy w.r.t base metal chemical composition.

TABLE 7.1 Percentage change in chemical composition of carbon and silicon

Exp. No.	Carbon %age (after spectroscopy)	Carbon %age in base metal	%age change in Carbon	Silicon %age (after spectroscopy)	Silicon %age in base metal	%age change in Silicon
1	0.0847	0.13	-34.846	0.4	0.25	60.000
2	0.0727	0.13	-44.077	0.219	0.25	-12.400
3	0.0621	0.13	-52.231	0.286	0.25	14.400
4	0.0709	0.13	-45.462	0.246	0.25	-1.600
5	0.101	0.13	-22.308	0.213	0.25	-14.800
6	0.0667	0.13	-48.692	0.211	0.25	-15.600
7	0.114	0.13	-12.308	0.331	0.25	32.400
8	0.0609	0.13	-53.154	0.267	0.25	6.800
9	0.0938	0.13	-27.846	0.227	0.25	-9.200
10	0.0639	0.13	-50.846	0.157	0.25	-37.200
11	0.0553	0.13	-57.462	0.171	0.25	-31.600
12	0.061	0.13	-53.077	0.171	0.25	-31.600
13	0.0765	0.13	-41.154	0.165	0.25	-34.000
14	0.083	0.13	-36.154	0.221	0.25	-11.600
15	0.056	0.13	-56.923	0.191	0.25	-23.600
16	0.0848	0.13	-34.769	0.199	0.25	-20.400
17	0.0615	0.13	-52.692	0.136	0.25	-45.600
18	0.0871	0.13	-33.000	0.163	0.25	-34.800

TABLE 7.2 Percentage change in chemical composition of manganese and phosphorus

Exp. No.	Manganese %age (after spectroscopy)	Manganese %age in base metal	%age change in Manganese	Phosphorus %age (after spectroscopy)	Phosphorus %age in base metal	%age change in Phosphorus
1	1.32	0.39	238.462	0.0228	0.003	660.000
2	0.508	0.39	30.256	0.0062	0.003	106.667
3	0.977	0.39	150.513	0.0094	0.003	213.333
4	0.667	0.39	71.026	0.0079	0.003	163.333
5	0.274	0.39	-29.744	0.005	0.003	66.667
6	0.554	0.39	42.051	0.0075	0.003	150.000
7	0.813	0.39	108.462	0.0072	0.003	140.000
8	0.818	0.39	109.744	0.0054	0.003	80.000
9	0.338	0.39	-13.333	0.0049	0.003	63.333
10	0.914	0.39	134.359	0.0104	0.003	246.667
11	0.846	0.39	116.923	0.0096	0.003	220.000
12	0.749	0.39	92.051	0.0092	0.003	206.667
13	0.586	0.39	50.256	0.0095	0.003	216.667
14	0.832	0.39	113.333	0.0138	0.003	360.000
15	0.973	0.39	149.487	0.0155	0.003	416.667
16	0.693	0.39	77.692	0.0103	0.003	243.333
17	1.04	0.39	166.667	0.0134	0.003	346.667
18	0.262	0.39	-32.821	0.0053	0.003	76.667

TABLE 7.3 Percentage change in chemical composition of sulphur and nickel

Exp. No.	Sulphur %age (after spectroscopy)	Sulphur %age in base metal	%age change in Sulphur	Nickel %age (after spectroscopy)	Nickel %age in base metal	%age change in Nickel
1	0.0226	0.01	126.000	0.428	1.76	-75.682
2	0.003	0.01	-70.000	1.01	1.76	-42.614
3	0.0034	0.01	-66.000	0.323	1.76	-81.648
4	0.003	0.01	-70.000	0.798	1.76	-54.659
5	0.004	0.01	-60.000	1.54	1.76	-12.500
6	0.0035	0.01	-65.000	0.79	1.76	-55.114
7	0.0034	0.01	-66.000	0.578	1.76	-67.159
8	0.003	0.01	-70.000	0.623	1.76	-64.602
9	0.0049	0.01	-51.000	1.45	1.76	-17.614
10	0.0045	0.01	-55.000	0.48	1.76	-72.727
11	0.0039	0.01	-61.000	0.454	1.76	-74.205
12	0.0042	0.01	-58.000	0.569	1.76	-67.670
13	0.005	0.01	-50.000	0.776	1.76	-55.909
14	0.0073	0.01	-27.000	0.79	1.76	-55.114
15	0.0058	0.01	-42.000	0.33	1.76	-81.250
16	0.0066	0.01	-34.000	0.842	1.76	-52.159
17	0.0048	0.01	-52.000	0.211	1.76	-88.011
18	0.0033	0.01	-67.000	1.38	1.76	-21.591

TABLE 7.4 Percentage change in chemical composition of copper and chromium

Exp. No.	Copper %age (after spectroscopy)	Copper %age in base metal	%age change in Copper	Chromium %age (after spectroscopy)	Chromium %age in base metal	%age change in Chromium
1	0.241	0.5	-51.800	0.113	0.41	-72.439
2	0.405	0.5	-19.000	0.249	0.41	-39.268
3	0.246	0.5	-50.800	0.0881	0.41	-78.512
4	0.36	0.5	-28.000	0.195	0.41	-52.439
5	0.568	0.5	13.600	0.361	0.41	-11.951
6	0.347	0.5	-30.600	0.2	0.41	-51.220
7	0.307	0.5	-38.600	0.157	0.41	-61.707
8	0.321	0.5	-35.800	0.146	0.41	-64.390
9	0.517	0.5	3.400	0.332	0.41	-19.024
10	0.28	0.5	-44.000	0.118	0.41	-71.220
11	0.255	0.5	-49.000	0.119	0.41	-70.976
12	0.291	0.5	-41.800	0.162	0.41	-60.488
13	0.353	0.5	-29.400	0.203	0.41	-50.488
14	0.355	0.5	-29.000	0.202	0.41	-50.732
15	0.232	0.5	-53.600	0.0884	0.41	-78.439
16	0.389	0.5	-22.200	0.237	0.41	-42.195
17	0.189	0.5	-62.200	0.0577	0.41	-85.927
18	0.528	0.5	5.600	0.347	0.41	-15.366

The results listed above in Table 7.1-7.4 are shown in Figure 7.3 (a-h) respectively

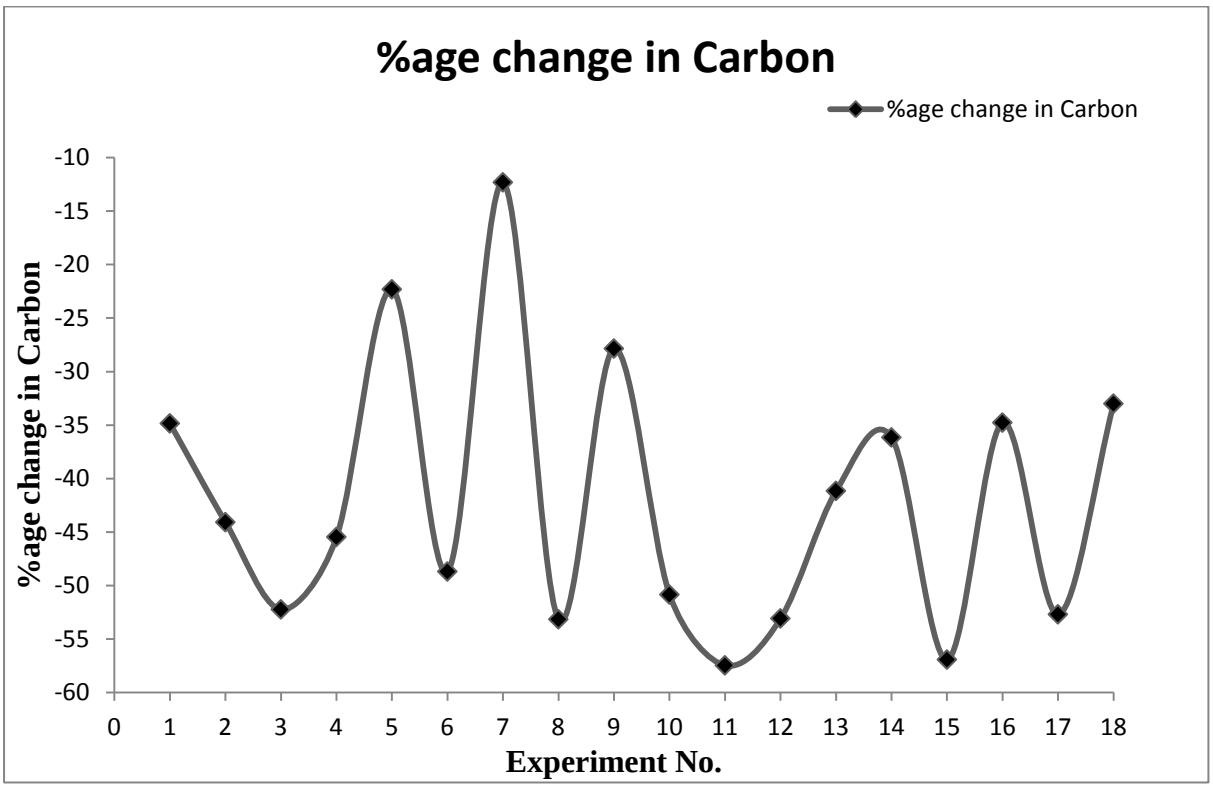

FIGURE 7.3 (a) - Variation in %age change in composition of carbon at weld centre

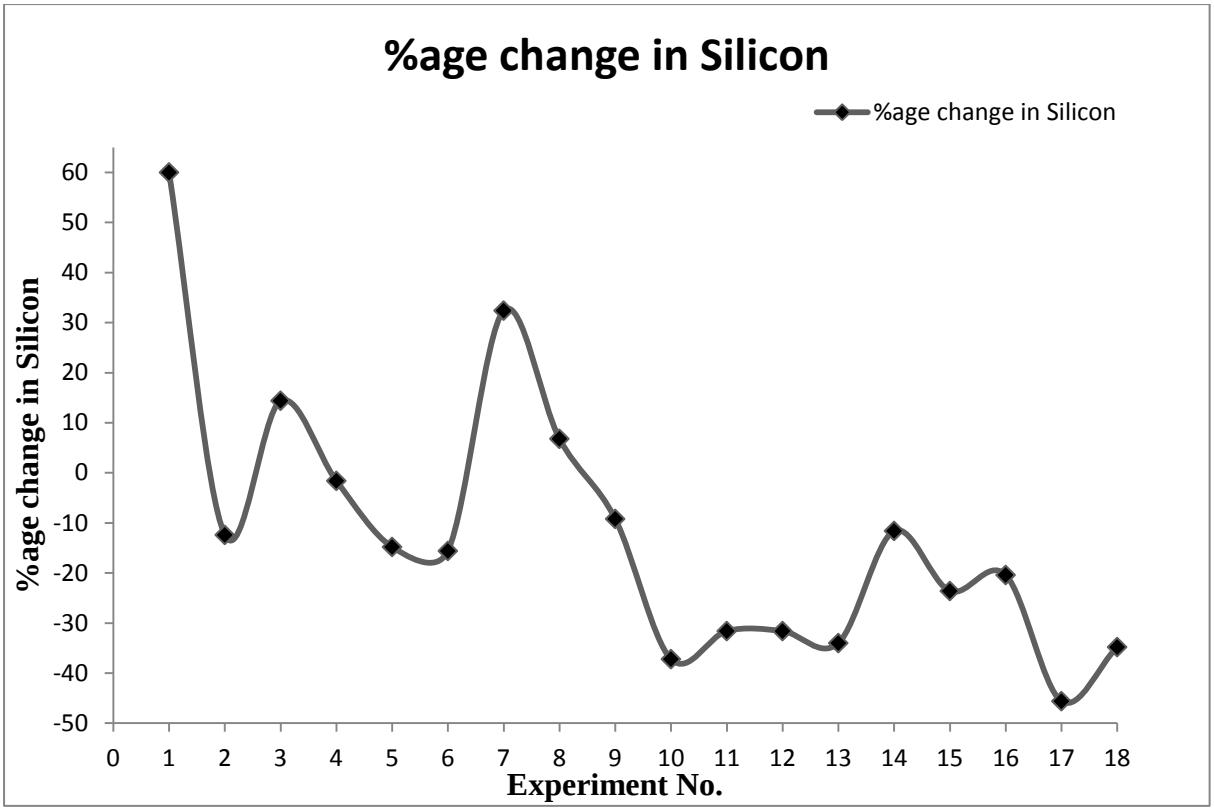

FIGURE 7.3 (b) - Variation in %age change in composition of silicon at weld centre

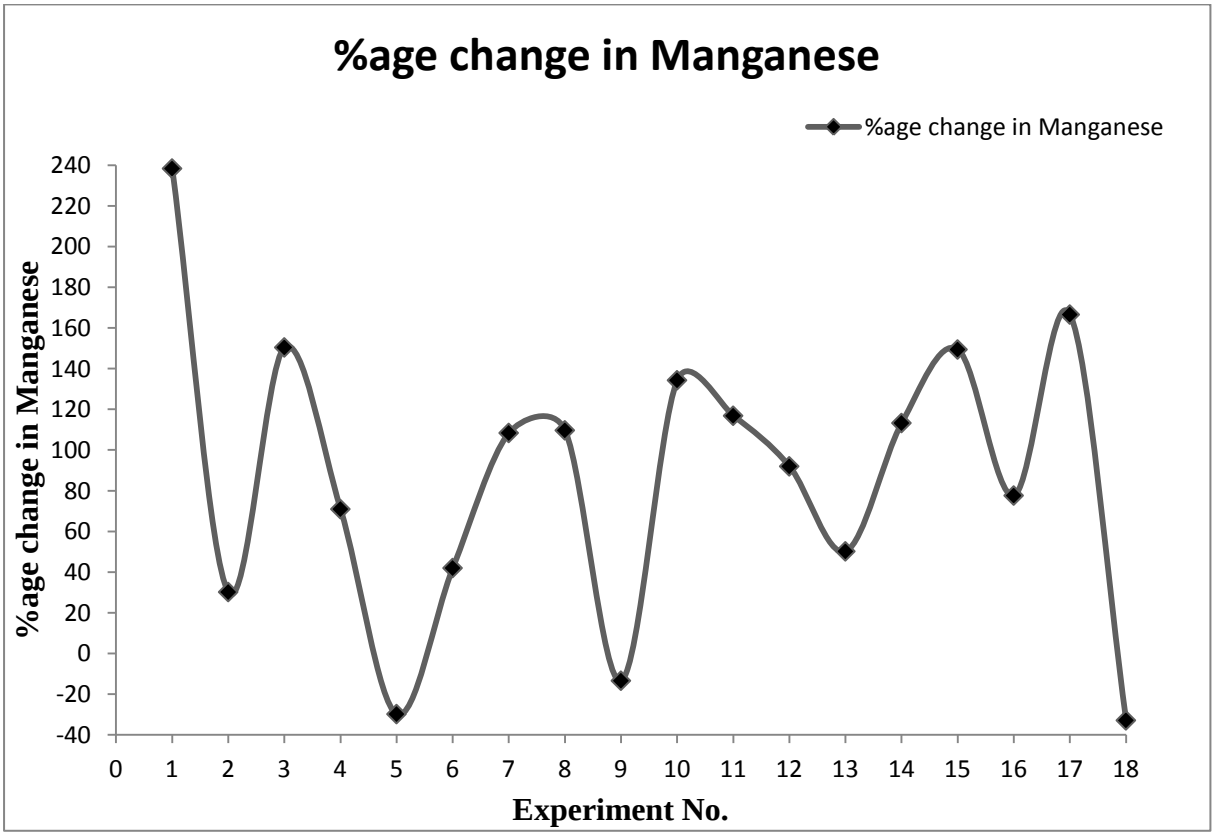

FIGURE 7.3 (c) - Variation in %age change in composition of manganese at weld centre

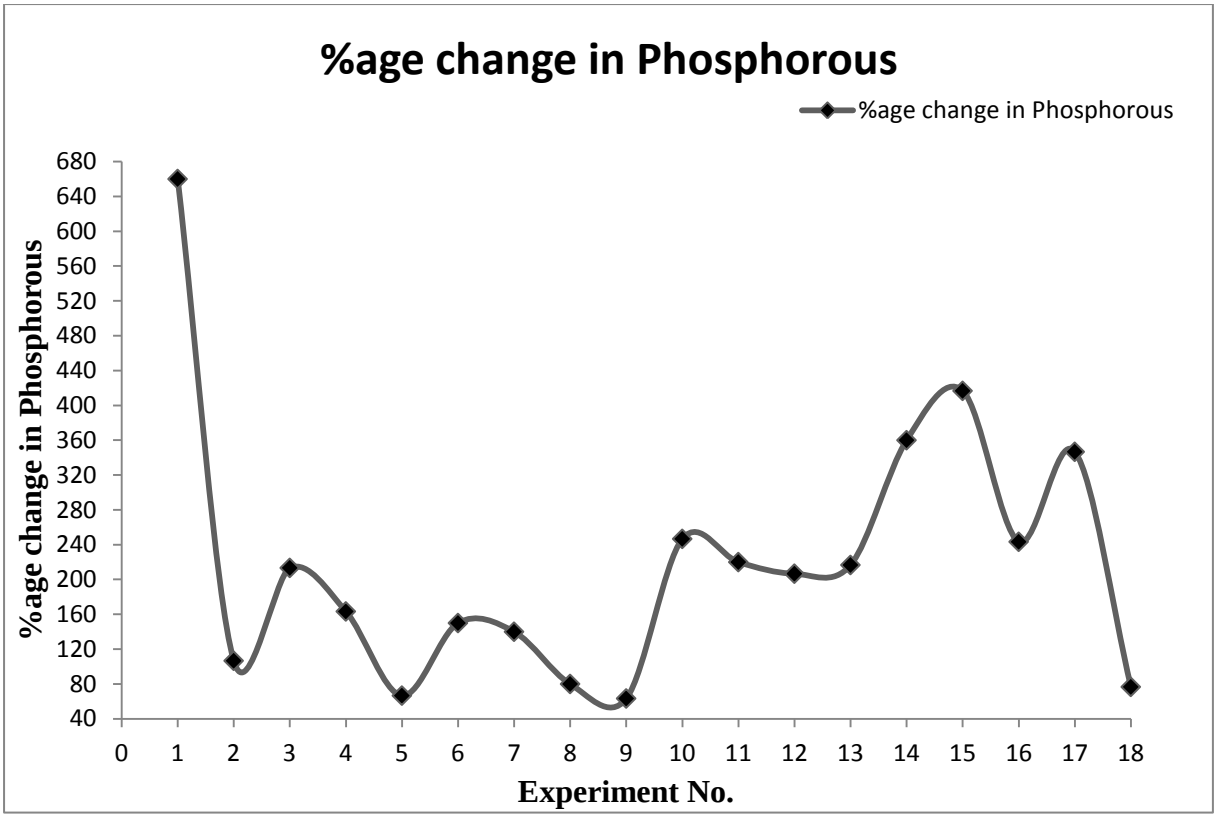

FIGURE 7.3 (d) -Variation in %age change in composition of phosphorus at weld centre

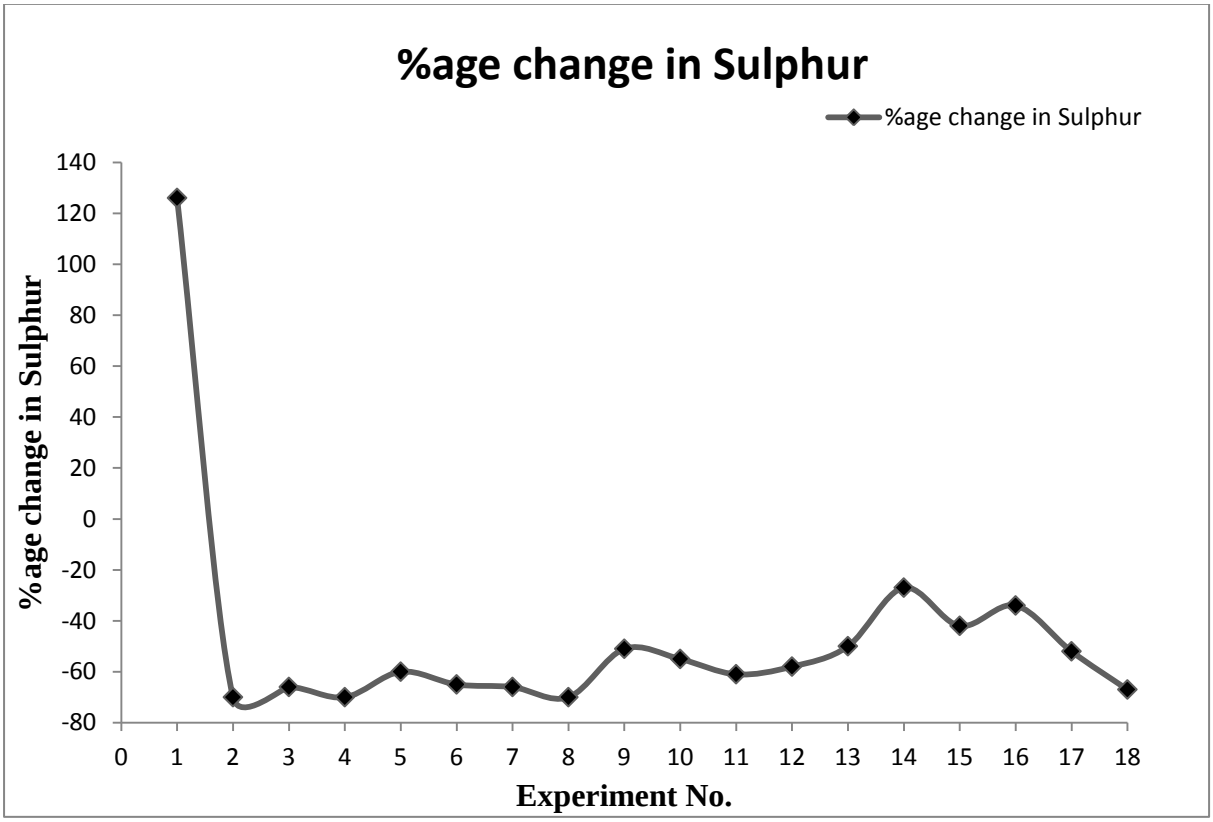

FIGURE 7.3 (e) - Variation in %age change in composition of sulphur at weld centre

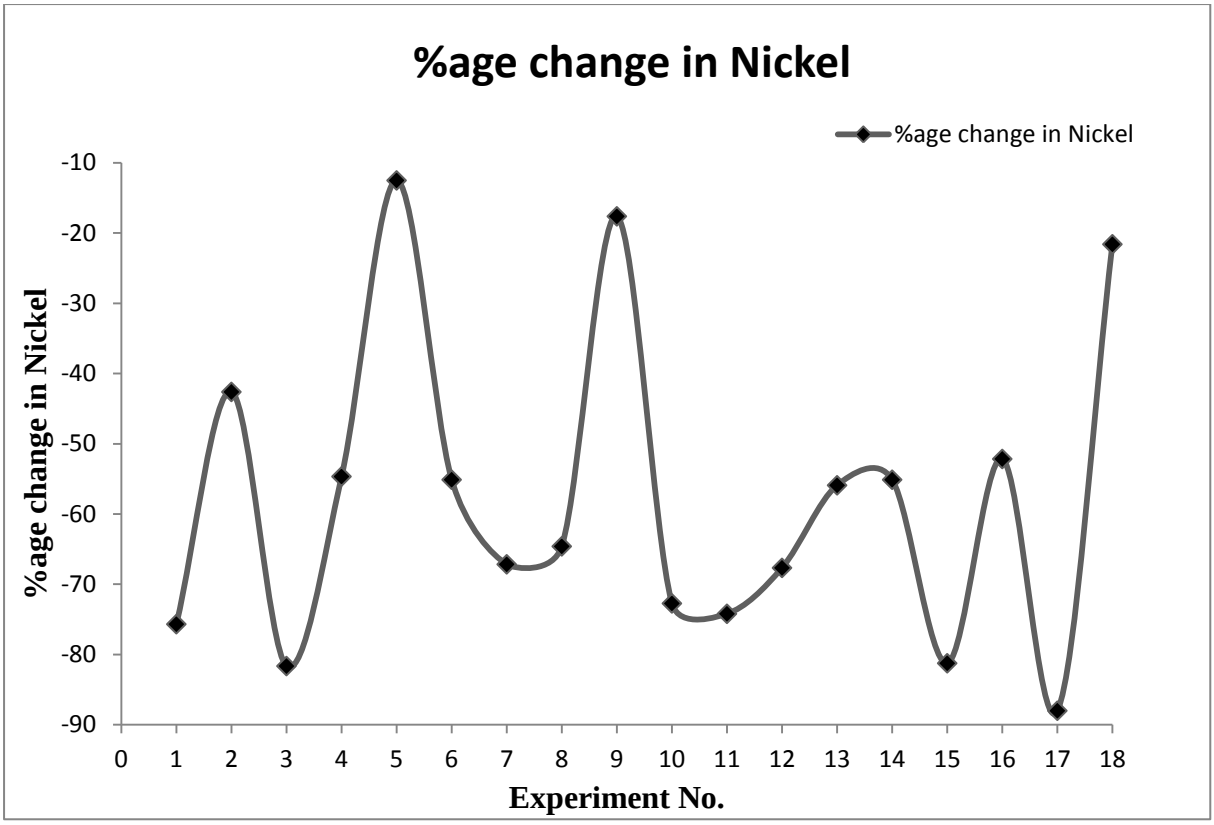

FIGURE 7.3 (f) - Variation in %age change in composition of nickel at weld centre

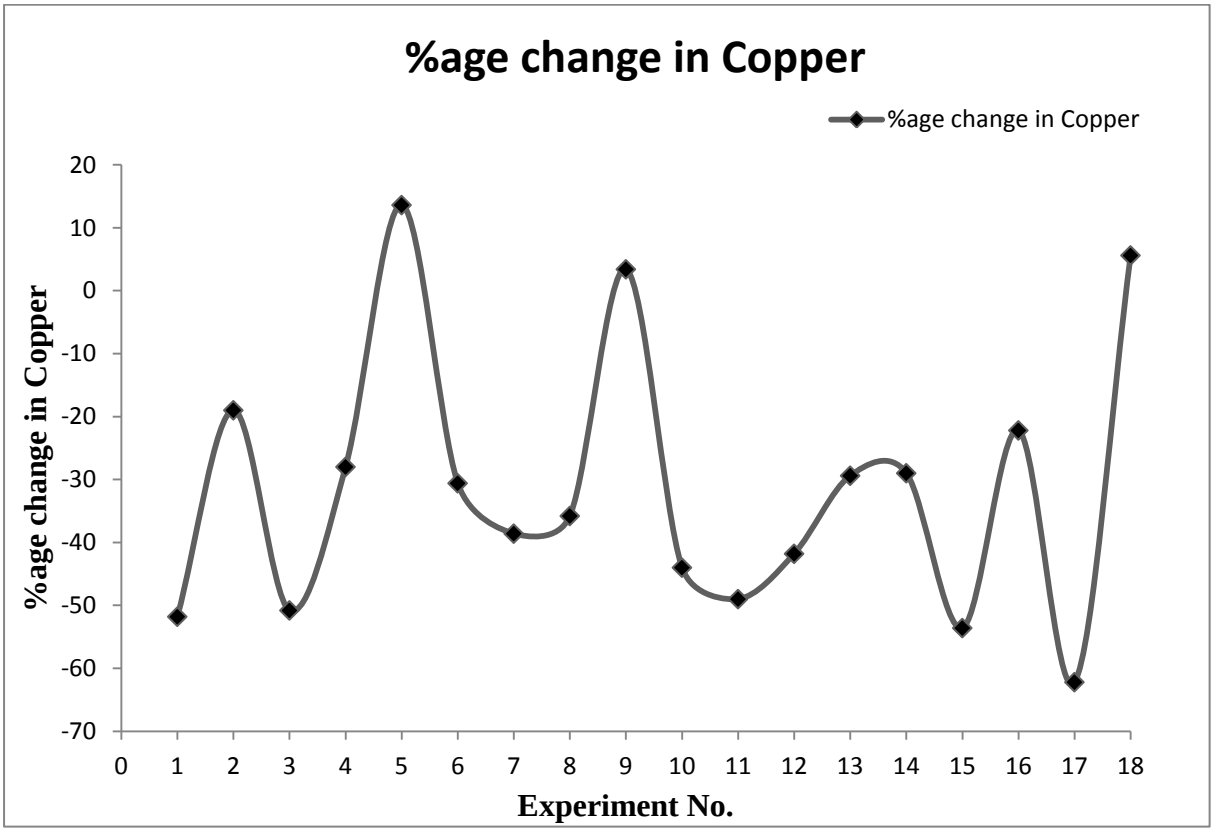

FIGURE 7.3 (g) - Variation in %age change in composition of copper at weld centre

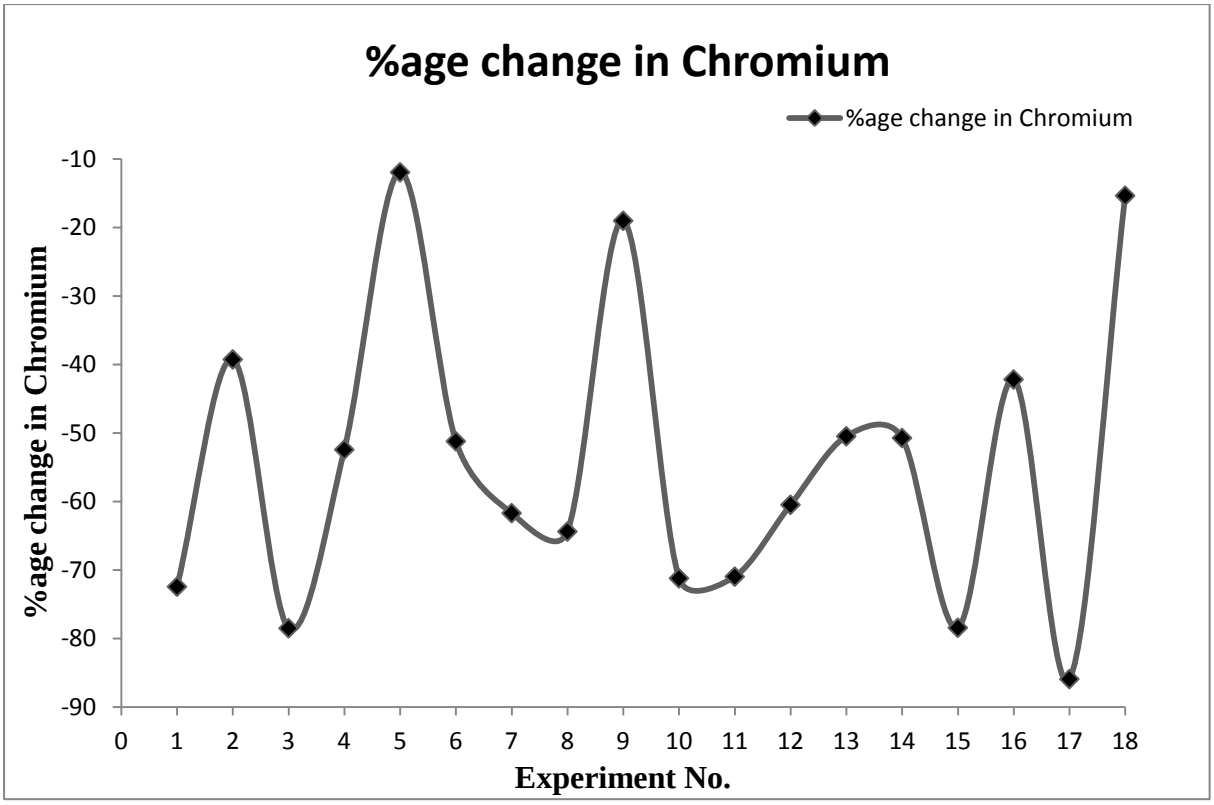

FIGURE 7.3 (h) - Variation in %age change in composition of chromium at weld

7.3 DISCUSSION OF CHEMICAL COMPOSITION

It is clear from Figure 7.3 (a-h) that percentage change in phosphorous was increasing in weld region but carbon, sulphur, nickel and chromium contents were decreasing whereas for silicon, manganese and copper shows the mixed trend. So, it concludes that some compounds of flux goes into the weld region.

CHAPTER-8

SUMMARY, CONCLUSIONS & FUTURE SCOPE

8.1 RESULTS

The effect of eight input factors was studied on the tensile strength, toughness, microhardness and chemical composition using the L18 Taguchi experimental design. Tensile strength, toughness at room temperature, toughness at -40 ^{o}C and microhardness at weld centre were measured as the response parameters. ANOVA was completed for all the responses to analyze the significance of the input factors. Main effect plots for mean values has been developed and analyzed. Table 8.1 shows the value of responses measured.

TABLE 8.1 Table for mean value of results

Experiment No.	**Mean Tensile Strength (N/mm^2)**	**Mean Toughness at room temperature (Joule)**	**Mean Toughness at -40 ^{o}C (Joule)**	**Mean Microhardness at weld centre (HVN)**
1	522.840	201	98	70.90
2	554.069	250	123	62.24
3	525.982	255	128	60.57
4	443.687	172	108	62.49
5	527.750	242	121	71.27
6	530.892	221	113	72.09
7	567.621	245	123	65.02
8	482.183	235	128	94.42
9	590.011	196	119	74.18
10	583.333	204	110	61.14
11	601.010	231	116	61.27
12	606.706	206	103	62.86
13	561.728	191	123	61.88
14	588.047	177	93	72.43
15	544.052	186	114	67.49
16	594.040	199	120	76.08
17	570.370	181	111	60.43
18	623.597	233	131	68.91

8.1.1 Tensile Strength

- Electrode Diameter, welding current and travel speed was found as the most significant factor with p value of 0.006, 0.036 and 0.049 respectively. Voltage, electrode stick-out, preheat temperature, flux and edge including angle did not show any significant effect on tensile strength.
- The mean tensile strength using the optimal condition would be 616.398 ± 38.26 N/mm^2 with electrode diameter should be 4 mm, welding current should be 450 Ampere and travel speed should be 15 m/hr.

8.1.2 Toughness at Room Temperature

- Electrode diameter, electrode stick-out, current, preheat temperature, voltage and flux was found as the most significant factor with p value of 0.007, 0.009, 0.015, 0.018, 0.031 and 0.039 respectively. Travel speed and edge including angle did not show any significant effect on toughness at room temperature.
- The mean toughness at room temperature using the optimal condition would be 279 ± 22.13 Joule with electrode diameter should be 3.2 mm, electrode stick-out should be 28 mm, welding current should be 350 Ampere, preheat temperature should be 150 ^oC and welding voltage should be 30 Volts and flux should be of type 3 i.e. GEEFLUX 541 (Basic).

8.1.3 Toughness at -40 ^oC

- Flux, current and electrode stick-out was found as a most significant factor with p value of 0.023, 0.033 and 0.042. Electrode diameter, voltage, travel speed, preheat temperature and edge including angle did not show any significant effect on toughness at -40 ^oC.
- The mean toughness at room temperature using the optimal condition would be 133.666 ± 10.87 Joule with flux should be of type 3 i.e. GEEFLUX 541 (Basic), current should be 450 Ampere and electrode stick-out should be 28 mm.

8.1.4 Microhardness at weld centre

- Current was found as the most significant factors that affect microhardness at weld centre.

- As the welding current increases from 350 Ampere to 450 Ampere, microhardness will also increase. As the edge including angle increases from 60 to 90 degree, microhardness will decrease.
- The microhardness would be maximum when edge including angle should be 60 degree, flux should be of type 1 i.e. AUTOMELT B31 (Neutral), current should be 450 Ampere and electrode stick-out should be 35 mm.
- Microhardness is greatly affected by the composition of flux. Contribution of flux type 1 and 3 is more as compared to flux 2 towards the micro hardness.

8.1.5 Chemical Composition

- Percentage change in phosphorous was increasing in weld region but carbon, sulphur, nickel and chromium contents were decreasing whereas for silicon, manganese and copper shows the mixed trend. So, it concludes that some compounds of flux goes into the weld region.

8.2 CONCLUSIONS

The present study was carried out to study the effect of process parameters on weld joint quality during submerged arc welding of HSLA steel. The process parameters that has been considered for changing are current, voltage, travel speed, electrode diameter, flux composition, pre heating of workpiece, electrode stick-out and angle of edge preparation were varied at different levels. The following conclusions have been drawn from the study-

- Welding current was found to be the most significant factor that affects the tensile strength, toughness and microhardness.
- The flux composition did not show any significant affect on tensile strength, but had a major effect on impact strength and microhardness.
- Tensile strength is majorly affected by electrode diameter, but did not show any significant effect on microhardness and toughness at -40 ^{o}C.
- Travel speed did not show any significant effect on microhardness and toughness, but had a major effect on tensile strength.
- Voltage has no significant effect on tensile strength, toughness at -40 ^{o}C and microhardness, but has a little affect on toughness at room temperature.
- Edge including angle did not show any significant affect on tensile strength and toughness, but had a major effect on microhardness.

- Preheating of workpiece did not show any significant effect on tensile strength, toughness at -40 ^{o}C and microhardness.
- Electrode stick-out has a significant effect on toughness, but did not show any significant effect on tensile strength and microhardness.

In addition to the present work further work can be done in following directions:

- There are lot of parameters (Current, voltage, travel speed, electrode diameter, flux composition, electrode stick-out, preheating of flux, edge including angle and preheating of workpiece) which can be varied individually to see their individual effects and combining these parameters to see their combine effect by experimental study & Taguchi method.
- Study the Effect of metal powder addition in order to increase toughness by using tabular electrode.
- Different flux can be made with different composition and study their effect on mechanical properties.
- Modeling of submerged arc welding process can be carried out by using finite element packages.

CHAPTER-9

REFERENCES

1) Jonathan S. Ogborn, the Lincoln Electric Company, "Welding, Brazing and Soldering", ASM Handbook, Volume-6, pp. 618-641, ISBN 0-87170-377-7(V.1), 1993.
2) www.niir.org/g/c/ni-167/6.jpg, downloaded on Dated-Nov, 29-2011.
3) www.twi.co.uk/services/technical-information/job-knowledge-16-equipment-for-submerged-arc-welding-apr1996/, downloaded on Dated-Dec, 08-2011.
4) ESAB, "Technical Handbook on Submerged Arc Welding" Reg. No: XA00136020 05, 2008.
5) Plessis John Du, "Control of Diffusible Weld Metal Hydrogen through Arc Chemistry modification", University of Pretoria, 2006.
6) R. S. Parmar, "Welding processes and technology", 2th Ed, 2008.
7) Larry Jeffus, "Welding Principles and Application", Thomsom Delmer Learning, 2004.
8) http://www.gowelding.com/weld/hotc.jpg, downloaded on Dated-May, 13-2012.
9) http://www.exponent.com/files/Uploads/Images/Mechanical/Project_experience_Malongo%20_2_.jpg, downloaded on Dated-May, 13-2012.
10) http://www.esab.com/global/en/education/images/Lean-Duplex-Porosity-formed surface-breaking.jpg, downloaded on Dated-May, 13-2012.
11) Vincent Van Der Mee, Fred Neessen, "Development of High Strength Steel Consumables from Project to Product", Lincoln Smitweld, Netherlands, 2007.
12) http://www.chasealloys.co.uk/steel/alloying-elements-in-steel/, downloaded on Dated-May, 13-2012.
13) Saurav Datta, A. Bandyopadhyay, Pradip Kumar Pal, "Application of Taguchi philosophy for parametric optimization of bead geometry and HAZ width in submerged arc welding using a mixture of fresh flux and fused flux", Int. J. Adv. Manufacturing Technology, Volume 36, pp. 689-698, 2008.
14) A. Patnaik, S. Biswas, S.S. Mahapatra, "An evolutionary approach to parameter optimisation of submerged arc welding in the hard facing process", Int. J. Manufacturing Research, Volume 2, pp. 462–483, 2007.
15) S.C. Moi, A. Bandyopadhyay, P.K. Pal, "Submerged arc welding with a mixture of fresh flux and fused Slag", Proc National Seminar on Advances in Material & Processing, IIT Roorkee, 2001.

16) E.A. Elsayed, A. Chen, "Optimal levels of process parameters for products with multiple characteristics", International Journal Production Research, Volume 31, pp. 1117-32, 1993.
17) R. Myers, D. Montgomery, “Response Surface Methodology. Wiley”, New York, 1982.
18) Aniruddha Ghosh ,Somnath Chattopadhyaya, R.K.Das, “Effect of Heat input on Submerged Arc Welded Plates” Procedia Engineering, Volume 10, pp. 2791–2796, 2011.
19) P Kumar, A Batish, A Bhattacharya, and R K Duvedi, “Effect of process parameters on microhardness and microstructure of heat affected zone in submerged arc welding”, Proceedings of the Institution of Mechanical Engineers, Part B: Journal of Engineering Manufacture, Volume 225, pp. 711-721, 2010.
20) Keshav Prasad, D. K. Dwivedi, “Some investigations on microstructure and mechanical properties of submerged arc welded HSLA steel joints”, Journal of Advanced Manufacturing Technology, Volume 36, pp. 475-483, 2006.
21) Behcet Gulenc, Nizamettin Kahraman, “Wear behaviour of bulldozer rollers welded using a submerged arc welding process”, Materials and Design, Volume 24, pp. 537–542, 2003.
22) R. S. Chandel, H. P. Seow, F. L. Cheong, “Effect of metal powder addition on mechanical properties of submerged arc welds”, Journal of Materials Science Letters , Volume 17, pp. 1785-1786, 1988.
23) N.D. Pandey, A. Bharti, “Effect of submerged arc welding parameters and fluxes on element transfer behaviour and weld-metal chemistry”, Journal of Materials Processing Technology, Volume 40, pp. 195-211, 1994.
24) M.L.E. Devis, “How submerged arc flux composition influence element transfer Weld.Pool Chem.and Metall”, The WI, Cambridge, UK, Volume 8, pp. 289-310, 1980.
25) W. Troyer, J. Mikurak, “Study of Mechanical Properties of Submerged Arc Welds after metal powder addition”, Welding J., Volume 53, pp. 494-498, 1974.
26) Vinod Kumar, Narendra Mohan, J.S. Khamba, “Development Of Cost Effective Agglomerated Fluxes From Waste Flux Dust For Submerged Arc Welding”, Proceding the World Congress of Engineering, 2009.
27) P. Kanjilal, T.K. Pal, S.K. Majumdar, “Combined effect of flux and welding parameters on chemical composition and mechanical properties of submerged arc weld metal”. Journal of Materials Processing Technology, Volume 171, pp. 223–231, 2006.

28) Ana Ma. Paniagua-Mercado, Victor M. Lopez-Hirata, Maribel L. Saucedo Munoz, "Influence of the chemical composition of flux on the microstructure and tensile properties of submerged-arc welds". Journal of Materials Processing Technology, Volume 169, pp. 346–351, 2005.

29) T.W. Eagar, "Oxygen and nitrogen contamination during submerged arc welding of titanium", Proc International Conference of Welding Research, Osaka University, Osaka, Japan, 1980.

30) C.S. Lee, R.S. Chandel, H.P. Seow, "Effect of Welding Parameters on the Size of Heat Affected Zone of Submerged Arc Welding", Materials and Manufacturing Processes, Volume 15, No.5, pp. 649-666, 2000.

31) M. Eroglu, M. Aksoy, N. Orhan, "Effect of coarse initial grain size on microstructure and mechanical properties of weld metal and HAZ of a low carbon steel", Material Science Engg, Volume 269, pp. 59–66, 1999.

32) B. Beidokhti, A.H. Koukabi, A. Dolati, "Effect of titanium addition on the microstructure and inclusion formation in submerged arc welded HSLA pipeline steel." Journal of Materials Processing Technology, Volume 209, pp. 4027–4035, 2009.

33) M. Zrilic, V.Grabulov, Z. Burzic, M. Arsic, S. Sedmak, "Static and impact crack properties of a high-strength steel welded joint" International Journal of Pressure Vessels and Piping, Volume 84, pp. 139–150, 2007.

34) S.D. Bhole, J.B. Nemade, L. Collins, Cheng Liu, "Effect of nickel and molybdenum additions on weld metal toughness in a submerged arc welded HSLA line-pipe steel". Journal of Materials Processing Technology, Volume 173, pp. 92–100, 2006.

35) S. Ravi, V. Balasubramaniana, S. Nemat Nasser, "Influences of post weld heat treatment on fatigue life prediction of strength mis-matched HSLA steel welds". International Journal of Fatigue, Volume 27, pp. 547–553, 2005.

36) S. Ravi, V. Balasubramanian, S. Babu, S. Nemat Nasser, "Influences of MMR, PWHT and notch location on fatigue life of HSLA steel welds". Engineering Failure Analysis, Volume 11, pp. 619–634, 2004.

37) J. Vojvodic Tuma, A. Sedmak, "Analysis of the unstable fracture behaviour of a high strength low alloy steel weldment" Engineering Fracture Mechanics, Volume 71, pp. 1435-1451, 2004.